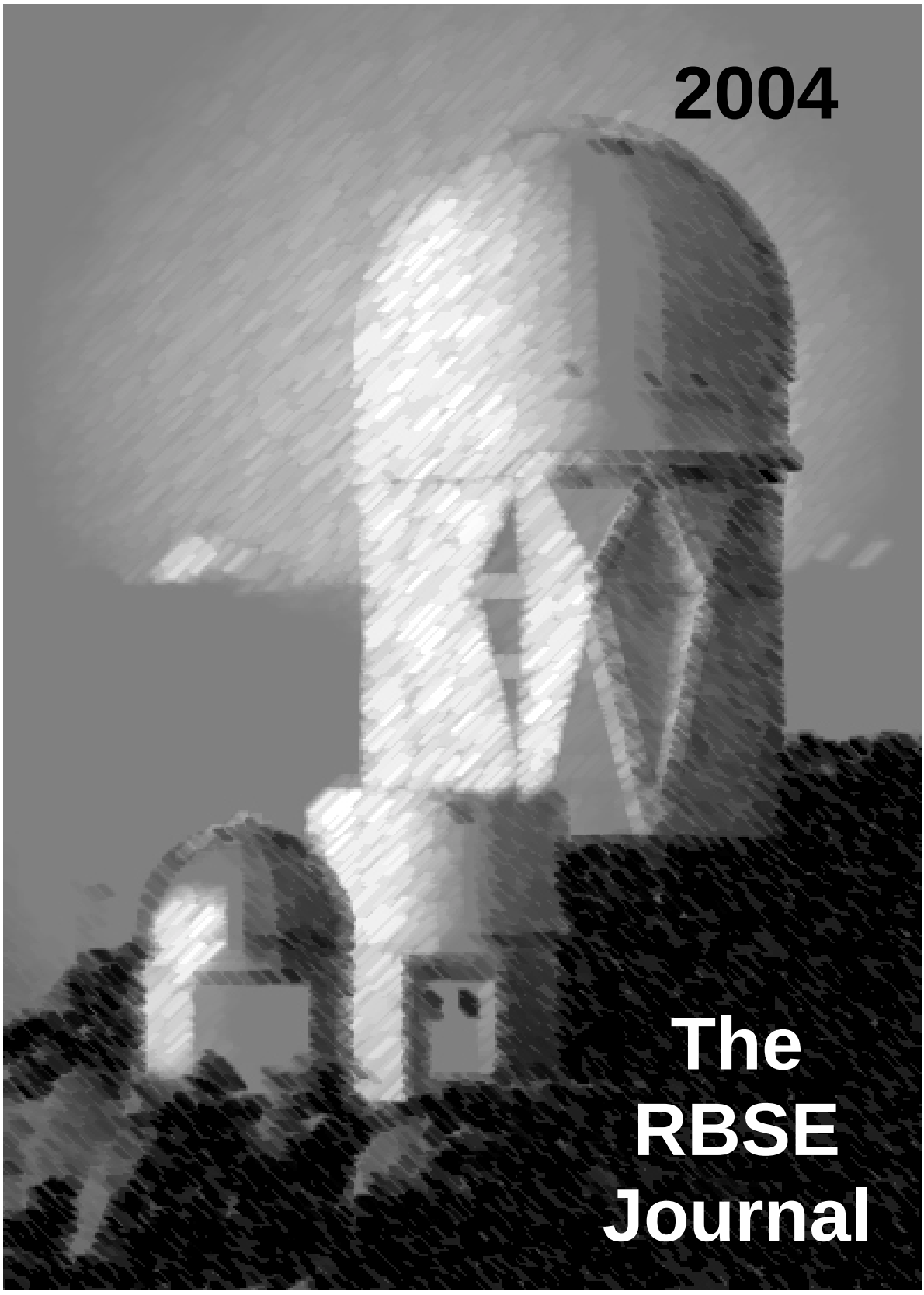

NOAO AURA NSF

The RBSE JOURNAL

2004

"Teacher Leaders in Research Based Science" (TLRBSE) is a Teacher Enhancement Program funded by the National Science Foundation. It consists of a distance learning course and a summer workshop for middle and high school teachers interested in incorporating leadership and research within their classes and school. TLRBSE brings the research experience to the classroom with materials, datasets, support, and mentors during the academic year. The RBSE Journal is an annual publication intended to present the research of students and teachers participating in the TLRBSE program.

Table of Contents

SOLAR RESEARCH

NOVA RESEARCH

OTHER RESEARCH

Horizontal Evershed Flow Velocities Of Ni I And Fe I Within Sunspots

Cayle Castor and Matt Crevier
Belmont High School, Belmont, New Hampshire
Teacher: Thomas R. Morin TLRSBE 2003

ABSTRACT

Using the McMath Pierce Telescope, a two-day observation was conducted of sunspots AR0564, AR567, and AR0563. The initial focus of the experiment was to determine the velocities of particles in the horizontal component of Evershed Flow. After a preliminary examination of spectra taken from the sunspots, a spectral line of unionized particles was located. The opportunity to compare velocities of ionized and unionized particles in Evershed flow was taken and the research was promptly aimed to determine the velocities of iron (ionized) and nickel (unionized) in the sunspots.

BACKGROUND

The sun has a strong magnetic field. This magnetic field can restrict movement of particles in the convection layer. Consequently, the transfer of heat energy is also restricted, resulting in a cool dark spot on the photosphere called a sunspot. Within the sunspot, there is a flow of ions along the magnetic field lines, starting from the center of the umbra and ending at the edge of the penumbra. This phenomenon is called Evershed Flow.

PROCEDURE FOR TELESCOPE OPERATION

MCMATH-PIERCE SOLAR TELESCOPE

Opening Telescope:

- Power on and open the telescope.
- Move to the Sun
- Focus and collimate to the main spectrograph.
- Power up the spectrograph and reboot spectrograph control computer.
  - Rotate spectrograph tank to orient the slit to solar coordinates and turn on tank rotation drive.

IR Array:

- Fill the array's dewar with liquid nitrogen (inner and outer cryogen flasks).
- Connect vacuum pump to the dewar's center nitrogen flask and evacuate (open valve slowing so that the dewar is pumped gently).
- Power on array's control electronics and computer.
- Select desired filter from the internal (cold) filter wheels.
- Wait for the dewar to cool to a stable temperature (indicated by the vacuum gauge dropping to and settling at around 45 torr).
- Open the spectrograph collimator and photoelectric port mirror covers.
- Move the grating to the desired wavelength.
- Adjust the array integration time for good signal strength.
- Verify the spectral lines are visible on the array monitor.
- Create subdirectories for the day's observations and set the data collection path on the control computer.

Scanning an active region:

- Setup solar limb guiders on a computer controlled stepper motor translation stage.
- Align limb guider translation to scan the spectrograph slit across an active region.
- Experimentally determine the array frame rate (files / seconds). Use this information to determine the desired stepping rate for the limb guider translation stage and the number of spectral frame to collect. (Take into account that one slit width is about half an arcsecond and the diffraction limit of the telescope at 5 microns is ~0.8 arcseconds. Spatially sampling at ~0.4 arcseconds would then be about right under good seeing.)
- Input scan parameters (number of steps, number of spectral frames, integration time, etc.)
- Start the scan sequence and simultaneously begin stepping the translation stage.
- Optional: Are there absorption lines in the spectra that only appear in the sunspot? If so, they are likely due to molecules. Sunspots can be cool enough for some molecules to exist! Find the wavelength of the line(s) and try to determine what molecule it represents. Make a spectroheliogram from the line center. Finally, see if you can look up the dissociation temperature of that molecule. The spectroheliogram conclusively maps where in the sunspot the temperature is below that dissociation temperature!

Scale Calibrations: Parameter Input Menus for Data Taking

- Measure the linear distance the translation stage displaced the limb guiders during the scanning sequence. From this the spatial scale between spectral frames can be calculated. (Note: The telescope image scale is 2.37 arcseconds/mm.)
- Place the 5mm scale plate across the slit and take a spectral image. This will be used to calculate the image scale (pixels/arcsec) in the slit axis.

Darks:

- Close the spectrograph slit.
- Reset the file name (like to "dark") and path.
- Take a series of observations using the same parameters as used in the scan sequence.

Flat Fields:

- Open a telnet window and log into "pacifico.tuc.noao.edu".
- Login: nim
- Password: teamnim
- Change directory (cd) to /home/vxworks/binPacifico

- Run the executable file "scan_client". This program rocks the spectrograph diffraction grating back-and-forth between to wavelength limits specified by the operator. The grating is rocked to average out spectral features to produce a smooth continuum for the flat field files. The Observing Support Engineer (me) will assist in the parameter selections. Listed here is an example run (Italics indicate user input):

  p% cd /home/vxworks/binPacifico
  p% scan_client
  scan - Pacifico-Indio version 1.0 3/27/98

  Enter wavelength units (n=nm, w=wave#, a=ang) > *w*
  Starting Wavelength > *2120*
  Ending Wavelength > *2130*
  Speed: Percentage of max speed (4%) > *20*
  Scan mode: 1=slew, 2=step > *2*
  Scan time (seconds: max = 600 seconds) > *600*
  Type 'q' (quit), 'c' (change data), 'g' (go), 's' (save mark), 'b' (back to mark)
  >*s*
  Type 'q' (quit), 'c' (change data), 'g' (go), 's' (save mark), 'b' (back to mark)
  >*g*

- Reset the file name (like to "flat") and path.
- In the Array control computer observations window, change the number of coadds from 1 to 8 and the exponent to 3 (divide by 8) and the number of repeats (frames to be taken to 32).
- Begin moving the Sun randomly over the spectrograph slit and a random fashion avoiding active regions. Moving the Sun while taking many spectral frames will average out any spatial structure across the slit. This is done on conjunction with the rocking of the grating to produce flat field frames that are featureless in both the wavelength and spatial axes.
- Begin the scan sequence while continuing to scan the grating and Sun.
- Stop the grating scanning with command "s" or wait for it to time out.
- Return to the original wavelength with command "b" (meaning back).

Procedure for Producing Dopplergrams

- Open the data reduction.exe program.
- Click on Image Frame and select the first file in a raw data sequence.
- Click on Image Dark and select a dark file that corresponds to the Image Frame in terms of scan number and the time of day in which it was taken. If done properly, the program should select the appropriate file(s) for the Dark Flat as well.
- Click on flat frame, and select a Flat that corresponds to the scan number and the time of day in which the Image Frame was taken.
- Save results in a desired destination. (It does not have to be an existing folder.)
- Be certain that the “Process all Matching Files” option is selected.

- Choose the number of discrete median replacement passes.
- (5 passes are recommended, 10 is the maximum)
- Process the data.

Procedure for Producing Dopplergrams in IDL

- Open the pro_dopplergram program file, IDL should automatically open.
- Press Ctrl-F5 to compile the program.
- Press F5 to run the program.
- Select first file from a reduced a data sequence.
- Select last file from the same reduced data sequence.
- Click the cursor on the left side of the target line.
- Click the cursor the right side of the target line.
- Click the cursor on the left side of a clean region.
- Click the cursor on the right side of a clean region.
- To view the spectral line fitting press 1, otherwise press zero.
- Save as a FITS file in a desired destination.

Procedure for Scaling the Dopplergram

- Open pro_dop_scale program file, IDL should automatically open.
- Press Ctrl-F5 to compile the file.
- Press F5 to run file.
- Select the continuum file (contin) produced by the dopplergram program.
- Select the dopplergram file (dop_gram) produced by the dopplergam program.
- Mask any bad pixel regions by clicking “yes” otherwise click no.
- Choose and click a corner of an area surrounding a zero velocity region.
- Choose and click the opposite corner of an area surrounding a zero velocity region.
- Left click on dopplergram image to display velocity at that point.

HYPOTHESIS

The goal of this research project is to determine if there is a direct correlation between the flow velocities of Iron ions and Nickel within a sunspot. This flow is a horizontal component known as Evershed Flow and can only be viewed edge on.

DATA

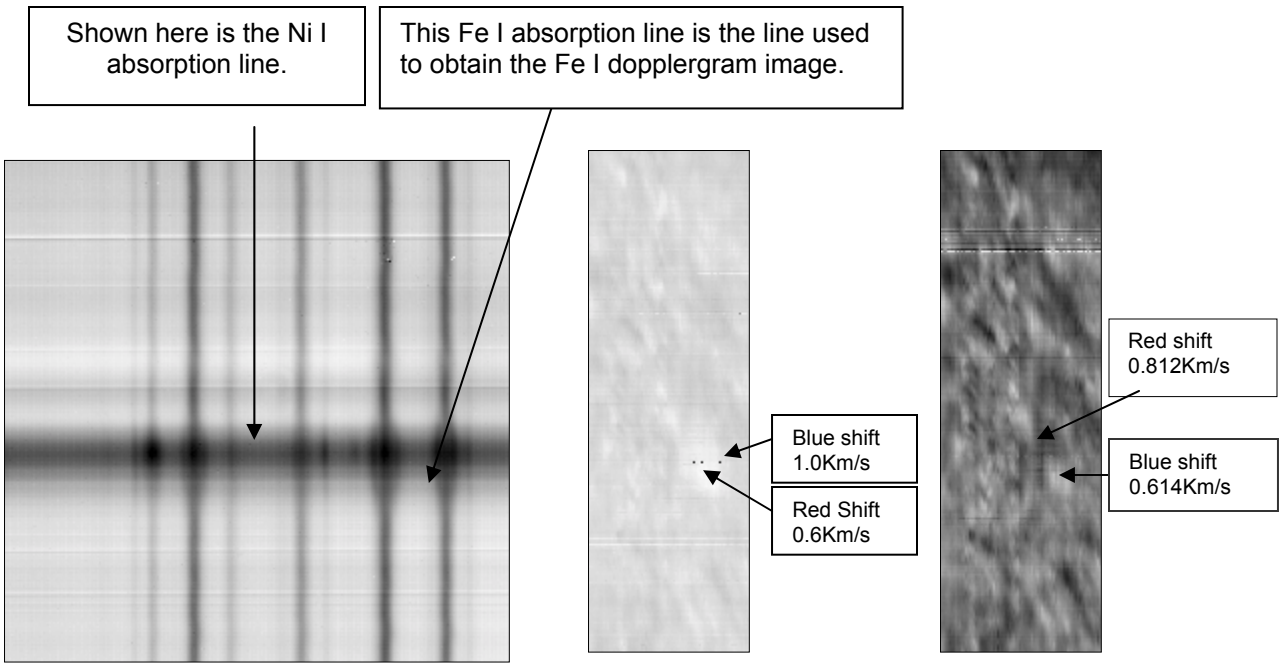

Infrared Spectrum at 15540Å Dopplergram of Ni I Line Dopplergram of Fe I line

CONCLUSION

Movement of the Iron ions is restricted to the magnetic field lines from within the umbra to the edge of the penumbra. This is supported by the data, which shows an initial outward flow of the ions and then a downward flow near penumbra.

Because the nickel particles are not ionized, their velocities would not correspond to the magnetic field lines unless there was an indirect mechanism for their flow, namely, other materials that are directed by the magnetic field.

The data seems to indicate that the mechanism for the nickel's movement is not the flow of iron directed by the magnetic fields. The nickel displays greater values for red and blue shift, indicating greater speeds than the iron. If the Iron particles were colliding with the more massive nickel particles, and the nickel had no other outside force causing its motion, then the transfer of energy would result in the nickel moving with less speed than the Iron.

If the data is accurate then there must be an unknown mechanism for the nickels particle's flow. The data may be inaccurate due to the small size of the sunspot and/or difficulties with the scan. Instead of conducting scans with 200 steps, scans with 100 steps were used. This resulted in slightly less precise data.

BIBLIOGRAPHY

Wallace, L, and W. Livingston. An atlas of the Solar Spectrum in the Infrared from 1850 to 1900 cm (1.1 to 5.4 um), revised. Tucson, Arizona: National Solar Observatory, 2003.

"The Sun." Discovering the Universe. 6th ed. 2003.

"Magnetic Maps of the Sun." SOHO Exploring the Sun. 1 Feb. 2004 <http://soi.stanford.edu/data/farside/>.

Landsman, Wayne. "Searchable Index of all IDL Astronomy Library Procedures ." IDL Astronomy User's Library. 24 Feb. 2004. NASA and GFSC. 15 Mar. 2004 <http://www.noodletools.com/noodlebib/refer/defineEntryMLA.php>.

"The Nature of Magnetic Fields." Conceptual Physics. 2nd ed. 1992.

The data reduction program was provided by Dr. Bergman.
The IDL Dopplergram programs were provided by Claude Plymate.
Special thanks to Dr. C. Walker and Dr. F. Hill.

Active Longitudes

Danny Matarese, Lee Braun, and Michael Tiu
Cranston High School East, Cranston, RI
Teacher: Howard Chun, RBSE 1999

ABSTRACT

Active longitudes have been theorized to be the points of origination for sunspots. Using the Carrington Longitude, the path of the sunspots can be tracked, and using this method, the active longitude can be found. After comparing the Carrington longitude and local longitude, it was difficult to find consistent and convincing evidence of Active Longitudes. Some data however, supported the theory with repeated origins of the sunspots.

PURPOSE

The paths of sunspots are tracked, and studied, in order to discover active longitudes

HYPOTHESIS

Some longitudes of the sun's surface will have a greater sunspot activity than other regions, according to their Carrington longitudes.

Procedure

1) Open ImageJ on your computer

2) Insert the Magnetograms CD

3) Using ImageJ track a sunspot's coordinates across the sun's surface, repeat as many times as possible.

4) Save your results to the computer's hard drive and organize them in a program such as Excel.

5) Compare the results of the sunspots and look for active longitudes.

CONCLUSION

Active Longitude is the longitudinal coordinates where sunspots are believed to repeatedly originate. The theory of active longitudes existing on the solar surface was hypothesized to be supported if the sunspot paths were tracked, and they were found to have similar longitude of origination within the same Carrington longitude. Some of the data was found to support the hypothesis. There were sunspots found with the same Carrington Longitude at around 285, 280, 345, 245, 255, 50, 28, and 22. These conclusive sets were out of about 30 sets of data total. This was not conclusive enough. Although these potential active longitudes were observed, further, more extensive research is needed to support the theory. All other Carrington Longitudes were found to be unique. There is a possibility that the Longitudes found were coincidental and not active.

REFERENCES

Porter, R.; The Biographical Dictionary of Scientist; Oxford Press; 1998

Meadows, AJ.; Early Solar Physics; Pergamon; 1970

Corrente, Marc and Ryan Loftus; The RBSE Journal; 2003

Magnetograms; NOAO, NSO; 2003

DATA

Image Date	Julian Date	Latitude	Longitude	Area	Carr. Rot	Carr. Long
02/14/1991	2448302.2528	25.8198	-33.9050	25.5880	1839.2003	287.9100
02/16/1991	2448304.2083	25.372	-8.8925	24.2793	1839.2025	287.1116
02/19/1991	2448307.2382	25.3991	28.8250	15.1909	1839.2088	284.8386
02/20/1991	2448308.1618	25.356	42.2573	11.0783	1839.2053	286.0805
01/11/1991	2448268.1653	-6.7783	-62.5095	28.7664	1838.0299	349.2180
01/12/1991	2448269.1778	-7.2900	-49.5248	35.2928	1838.0310	348.8390
01/13/1991	2448270.1771	-7.9618	-38.2728	47.5143	1838.0364	346.9014
01/14/1991	2448271.1771	-8.2962	-24.3189	49.3928	1838.0343	347.6565
01/15/1991	2448272.1965	-8.5283	-10.9573	55.2658	1838.0345	347.5628
01/17/1991	2448274.3722	-9.4172	15.7102	65.7824	1838.0402	345.5138
01/18/1991	2448275.1785	-9.8766	24.8723	63.1906	1838.0443	344.0344
01/19/1991	2448276.2076	-10.3939	38.6810	48.4447	1838.0437	344.2594
01/21/1991	2448278.1931	-9.9303	67.2021	24.0094	1838.0373	346.5755
07/31/1991	2448469.1549	21.8759	-34.1961	42.5779	1845.3202	244.7192
08/01/1991	2448470.0847	21.8900	-20.9222	48.1283	1845.3174	245.7201
08/02/1991	2448471.0826	21.9675	-7.2307	57.3554	1845.3160	246.2404
08/03/1991	2448472.0833	22.0707	6.0352	53.1806	1845.3158	246.2983
08/04/1991	2448473.1042	22.2885	19.4744	52.6495	1845.3159	246.2638
08/05/1991	2448474.1007	22.5073	32.0797	51.9164	1845.3175	245.7161
08/06/1991	2448475.1438	22.2011	45.9616	39.7111	1845.3171	245.8310
08/07/1991	2448476.1368	22.1988	59.1525	42.6490	1845.3169	245.9148
06/02/1991	2448410.2813	19.4893	-55.8039	22.9701	1843.2218	280.1697
06/03/1991	2448411.1618	19.2989	-44.0708	22.2498	1843.2214	280.2806
06/04/1991	2448412.2292	19.1472	-30.6645	25.4746	1843.2233	279.5990
06/05/1991	2448413.3396	19.3685	-16.5171	32.1898	1843.2247	279.0903
06/06/1991	2448414.1708	19.5301	-5.4876	35.8183	1843.2246	279.1483
06/07/1991	2448415.0764	19.9780	6.5025	37.4525	1843.2245	279.1863
06/08/1991	2448416.1090	19.6199	20.0850	32.0461	1843.2246	279.1392
06/09/1991	2448417.1208	19.7324	33.8551	26.6118	1843.2235	279.5547
06/10/1991	2448418.1653	19.670	48.0748	25.5105	1843.2223	279.9891
05/01/1991	2448378.0688	-13.0792	-56.1915	32.6451	1842.0418	344.9470
05/02/1991	2448379.1278	-12.7789	-41.2158	34.6985	1842.0390	345.9449
05/03/1991	2448380.0743	-11.9846	-28.0591	39.1549	1842.0372	346.6086
05/04/1991	2448381.1139	-12.3992	-13.7536	52.1912	1842.0356	347.1929
05/05/1991	2448382.1083	-10.7736	0.4502	53.6556	1842.0326	348.2712
05/06/1991	2448383.1583	-9.7430	13.4596	54.9946	1842.0349	347.4220
05/07/1991	2448384.0653	-8.9569	27.1153	51.9594	1842.0303	349.1072
05/08/1991	2448385.1729	-8.9388	42.8651	55.8556	1842.0271	350.2375
12/27/1987	2447157.1972	-34.5584	-55.8183	39.0668	1797.2797	259.3043
12/28/1987	2447158.1590	-34.6058	-43.3366	35.6624	1797.2803	259.0914
12/29/1987	2447159.1583	-34.6073	-30.6956	36.3780	1797.2818	258.5428
12/30/1987	2447160.1924	-34.3888	-18.6894	42.5735	1797.2864	256.9012
01/01/1988	2447162.2667	-34.8228	6.7109	40.8339	1797.2919	254.9231
01/02/1988	2447163.1826	-34.7127	18.5733	38.4975	1797.2925	254.6959
01/03/1988	2447164.1931	-35.0798	32.2296	33.7024	1797.2916	255.0160
01/04/1988	2447165.1729	-36.1002	45.5338	15.6929	1797.2906	255.3871
12/10/1985	2446410.1424	2.0833	-68.2381	5.7217	1769.9109	32.0874
12/14/1985	2446414.1618	3.5930	-11.3960	19.6465	1769.9143	30.8689
12/15/1985	2446415.1979	2.8843	0.2799	23.4387	1769.9198	28.8695
12/17/1985	2446417.1438	2.0852	24.1750	16.9689	1769.9248	27.0820
12/18/1985	2446418.1917	2.6734	38.6640	15.7301	1769.9229	27.7398
12/19/1985	2446419.1521	1.7196	51.2669	10.9231	1769.9231	27.6665
12/02/1991	2448593.1847	19.2854	-57.7340	21.0218	1849.9329	24.1415
12/03/1991	2448594.2014	18.5202	-44.8333	29.1162	1849.9344	23.6235
12/06/1991	2448597.2465	19.3231	-5.3672	51.1903	1849.9364	22.8975
12/07/1991	2448598.1618	19.3531	6.7825	46.9555	1849.9362	22.9667
12/08/1991	2448599.1583	19.5466	19.6119	39.9872	1849.9371	22.6432

Image Date	Julian Date	Latitude	Longitude	Area	Carr. Rot	Carr. Long
09/18/1987	2447057.0875	12.1553	-63.5153	2.0580	1793.6307	132.9310
09/19/1987	2447058.0840	12.1356	-50.3220	2.1759	1793.6306	132.9714
09/20/1987	2447059.2438	12.4742	-35.7859	3.7178	1793.6328	132.2006
12/27/1987	2447157.1972	-34.5584	-55.8183	39.0668	1797.2797	259.3043
12/28/1987	2447158.1590	-34.6058	-43.3366	35.6624	1797.2803	259.0914
12/29/1987	2447159.1583	-34.6073	-30.6956	36.3780	1797.2818	258.5428
12/30/1987	2447160.1924	-34.3888	-18.6894	42.5735	1797.2864	256.9012
01/01/1988	2447162.2667	-34.8228	6.7109	40.8339	1797.2919	254.9231
01/02/1988	2447163.1826	-34.7127	18.5733	38.4975	1797.2925	254.6959
01/03/1988	2447164.1931	-35.0798	32.2296	33.7024	1797.2916	255.0160
01/04/1988	2447165.1729	-36.1002	45.5338	15.6929	1797.2906	255.3871
02/28/1982	2445029.1326	-21.4671	-57.4624	40.3242	1719.2626	265.4631
03/03/1982	2445032.1306	-19.2358	-17.9346	78.1046	1719.2627	265.4221
03/04/1982	2445033.1188	-19.2246	-4.9061	90.1659	1719.2628	265.4077
03/05/1982	2445034.1590	-17.8480	8.6816	81.0088	1719.2632	265.2650
03/06/1982	2445035.1403	-17.9263	21.8428	86.6693	1719.2626	265.4750
03/07/1982	2445036.1257	-17.3971	34.8574	79.4617	1719.2625	265.4833
03/09/1982	2445038.1125	-15.2929	62.4310	38.2835	1719.2588	266.8335
11/02/1991	2448563.1160	-8.5840	-67.8767	10.6906	1848.8587	50.8690
11/03/1991	2448564.1285	-9.0277	-55.6351	12.0404	1848.8618	49.7467
11/04/1991	2448565.2035	-9.1802	-41.7843	16.8207	1848.8628	49.4089
11/05/1991	2448566.1813	-8.8565	-29.4385	17.3851	1848.8643	48.8493
11/06/1991	2448567.2646	-9.4038	-14.6864	19.8795	1848.8630	49.3027
11/07/1991	2448568.1847	-9.1058	-1.3297	11.0695	1848.8597	50.5148
11/11/1991	2448572.1965	-12.8628	8.9089	4.7095	1848.9783	7.8025
11/12/1991	2448573.1715	-12.2828	20.4622	9.9778	1848.9820	6.4870
11/13/1991	2448574.2549	-12.4796	34.6637	4.2558	1848.9823	6 .3898
08/07/1991	2448476.1368	9.0531	-62.5178	10.5894	1845.6549	124.2445
08/08/1991	2448477.0931	8.3669	-51.0983	17.8488	1845.6582	123.0427
08/11/1991	2448480.2326	3.8553	-42.0472	14.0535	1845.7482	90.6552
08/12/1991	2448481.2618	3.9433	-27.9182	16.5984	1845.7467	91.2005
08/13/1991	2448482.0743	4.0302	-17.3566	19.3242	1845.7471	91.0381
08/14/1991	2448483.1188	4.0070	-3.6882	16.7679	1845.7474	90.9212
08/17/1991	2448486.1063	4.4365	36.5557	9.0514	1845.7452	91.7338
08/18/1991	2448487.2035	3.9482	51.9530	3.4386	1845.7426	92.6491
08/19/1991	2448488.2264	3.2465	66.2929	0.4392	1845.7403	93.4878
01/07/1991	2448264.2861	6.2918	-46.7820	13.8541	1837.8440	56.1457
01/08/1991	2448265.1750	8.5308	-38.9262	18.8514	1837.8548	52.2693
01/09/1991	2448266.1729	8.9874	-27.7979	34.7468	1837.8605	50.2263
01/11/1991	2448268.1653	5.9316	2.3606	26.0419	1837.8498	54.0881
01/12/1991	2448269.1778	6.9299	14.2304	28.2031	1837.8539	52.5942
01/13/1991	2448270.1771	7.5877	26.6954	20.1635	1837.8559	51.8696
01/14/1991	2448271.1771	5.7943	41.7519	5.6082	1837.8508	53.7274
01/15/1991	2448272.1965	10.7593	46.7187	8.7149	1837.8743	45.2388
06/02/1991	2448410.2813	19.4893	-55.8039	22.9701	1843.2218	280.1697
06/03/1991	2448411.1618	19.2989	-44.0708	22.2498	1843.2214	280.2806
06/04/1991	2448412.2292	19.1472	-30.6645	25.4746	1843.2233	279.5990
06/05/1991	2448413.3396	19.3685	-16.5171	32.1898	1843.2247	279.0903
06/06/1991	2448414.1708	19.5301	-5.4876	35.8183	1843.2246	279.1483
06/07/1991	2448415.0764	19.9780	6.5025	37.4525	1843.2245	279.1863
06/08/1991	2448416.1090	19.6199	20.0850	32.0461	1843.2246	279.1392
06/09/1991	2448417.1208	19.7324	33.8551	26.6118	1843.2235	279.5547
06/10/1991	2448418.1653	19.6704	48.0748	25.5105	1843.2223	279.9891
02/28/1982	2445029.1326	-21.4671	-57.4624	40.3242	1719.2626	265.4631
03/03/1982	2445032.1306	-19.2358	-17.9346	78.1046	1719.2627	265.4221
03/04/1982	2445033.1188	-19.2246	-4.9061	90.1659	1719.2628	265.4077
03/05/1982	2445034.1590	-17.8480	8.6816	81.0088	1719.2632	265.2650
03/06/1982	2445035.1403	-17.9263	21.8428	86.6693	1719.2626	265.4750
03/07/1982	2445036.1257	-17.3971	34.8574	79.4617	1719.2625	265.4833
03/09/1982	2445038.1125	-15.2929	62.4310	38.2835	1719.2588	266.8335

Image Date	Julian Date	Latitude	Longitude	Area	Carr. Rot	Carr. Long
10/23/1989	2447823.3833	-19.8974	-34.1986	32.0563	1821.5525	12639073
10/24/1989	2447824.2437	-20.1063	.22.3649	32.9625	1821.584	127.3846
10/25/1989	2447825.7076	-19.9529	-9.5086	25.6749	1821.6194	127.2628
10/26/1989	2447826.2611	-20.5781	3.8528	27.9985	1821.658	12639756
10/27/1989	2447827.2160	-21.2517	16.4166	20.0509	1821.693	126.9364
10/28/1989	2447828.2083	-21.4233	29.4959	15.0839	1821.7294	126.9178
10/29/1989	2447829.2160	-21.5699	452.8657	12.4159	1821.7663	126.988
10/30/1989	2447830.2062	-21.2796	56.7511	7.4033	1821.8026	127.803
11/3/1989	2447834.7139	17.767	-9.5733	31.645	1821.9496	8.5828
11/4/1989	2447835.1097	24.0158	3.9237	50.5548	1821.9861	8.936
11/5/1989	2447836.1965	23.9441	16.4274	46.1054	1821.0223	8.4151
3/18/85	2446143.1278	-10.8999	-43.877	2.392	1759.9489	334.5102
3/20/85	2446145.1187	-10.7664	-18.8969	4.467	1760.0219	333.2127
3/21/85	2446146.0896	-11.0523	-5.7442	4.0314	1760.0575	333.5516
3/22/85	2446147.0944	-10.9374	7.02894	4.2858	1760.0944	333.3223
3/23/85	2446148.1042	-10.97.26	22.0914	3.1014	1760.1314	334.7972
3/24/85	446149.1234	-12.3418	34.9594	1.4982	1760.1688	334.2006
3/25/85	2446150.1181	6.0112	-41.0844	13.1019	1760.2052	245.0406
3/26/85	2446151.2701	6.3082	-25.7057	15.2297	1760.2474	245.2132
3/27/1985	2446152.1299	6.155	-14.5375	16.3562	1760.279	245.0341
3/30/1985	2446155.1486	6.0876	25.9945	10.8989	1760.3896	245.7033
3/31/1985	2446156.1903	5.7699	40.5883	6.9675	1760.4278	245.3172
4/1/1985	2446157.0903	5.9944	53.0241	5.2771	1760.4608	245.0406
5/9/1985	2445830.1201	11.5429	-40.9807	86.6691	1748.4731	148.7712
5/10/1985	2445031.1979	6.5583	-27.1035	99.2484	1748.5107	149.1357
5/11/1985	2445832.1083	6.6628	-14.1187	104.6015	1748.543	149.797
5/12/1985	2445833.1993	7.0334	-0.8513	98.4601	1748.5859	148.4176
5/13/1985	2445834.1976	7.0804	12.56	104.7523	1748.6225	148.7185

Sunspot Activity And Mars Exploration

Michael TW Huang, Michael Paul St. Laurent, Michael Geary King
Cranston High School East, Cranston, RI
Teacher: Howard Chun, RBSE 1999

ABSTRACT

A relationship between the occurrences of sunspots and the success rate of several missions to Mars was examined. Tapping into NASA databases and other resources containing data of different missions sent to Mars, data was collected on each mission dating back to the 1970s along with its success rate and its cause of failure if it was unsuccessful. From the twelve different missions examined, five missions failed during periods of high solar activity, while only one succeeded during high solar activity. Of the four successful missions, three of them occurred during periods of low solar activity. A correlation between the success rate can then be concluded that the ejections from the sun have some effect on the spacecrafts heading towards Mars.

BACKGROUND INFORMATION

Sunspots

Sunspots are dark spots visible in the sun's photosphere, some of which are big as 50,000 miles in diameter. They are dark because of their cooler temperature than the surrounding material, and their lowered temperature can be traced to a strong magnetic field that inhibits the conveying of heat. Even the largest sunspots can't be seen with the naked eye. They also rotate with the sun and fluctuate in size and shape. Even though sunspots aren't as luminous as their surroundings, they still radiate an amount of light about ten times brighter than the sun.

The composition of sunspots is broken down into two parts. The first part is the umbra, the dark, roughly circular central disk made of hot material rising from the sun's interior, and the penumbra, the lighter outer area in circumference of the umbra. The powdery appearance of the area outside of the sunspot can be traced to convection. The middle of each granule is hot material rising from the sun's interior, while the edges are cooler material sinking downward.

The number of sunspots follows a 22-year cycle. Sunspots most often are in the low latitudes near the solar equator, and as the sunspot cycle progresses, the visible sunspots move gradually towards the equator of the sun.

During these active solar periods, much material is ejected from the sun affecting space around the sun including the earth. Because the earth is surrounded by a magnetic field, the ejections generally only affect that field. The ejections also reach beyond earth affecting other planets and any spacecrafts beyond the earth's atmosphere.

MARS MISSIONS

Space probes have provided the most detailed information about Mars. Exploration of the planet began in 1960, when the former USSR launched its first probe to Mars. Their Mars missions were mainly unsuccessful until the Phobos missions which successfully studied Mars' moon Phobos. They have continued to explore Mars on a more modest scale since the fall of the Soviet Union. Soon after the Soviets began their space program, NASA began their Mars missions to rival the communists, with the Mariner. The US began with flyby missions which simply flew by Mars, taking as many photographs as possible en route. These missions took the first close up pictures of the planet, revealing their geographical similarities to Earth, such as polar ice caps and clouds in its atmosphere, seasonal weather patterns, volcanoes, and canyons. These missions included the early Mariner campaigns. Next were orbiter missions as our knowledge and technologies grew, so we began putting spacecraft in orbit around Mars for longer term, global studies. These missions included the later Mariner and early Viking campaigns. The Viking campaign had orbiters to map Mars and make global studies of its geology and chemistry. With even more capabilities over the years, we began to land on the surface, with landers and rovers. Today, we're not only landing in one place, but have shown that we can be mobile on the surface of Mars. These missions included some of the most recent campaigns, including the Pathfinder and Mars Express. Recently, interest in Mars has grown, including whether life can be sustained on the planet, with the recent traces of water evident.

PURPOSE

Through the analysis of solar data and space exploration, the correlation between sunspot activity and the failures/successes of Mars exploration is determined.

HYPOTHESIS

Sunspots are known to affect Earth's magnetic field, and they may be linked to the technical failures of missions to Mars. During times of lesser sunspot activity, there would be a higher success rate of missions aimed to explore Mars, and during times of higher sunspot activity, there would be a lesser success rate of missions.

PROCEDURE

Using the Internet, the dates and the status of past missions to Mars were collected. The dates were then compiled and were used for the solar data. The solar data that indicated sunspot activity was taken from several different sources such as the Internet and various programs such as ImageJ. The data given were the amount of groups of sunspots observed and the amount of sunspots individually. The R value was determined by multiplying the amount of groups by a factor of ten and then adding the amount of sunspots. Finally, this value is then multiplied by the constant k that varies with the years. The success of the various Mars missions were then compared to sunspot activity taken within the period of a week before the launch to compensate for the amount of time the sun's ejected material would reach the spacecraft.

DATA

Charts (g – Groups of Sunspots, f – Number of Sunspots, R – Relative Number of Sunspots)

Mariner 4 – Nov. 28 1964 – Succeeded			
Date	g	f	R
Nov. 21	2	3	16.6
Nov. 22	1	1	7.9
Nov. 23	0	0	0
Nov. 24	0	0	0
Nov. 25	1	2	8.6
Nov. 26	0	0	0
Nov. 27	0	0	0
Averages	0.6	0.9	4.7

Zond 2 – Nov. 30 1964 – Lost Contact			
Date	g	f	R
Nov. 23	0	0	0
Nov. 24	0	0	0
Nov. 25	1	2	8.6
Nov. 26	0	0	0
Nov. 27	0	0	0
Nov. 28	0	0	0
Nov. 29	0	0	0
Averages	.1	.3	1.2

Mars 1969A – Mar. 27 1969 – Failed			
Date	g	F	R
Mar. 20	12	103	160.6
Mar. 21	12	148	193.0
Mar. 22	11	147	185.0
Mar. 23	11	134	175.7
Mar. 24	8	95	126.0
Mar. 25	8	90	122.4
Mar. 26	11	73	131.8
Averages	10.4	112.9	156.4

Mariner 8 – May 8 1971 - Failed			
Date	G	f	R
May 1	5	17	48.2
May 2	-	-	-
May 3	7	26	69.1
May 4	-	-	-
May 5	4	62	73.4
May 6	-	-	-
May 7	4	51	65.5
Averages	5.0	39.0	64.1

Kosmos 419 – May 10 1971 – Failed			
Date	g	f	R
May 3	7	26	69.1
May 4	-	-	-
May 5	4	62	73.4
May 6	-	-	-
May 7	4	51	65.5
May 8	-	-	-
May 9	4	65	75.6
Averages	4.8	51.0	70.9

Mars 5 – July 25 1973 – Comp. Prob.			
Date	g	f	R
July 18	4	28	49.0
July 19	4	14	38.9
July 20	1	2	8.6
July 21	2	7	19.4
July 22	-	-	-
July 23	-	-	-
July 24	1	3	19.4
Averages	2.4	10.8	27.1

Phobos 2 – July 12 1988 – Comp. Prob.			
Date	g	F	R
July 5	-	-	-
July 6	6	92	91.2
July 7	8	78	94.8
July 8	10	66	99.6
July 9	6	66	75.6
July 10	-	-	-
July 11	-	-	-
Averages	7.5	75.5	90.3

Mars Observer – Sept. 25 1992 - Failed			
Date	g	f	R
Sept. 18	5	59	65.4
Sept. 19	6	33	55.8
Sept. 20	8	61	84.6
Sept. 21	9	57	88.2
Sept. 22	6	80	84.0
Sept. 23	7	76	87.6
Sept. 24	9	91	108.6
Averages	7.1	65.3	82.0

Pathfinder – Dec. 4 1996 – Succeeded			
Date	g	f	R
Nov. 27	-	-	-
Nov. 28	1	48	34.8
Nov. 29	1	42	31.2
Nov. 30	1	36	27.6
Dec. 1	2	26	27.6
Dec. 2	1	11	12.6
Dec. 3	0	0	0
Averages	1.0	27.2	22.3

Mars Odyssey – April 7 2001 – Succeeded			
Date	g	f	R
March 31	-	-	-
April 1	11	47	157
April 2	10	33	133
April 3	9	26	116
April 4	12	32	152
April 5	10	23	123
April 6	11	23	133
Averages	10.5	30.7	135.7

Mars Beagle 2 – June 2 2003 – Failed			
Date	g	f	R
May 26	-	-	-
May 27	-	-	-
May 28	4	18	58
May 29	5	15	65
May 30	4	15	55
May 31	-	-	-
June 1	-	-	-
Averages	4.3	16.0	59.3

Spirit – June 10 2003 – Succeeded			
Date	g	f	R
June 3	3	10	40
June 4	-	-	-
June 5	4	13	53
June 6	5	18	68
June 7	-	-	-
June 8	7	35	105
June 9	-	-	-
Averages	4.8	19.0	66.5

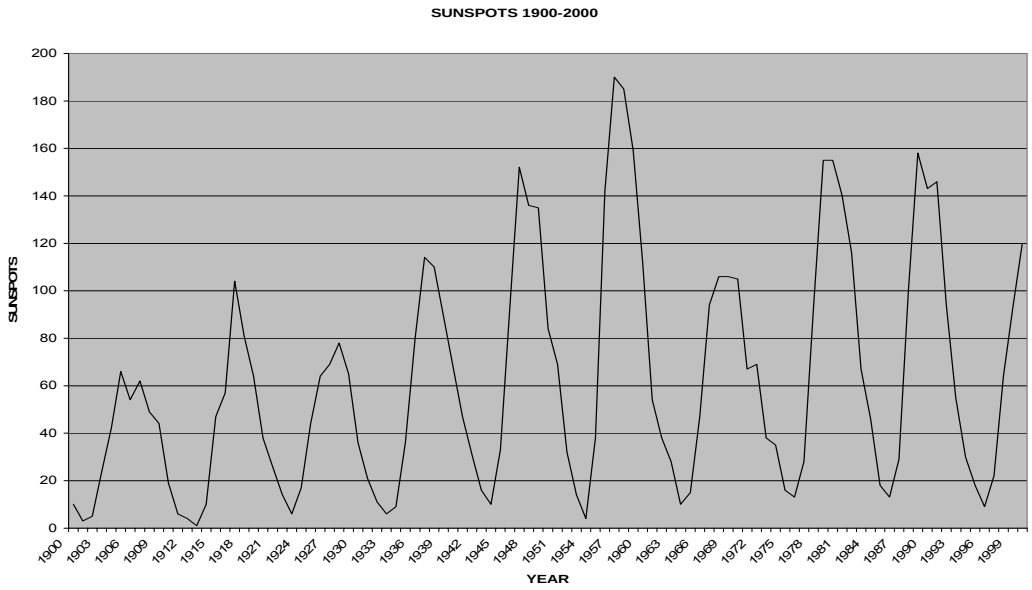

Magnetograms

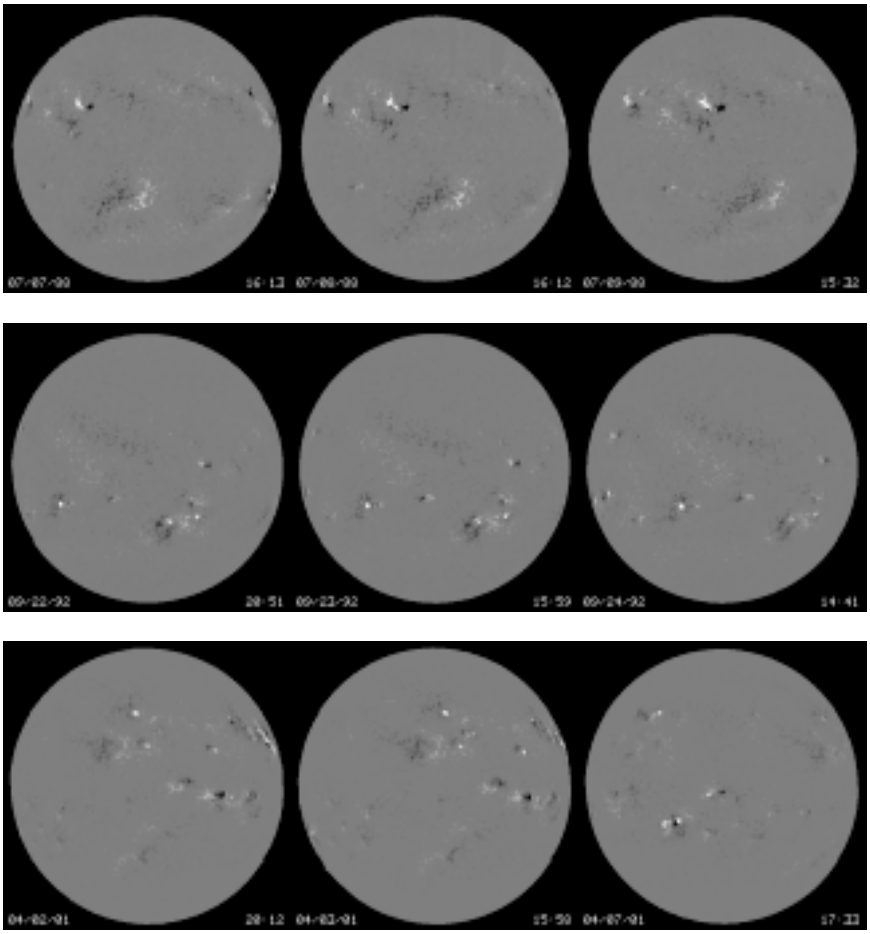

CONCLUSIONS

After comparing the two different sets of data, there is some evidence that sunspots affect the success rate of missions to Mars. Sunspots have been noted to have effects on the intensity of Earth's magnetic field. If the magnetic fields produced by the sunspots are strong enough to affect the planet earth's atmosphere and magnetic field, it is highly possible that it would send material beyond earth and affect any mechanical vessel attempting to reach Mars. Sunspots may affect the computer's or machinery's ability to function properly creating a failure in the mission. The outcomes of several different missions were examined, and sunspot activity that corresponded to those dates was collected. Mariner 4 sent in 1964 with a sunspot average of about 4.7 succeeded. Zond 2 failed though it was sent during a period of very low sunspots of about 1.2. Mars 1969A, Mariner 8, and Kosmos 419 all failed occurring during periods of relatively high amounts of sunspots. Mars 5 pertained to computer problems and failed in 1973 with a relative sunspot number of 27.1. In the year 1988, the Phobos 2 was sent into orbit heading towards Mars. It would end up shutting down due to a computer failure in the year 1989, which had a sunspot index of about 90.3 indicating that there was a high amount of sunspot activity. The year was also recorded to be near the maximum peak during the sunspot cycle. In 1992, the Mars Observer was sent, but it was lost due to an unknown reason. Because the true cause for its outcome was unknown, no conclusion could be drawn from this mission, though it occurred during a period of low sunspot activity. The Mars Pathfinder was sent to Mars in late 1996 and succeeded in 1997, which was recorded to have a very low sunspot index of about 22.3. By 2001, when there was more solar activity, the Mars Odyssey succeeded in its mission, which contradicts the hypothesis. In the year 2003, the Mars Beagle 2 failed with solar activity of 59.3, and the Spirit succeeded with a sunspot number of 66.5. From this data, it may be concluded that the amount of sunspot activity does affect the success rate of missions headed towards Mars. It was noted that three of the four successes occurred during periods of relatively low sunspot activity, while about 6 of 8 missions failed during periods of relatively high sunspot amounts. Failures due to human error should also be kept in mind. Though the data supports the hypothesis, more data should be collected and further examination on how the material ejected by sunspots may affect specific equipment should be analyzed before any definite conclusions may be drawn.

REFERENCES

http://www.wdcb.ru/stp/data/solar.act/sunspot/

http://solarwww.mtk.nao.ac.jp/solar/sunspots/number/

http://www.stoughton.k12.wi.us/Schools/RvrBluff/Astronomy/docs/SUNSPOT%20GRAPH%201900-2000.xls

http://www.planetary.org/learn/missions/marsmissions.html

Magnetic Field Strength Comparisons Between Lone Sunspots And Clustered Sunspots Of Similar Size.

Daniel Young co-PI, Rosalind Mallet co-PI, Elias Hayes
Cornerstone Community Christian School, Kelso WA
Teacher: Diedre Young, TLRBSE 2003

ABSTRACT
Zeeman splitting was measured in infrared images using the McMath-Pierce Solar Telescope at Kitt Peak National Observatory in Arizona. Recent images taken from the observatory on February 26, 2004 and additional archived sunspots of AR3966, AR563, AR564, AR565, and AR567 in July 2003 were used for research and analysis. This research was conducted to ascertain magnetic field strengths when comparing similarly sized sunspots in clusters versus pairs or singles. This was necessary in order to determine if the location and size of a sunspot(s) is an indicator of magnetic field strength.

BACKGROUND
The famous astronomer Galileo first recorded the phenomenon of sunspots in 1609, and thought that the spots were merely dark cloud-like formations drifting through the atmosphere of the Sun. Later observers of the 1800s hypothesized that the dark spots were unknown planets traveling Mercury's orbit and only became visible when they crossed in front of the sun. Shortly thereafter, however, observers discovered that the unknown spots changed drastically in number and when they exploded the earth would receive intense magnetic storms. It was therefore concluded that these spots were not planets and astronomers speculated that fascinating splotches were caused by the horrendous amount of magnetism on the sun.

They were indeed correct, as in 1896 Pieter Zeeman became the founder of the "Zeeman Effect" by which one could calculate the magnetic field strength of a sunspot by measuring the splitting of electron energy levels in the spectra of elements like Fe I; to state it simply, the wider the split in the spectral line, the stronger the magnetic field strength. George Ellery Hale, an American astronomer and inventor of the spectroheliogram, proved the Zeeman Effect. He combined Zeeman's theory with his invention and imaged the affects of magnetism on pairs of sunspots. He was then able to calculate the magnetic field intensity to approximately 1500 Gauss.

As we now know from technological advancements, that the Sun is a ball of plasma powered by a natural fusion process and sunspots are in fact products of the sun's intense magnetic fields located in the photosphere. It is now understood that these magnetic fields eventually knot, causing cooler, denser areas thereby giving birth to sunspots. From the observations of astronomers, they have noted that sunspots both shrink and grow in their size, lasting a few days or even several weeks. As the magnetic force continues to build up, it eventually causes ``magnetic flux tubes" to break, releasing enormous amounts of energy. A smaller scale eruption on the solar surface is called a prominence and because the Sun has such strong magnetic fields, the charged particles will be caught and brought back the surface. The more powerful eruptions are known as coronal mass ejections (CME's) or more commonly solar flares. Larger sunspots, when

they break, have been known to project charged particles through the Sun's dense magnetic fields and layered atmosphere into space. If the Earth happens to be in the solar flare's direct path, a magnetic storm will be experienced, causing what we know as the Aurora Borealis. Charged particles will enter through the Earth's magnetic "defenses" at the North and South Poles where shields are less pronounced, because the magnetic field lines are closer together, and the solar storm will "bend" the magnetic fields of the Earth, exposing satellites to the storm. There is always a danger of satellite and communications disruption because of this "bending" and the passing through of the charged particles.

RESEARCH PROBLEM

Based on past research and observation (determining whether or not magnetic field strength varies across a sunspot), it is reasonable to believe that the magnetic field strength of a sunspot also varies based on its location in relation to other sunspots. This project investigates whether or not the magnetic field strength of a sunspot varies if that spot is by itself or as a part of a larger cluster.

PROCEDURE

This study was done by scanning AR (active regions) 396, 563, 565, and 567 in infrared light, and measuring the Zeeman splitting of the iron spectral line at 15,650 angstroms. Images were taken from the McMath-Pierce solar telescope at Kitt Peak on July 3-7, 2003, and February 23-24, 2004. On July 3, 2003, the sunspots were at the center of the Sun. Three sets of scans were taken on July 3, each set encompassing a different area of the active region. Two sets of scans of the same areas were taken on July 7. An additional set of scans was taken to determine plate scale, and other scans were taken to determine the Sun's rotation rate and to provide data for darks and flats. Data in July was taken in the umbra and penumbra of the large sunspot, a nearby small sunspot and for a cluster of small sunspots in AR 396. Data on the 7th was taken of three active regions, the large sunspot (375/396), the small sunspot, and the cluster. In February, the sunspots were just off solar center, and six scans were taken (in addition to plate scale, rotation rate and the darks and flats) of each of the three active regions (563,565,567).

The magnetic fields were determined by using this formula (Klaveren et al. 10)

$$\mathbf{B = e/4\pi cm_e\ [\Delta\lambda/\ (\lambda^2\ x\ g)]}$$

Where B is the magnetic field in gauss,
$E/4\pi cm_e$ is a value from quantum mechanics that equals 2.13 x 10^{12} [Put in the units.] at this wavelength
λ is the wavelength in Ångstroms
G is the Landè factor which is determined from quantum mechanics, in this instance to be 3
$\Delta\lambda$ is the separation in Angstroms between the pi and sigma components of the spectral line.

The formula simplifies then to:

$$B = 2.13 \times 10^{12}(\Delta\lambda/\lambda^2 g)$$

To solve for B, the two variables, λ^2 and $\Delta\lambda$, had to be determined**.**

We already know λ because it is 15,650 Angstroms (the observed wavelength at which the scans were taken); thus, we need to find $\Delta\lambda$. This is done by reducing and analyzing the images using a program designed by Dr. Marcel Bergman. After the images were taken at Kitt Peak, the raw data was reduced (taking out the errors and background noise), which is done by subtracting the "dark" images (showing hot pixels from the instrument) and dividing (or normalizing) the data by the "flat" images. After the data is reduced, the spectra now show the Zeeman split lines clearly. The data set can be "rearranged" one step further into actual pictures of the sunspot, using a 'spectroheliogram' program. Spectroheliograms (SHG) are like snapshots of the sunspot at one wavelength, making use of the fact that the sunspot was scanned across in one spatial direction or dimension and that the slit on the instrument provided the second spatial dimension. After reducing and running the images through the spectroheliogram software, they are ready to be analyzed to determine $\Delta\lambda$

After the spectroheliogram files (SHG files) were opened, one SHG file was subtracted from the other, and the resulting image was displayed in a new window. A region was then selected to measure the magnetic field, usually in the center of the sunspot. A horizontal box was drawn on each image at the appropriate y-axis for the region, and then using "New Analysis Window" from the "Window" menu, a graphical spectrum was displayed, corresponding to the center of the sunspot. The set of three Zeeman lines was located in the spectrum. An x-axis pixel reading was taken for the left and center Zeeman lines. The pixel separation of the Zeeman split lines was therefore obtained. This measurement was converted into Angstroms from pixels and plugged into the formula for the magnetic field strength.

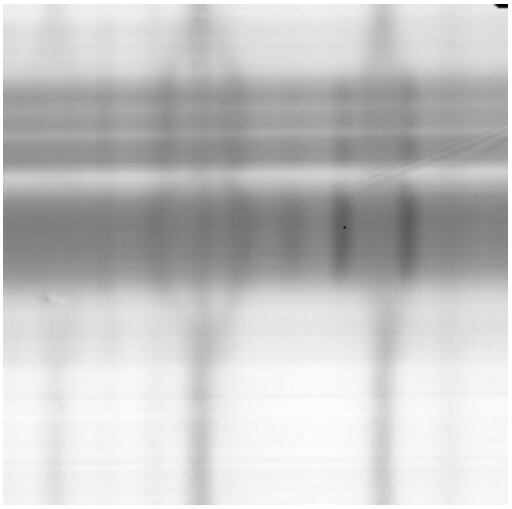

Fig. 3 Image of AR 375 Showing Zeeman Splitting

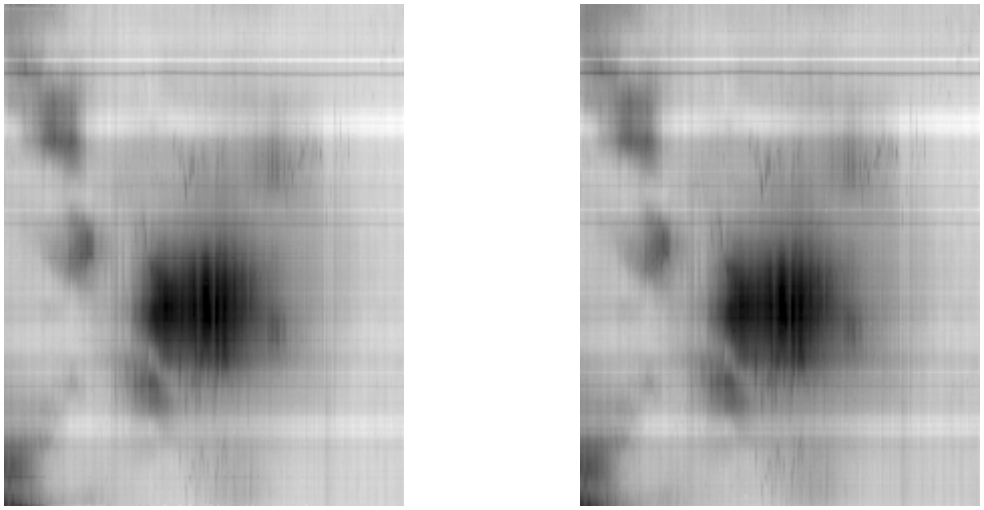

Fig. 4 001_200.67 & 001_200.167 SHG Images

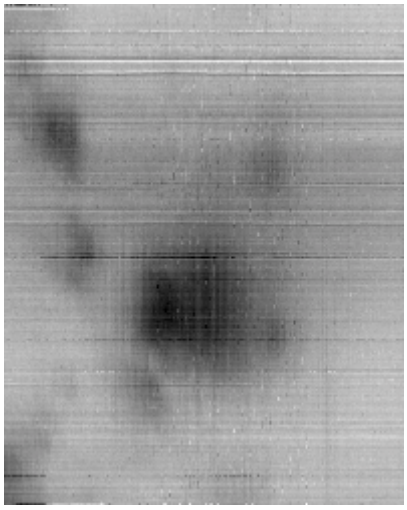

Fig. 5 Processed Image Of File 150.138 Minus File 150.154

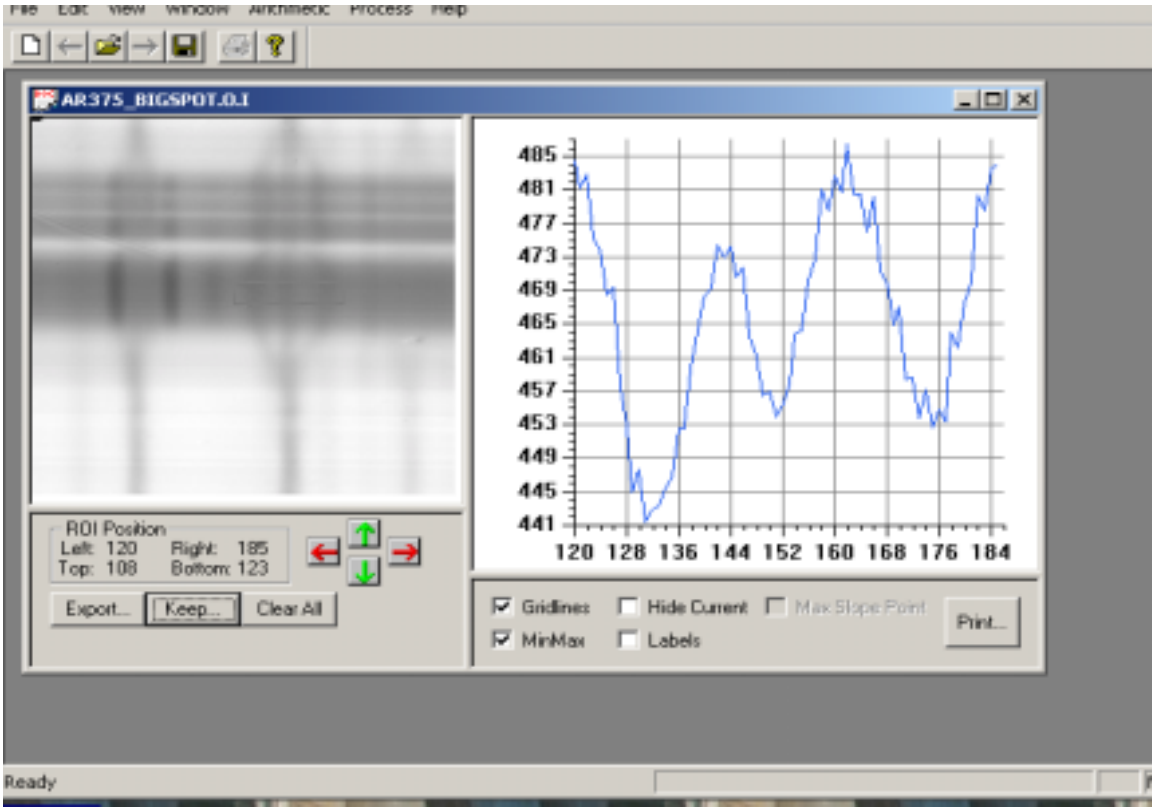

Fig. 6 Zeeman Split Line And Spectral Analysis Graph Using Kitt Peak Software Showing Peaks At 132, 151, And 175 From The Boxed Area

The value for "Δλ," was determined for 11 sunspots and the magnetic field in gauss was calculated for each sunspot. However, only sunspots of similar size (within 10%) can be compared, so the areas also had to be determined by doing a diameter on the SHG file and converting it to square kilometers. This was done by comparing the sun's diameter and pixel value, versus the sunspot's pixel value, and solving for the unknown factor, in this case, the sunspot's area in square kilometers. Unfortunately, not all sunspots are perfect circles. Because of this, the area for those sunspots was measured at the location of which the magnetic field strength was determined. In other words, magnetic field strength was calculated at the roundest portion of a sunspot, thus, the area was measured at that point. Thus, with area and magnetic field strength, the sunspots can be compared.

RESULTS

Eleven different sunspots for which the magnetic field strength could be determined were studied. Their size and magnetic field strength were calculated and plotted on the graphs shown below (Note, sunspots one through nine were taken from active region AR567 while sunspots ten and eleven were taken from AR 375).

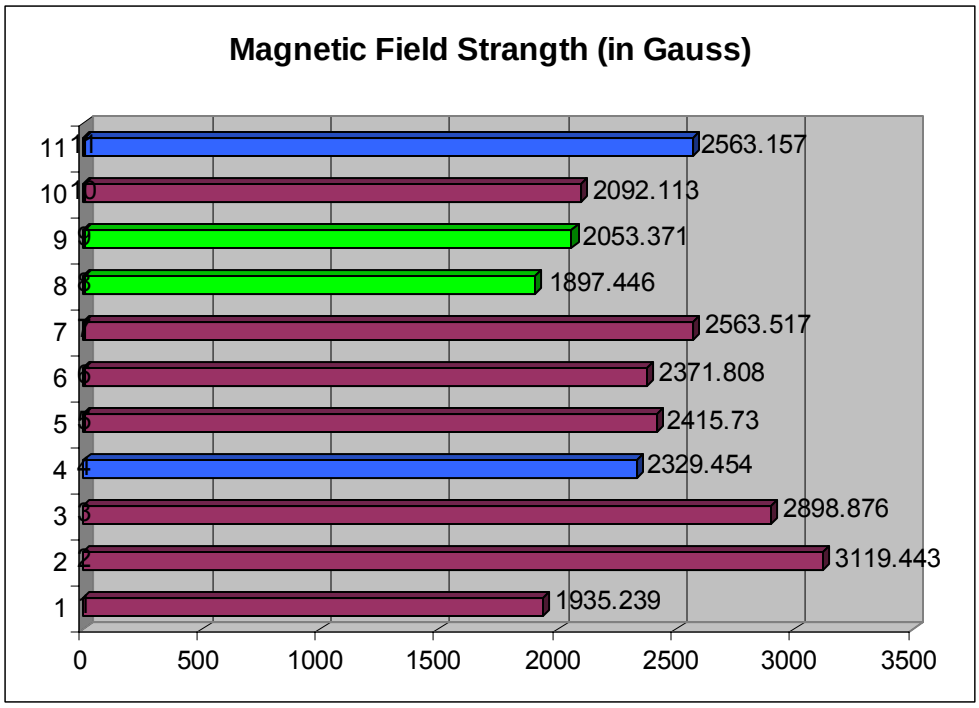

Graph 1
Sunspot Categorized Number Versus Magnetic Field Strength With Compared Sunspots (Size Within 10 Percent) In Blue And Green

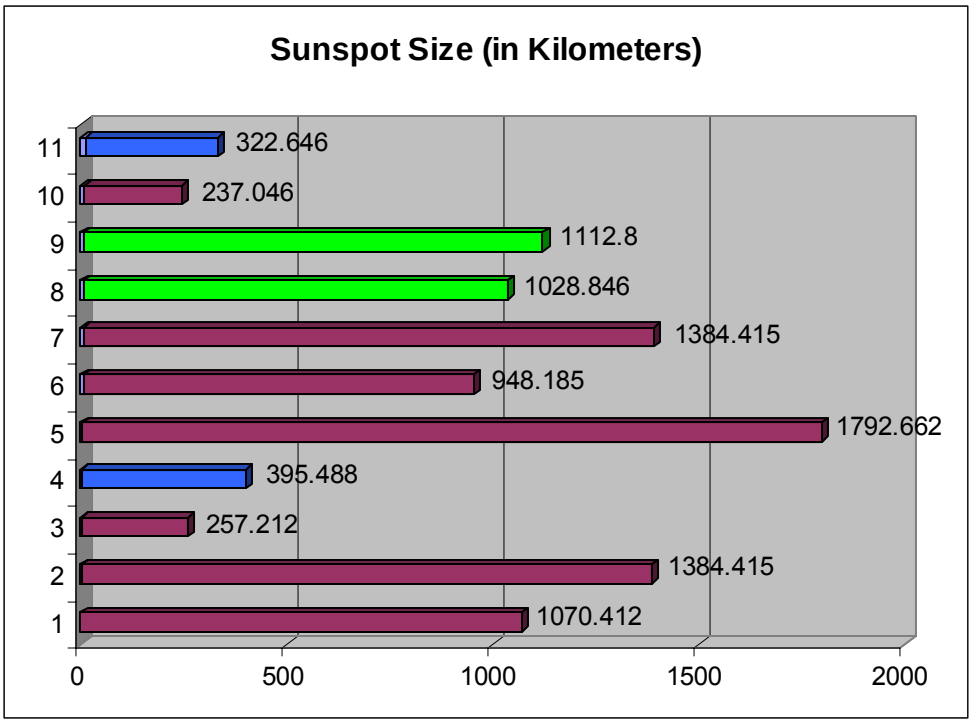

Graph 2
Sunspot Categorized Number Versus Size With Compared Sunspots (Size Within 10 Percent) In Blue And Green
Sunspots 11 and 9 are parts of clusters while sunspots 8 and 4 are lone sunspots.

CONCLUSION

Based on the processed data as seen in the final two graphs, the magnetic field strengths in sunspots of comparable size in clusters versus singled spots do not fluctuate. There are several possibilities why no relationship was seen. It is possible that the sunspots do not affect each other and their magnetic field strength is based on something other than their location in proximity to each other, such as their size or location on the sun. There could also be some unseen properties within sunspots we have not yet discovered that could account for not seeing a variation in magnetic field strength.

In addition, the methods used in analysis may have been flawed. Only a limited number of sunspots were available to be observed. If much more data were taken, the results might have been more accurate. Also, if the sunspots observed were more similar in size, more precise results could have been tabulated.

NEXT STEPS

This conclusion suggests several future studies of sunspots' magnetic field strengths. One would be to repeat the experiment in a different wavelength to see if the results are similar to what was found here. Another step would be to do archiving of data to find similarly sized sunspots and do comparison studies. Intense statistical techniques could also be employed to help determine a gauss-to-km^2 ratio in comparison of the sunspots. One step that is promising to consider would be the comparison of sunspots over the

twenty-two year magnetic cycle to determine if magnetic field strength varies with the cycle when comparing sunspots.

ACKNOWLEDGMENTS

NSF (National Science Foundation)
TLRBSE (Teacher Leaders in Research Based Science Education)
KPNO (Kitt Peak National Observatory)
Connie Walker Ph. D
Frank Hill Ph. D
Claude Plymate

REFERENCES

http://www.britannica.com/nobel/micro/653_3.html

Hathaway, Dr. David H. "The Photosphere." Solar Physics. 06 Jan. 2003.

http://science.nasa.gov/ssl/pad/solar/surface.html

"Magnetism-the Key to Understanding the Sun." Solar Physics.

http://science.nasa.gov/ssl/pad/solar/the key.html

Stern, Dr. David P. "Millennium of Geomagnetism." 31 Jan. 2003

http://www-spof.gsfc.nasa.gov/earthnag/mill_5.html

Avrett, Eugene H. Frontiers of Astrophysics. Cambridge: Harvard University Press, 1976.

Boozer, Christopher. Sunspots. Astrophysical and Planetary Sciences Department, University of Colorado Boulder. 12 May 2004 <http://www.genesismission.org/educate/kitchen/resource/factsheets/SunSpots>.

Brit, Robert Roy. "Sun On Fire, Releases 3 More Major Flares." Space.com. 3 Nov. 2003. 10 May 2004 <http://www.space.com/scienceastronomy/solar_flares_031103.html>.

Clark, Stuart. Towards the Edge of the Universe, A Review of Modern Cosmology. Praxis Publishing Co., 1999.

Geerts, B and E. Linacre. "Sunspots and Climate." Dec. 1997. 12 May 2004 <http://www-das.uwyo.edu/~geerts/cwx/notes/chap02/sunspots.html>.

Myers, Jim, Young, Diedre, Van Klavern, Karin, Stewart, Marty, Merriot, Ivy "Magnetic Field Variations across Solar Active Region AR 396." TLRBSE 2003 Cadre (21, April 2004): 1-13.

Philips, Tony. "A Twisted Tale of Sunspots." 29 Feb. 2000. 12 May 2004 <http://spacescience.com/headlines/y2000/ast29feb_1.htm>.

Plymate, Claude. Personal Interview. 23-24 Feb. 2004.
"Sunspots: Solar & Stellar Ball Lightning." 2004. 12 May 2004 <http://www.grandunification.com/hypertext/SunspotsSolarBallLightning.html>.

Wolff, Fraknoi Morrison. Voyager through the Universe. Saunders College Publishing, 2000.

Magnetic Field Variations Across Solar Active Region AR 396

Jim Myers, Warren Central High School, Bowling Green, KY – TLRBSE 2003
Ivy Merriot, Abaetern Academy, Bozeman, MT -- TLRBSE 2003
Marty Stuart, Bozeman High School, Bozeman, MT -- TLRBSE 2003
Karin van Klaveren, Golden West Middle School, Fairfield, CA – TLRBSE 2003
Diedre Young, Cornerstone Community Christian School, Kelso, WA – TLRBSE 2003

ABSTRACT

Zeeman splitting was measured in infrared images taken of sunspot AR 396 in July 2003 using the McMath-Pierce Solar Telescope at Kitt Peak to determine the magnetic field in the large sunspot, a small sunspot and in a cluster of small sunspots. This was done to determine if the size of a sunspot is an indicator of the strength of the magnetic field. A sunspot is an area where strong magnetic fields break through the sun's photosphere, or "surface". The magnetic turbulence of these fields creates cooler and thus darker areas on the photosphere. Sunspots may vary in duration from hours to months and may be as large as 50,000 km in diameter. The number of sunspots is directly related to solar radiation output which affects terrestrial temperatures.

BACKGROUND

The magnetic field of a sunspot can be 5,000 times that of the earth's magnetic field and several hundred times that of the surrounding solar area. It is believed that the differential rotation of the solar surface create eddy currents of charged particles in the solar plasma. This acceleration of charged particles creates magnetic fields and the magnetic field lines eventually "knot" and cause the magnetic eruptions that are seen as sunspots. Studies in helioseismology suggest that differential rotation is not limited to the sun's surface but also extends into its interior.[1] The magnetic fields erupt through the solar surface looping from one location to another. The magnetic field loops may extend far into the solar atmosphere with great influence on charged particles at various heights above the sun's surface creating active regions.

Observing the sun in different wavelengths of light shows that sunspots are related to active regions of the solar atmosphere and to coronal holes. It is from coronal holes that coronal mass ejections that cause polar auroras and solar storms, with their associated disruptions, on earth to occur. Sunspots are often predictors of these CME's. It is known that the size of the active region is proportional to the size of the sunspot. A study comparing the magnetic field strength using Zeeman splitting in the sunspot to its size may be beneficial in corroborating this.

The Zeeman Effect is the splitting of a spectral line into two or more components of different wavelength when a radiation source is subjected to a magnetic field. It was first observed in 1896 by the Dutch physicist Pieter Zeeman, who won the 1902 Nobel Prize for Physics. Hendrik Lorentz had earlier hypothesized that the vibrations of electrons inside an atom produce light and that a magnetic field would affect these vibrations and thus the wavelength of the light emitted. This theory was confirmed by Zeeman and later by quantum mechanics, according to which spectral lines of light are emitted when electrons change from one discrete energy level to another. Each of the levels is split in a

magnetic field into sublevels of equal energy. These sublevels of energy are revealed by the split spectral line components.[2]

RESEARCH PROBLEM

We can infer the presence of magnetic fields if we observe Zeeman splitting in the spectrum, and we can measure the strength of the field by measuring quantitatively the amount of Zeeman splitting. The distance of the splitting from the original spectral line is proportional to the magnetic force causing that splitting**.** This project investigates whether or not the size of the sunspot is determined by the intensity of the magnetic field.

PROCEDURE

This study was done by scanning AR 396 in infrared light and measuring the Zeeman splitting of the iron spectral line at 15650 A. Images were taken from the McMath-Peirce solar telescope at Kitt Peak on July 3 and July 7, 2003. On July 3, 2003, the sunspot was at the center of the Sun. Three sets of scans were taken on July 3, each set encompassing a different area of the active region. Two sets of scans of the same areas were taken on July 7th. An additional set of scans was taken to determine plate scale and other scans were taken to determine the Sun's rotation rate and to provide data for darks and flats. Data was taken in the umbra and penumbra of the large sunspot, a near by small sunspot and for a cluster of small sunspots in AR 396. Data on the 7th was taken of three active regions, the large sunspot (375/396), the small sunspot and the cluster. This data is available on the TLRBSE CD ROM "TLRBSE Solar Data" Version 1.0b July 2003.

The magnetic fields were determined by using the formula

$$B = e/4\pi cm_e \, [\Delta\lambda / (\lambda^2 \times g)]$$

where B is the magnetic field in gauss,
$e/4\pi cm_e$ is a value from quantum mechanics that equals 2.13×10^{12} at this wavelength
λ is the wavelength in angstroms,
and g is the Lande factor which is determined from quantum mechanics, in this instance to be 3.

The formula simplifies then to

$$B = 2.13 \times 10^{12}(\Delta\lambda/\lambda^2 g)$$

To solve for B, the two variables, $\lambda 2$ and $\Delta\lambda$, had to be determined. Thus, the images were analyzed to determine λ, from which we could calculate $\lambda 2$, and to determine $\Delta\lambda$ in each sunspot region that was studied. A spreadsheet template was developed to analyze and compile the data from several slices of the active area. The research team was divided into two teams at this point, one team gathered data from the images while the other team developed a spreadsheet and input data.

A spreadsheet template was developed so that the only variable was Δλ in pixels. This was done by rewriting the equation to

$$B = \frac{\Delta\lambda}{\left(4.69\text{x}\ 10^{-13}\right)\left(\lambda^2 g\right)}$$

where 4.69 x 10^{-13} is the reciprocal of 2.13 x 10^{12}.

When the number of pixels representing Δλ was determined it was entered into the spreadsheet. By multiplying Δλ by the plate scale, Δλ in angstroms was determined. This value is then divided by the quotient of g, λ^2, and 4.69 x 10^{-13} to calculate the value of B at each value of λ.

SPREADSHEET TEMPLATE

B value	λ^2	Δλ in pixel	plate scale	Δλ in Angstroms	J	g	yvalue
0.0000E+00	2.441E+08		0.04961	0	4.69E-13	3	
0.0000E+00	2.441E+08		0.04961	0	4.69E-13	3	
0.0000E+00	2.441E+08		0.04961	0	4.69E-13	3	
0.0000E+00	2.441E+08		0.04961	0	4.69E-13	3	
0.0000E+00	2.441E+08		0.04961	0	4.69E-13	3	
0.0000E+00	2.441E+08		0.04961	0	4.69E-13	3	
0.0000E+00	2.441E+08		0.04961	0	4.69E-13	3	
0.0000E+00	2.441E+08		0.04961	0	4.69E-13	3	
0.0000E+00	2.441E+08		0.04961	0	4.69E-13	3	
0.0000E+00	2.441E+08		0.04961	0	4.69E-13	3	
0.0000E+00	2.441E+08		0.04961	0	4.69E-13	3	
0.0000E+00	2.441E+08		0.04961	0	4.69E-13	3	
0.0000E+00	2.441E+08		0.04961	0	4.69E-13	3	
0.0000E+00	2.441E+08		0.04961	0	4.69E-13	3	
0.0000E+00	2.441E+08		0.04961	0	4.69E-13	3	

Heliograph images were processed using Kitt Peak image processing software to determine the Zeeman splitting at appropriate slices. These were the umbra, the penumbra and umbra/penumbra edge. The sunspots were designated for purposes of this study as "the big sunspot" (375/396), "sunspot #1", "sunspot #2", "the small sunspot", and "group D".

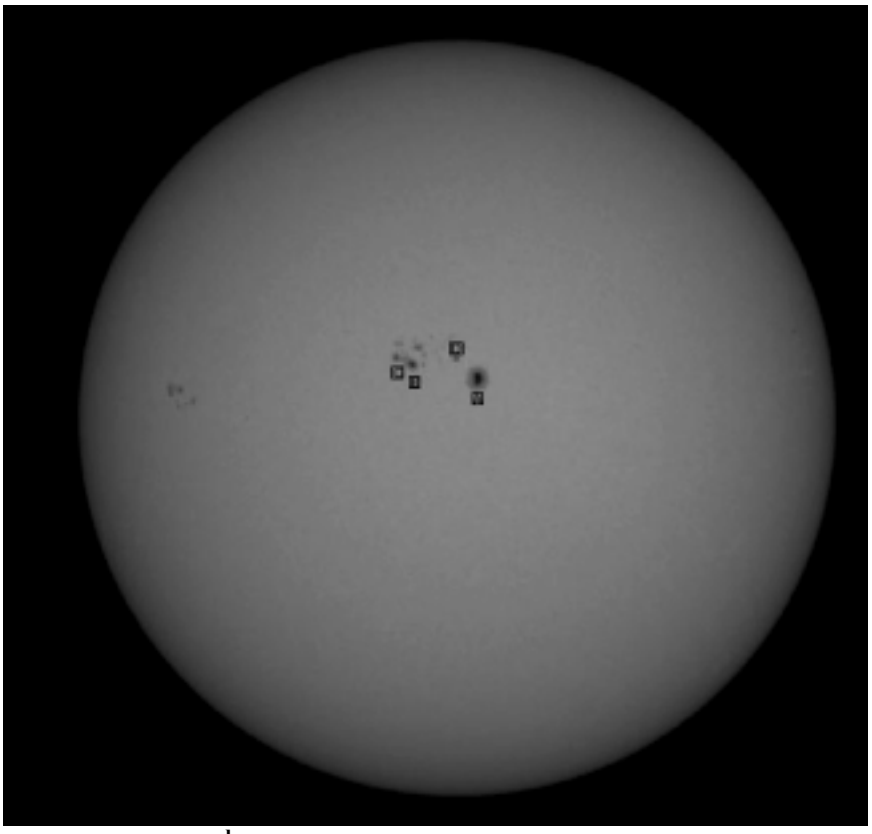

The Sun On July 3rd Showing The Location Of The Targeted Sunspots

First the plate scale was determined. The spectral lines were determined from the spectral atlas, "Sunspot Umbral Spectra in the Region 400 to 8640 cm^{-1} (1.16 to 2.50 μm)" to be 15653.0A and 15648.5A. Then by using the software to count the pixels from the iron spectral line at 15653.0A to the spectral line at 15648.5A the pixel distance between them was determined. Dividing spectral distance of 4.5 angstroms by the pixel separation of 91 gives us a plate scale of 0.049 angstroms/pixel. The pixel distance between the two iron spectral lines was determined by the software which reads the x and y coordinates as the cursor moves from the center of one line to the center of the opposite line.

The magnetic field was determined by measuring the pixel distance between the two Zeeman split lines and dividing by two to get an average from the center line. It was agreed by the researchers that this would be more accurate than measuring only one side of the Zeeman split.

To determine Δλ, an image was opened using Kitt Peak image processing software. (Image J will also work as may other IP software). A reduced file was opened and the set of three Zeeman lines was located. An x-axis pixel reading was taken for the left and center Zeeman lines and corresponding spectroheliographs (SHG files) were opened. (Step-by-step procedure is available.) Using the image processing software one SHG file was subtracted from the other and the resulting image was displayed in a new window. Regions were then selected to measure the magnetic field. These regions were outside the sunspot, through the center of the penumbra, the center of umbra, and the corresponding regions on the opposite side of the sunspot. A horizontal box was drawn on each image at the appropriate y-axis for each region, and then using "New Analysis Window" from the "Window" menu a graphical spectral analysis was displayed. Using these graphical representations, the pixel separation of the Zeeman split lines was obtained. This became **"Δλ" on the spreadsheet and the magnetic field in gauss was calculated.**

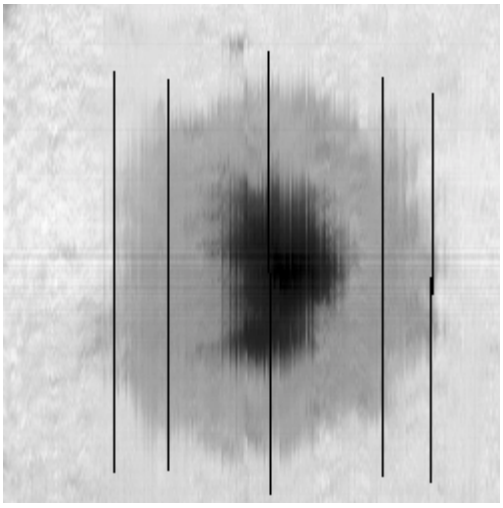

AR 396 Showing Where Regions Were Selected For Zeeman Split Readings

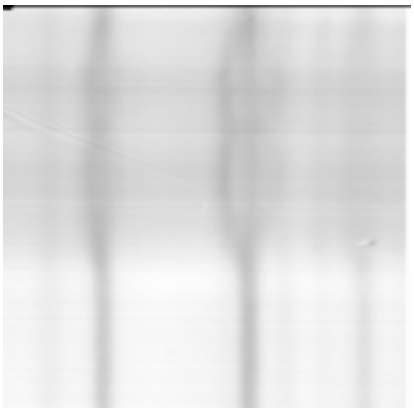

Image Of AR 396 Showing Zeeman Splitting

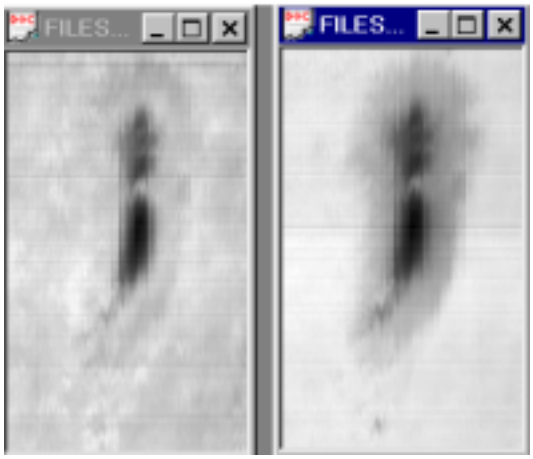

001_150.138 & 001_150.154 Shg Images

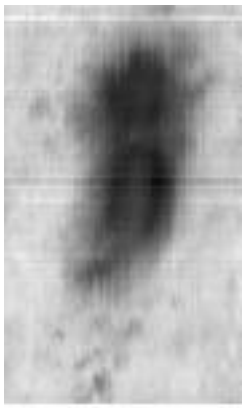

Processed Image Of File 150.138 Minus File 150.154

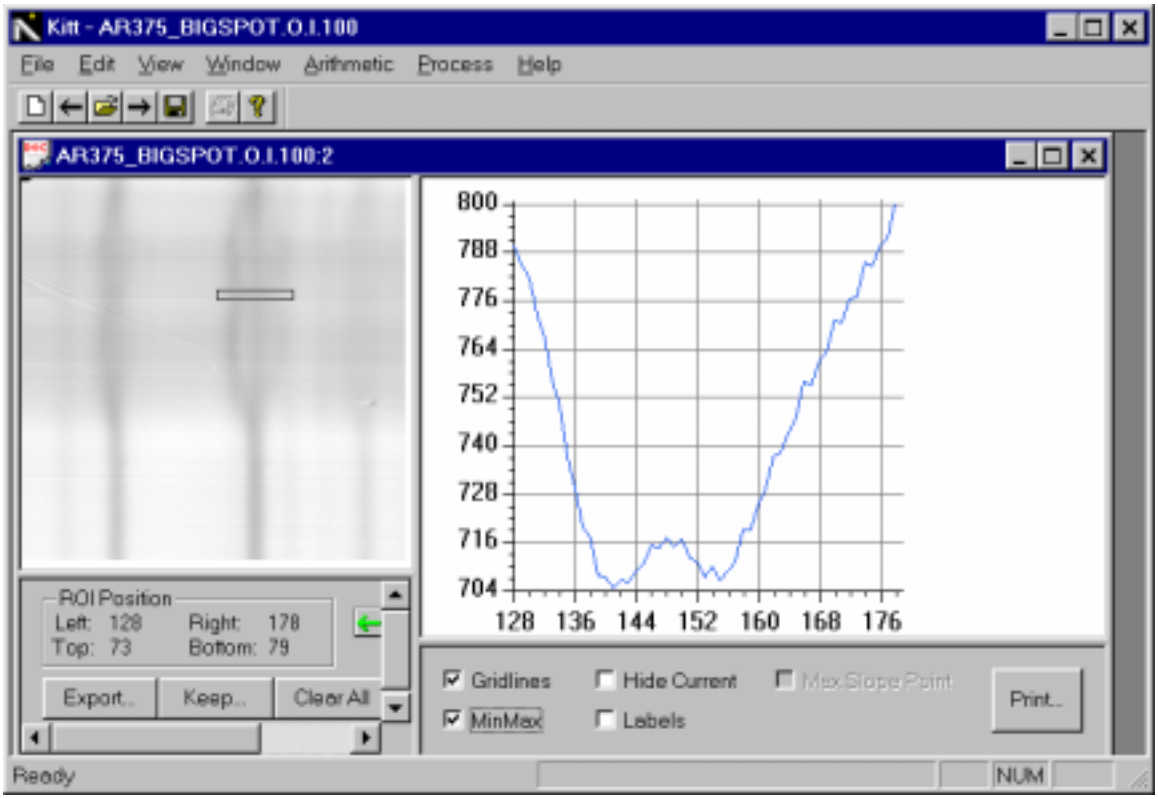

Zeeman Split Line And Spectral Analysis Graph Using KP Software Showing Peaks At 141 And 155 From The Boxed Area

RESULTS

After the magnetic field across each slice was computed a composite spreadsheet and graph for each sunspot was compiled. The values on the spreadsheets are of the magnetic fields in gauss of each slice at the y-axis location. The plate scale of the heliograph also indicates that each pixel represents 278 kilometers across the sun's surface. By subtracting the initial km reading from the final reading, the diameter of the sunspot along the y-coordinate may be obtained. The graphs give visual interpretations of magnetic field strength while the spreadsheet data yield digital information of a more exact nature. All the graphs are multi-line graphs of the values from the several slices of each sunspot to show the magnetic field variation at each slice. The line with the highest value in each graph includes error bars of 145 gauss which represents + or – one pixel on the heliographs. While great effort was exerted in reading the heliographs and spectroheliographs, it should be understood that each datum point may be ± 145 gauss which the researchers deem as reasonable human error.

SMALL SUNSPOT

y-axis	Km	Slice #36	Slice #107	Slice #152	Slice #164	Slice #176
91	25298	6.500E+02	0.000E+00	0.000E+00	5.778E+02	0.000E+00
106	29468	5.077E+02	1.011E+03	5.778E+02	8.666E+02	1.015E+03
114	31692	6.528E+02	1.156E+03	6.500E+02	5.778E+02	1.160E+03
123	34194	6.528E+02	1.733E+03	6.500E+02	7.944E+02	1.741E+03
127	35306	7.978E+02	1.878E+03	1.589E+03	6.500E+02	1.886E+03
133	36974	7.978E+02	2.528E+03	2.022E+03	7.944E+02	2.539E+03
140	38920	7.978E+02	2.311E+03	2.239E+03	6.500E+02	2.321E+03
146	40588	7.978E+02	2.528E+03	2.311E+03	5.778E+02	2.539E+03
153	42534	7.978E+02	2.094E+03	2.455E+03	7.222E+02	2.103E+03
169	46982	7.978E+02	1.950E+03	2.022E+03	6.500E+02	1.958E+03
175	48650	7.978E+02	1.228E+03	6.500E+02	6.500E+02	1.233E+03
178	49484	7.978E+02	6.500E+02	6.500E+02	6.500E+02	6.528E+02
181	50318	4.352E+02	5.778E+02	5.055E+02	5.778E+02	5.802E+02
184	51152	5.077E+02	4.333E+02	5.055E+02	5.778E+02	4.352E+02
		0.000E+00	0.000E+00	4.333E+02	6.500E+02	0.000E+00

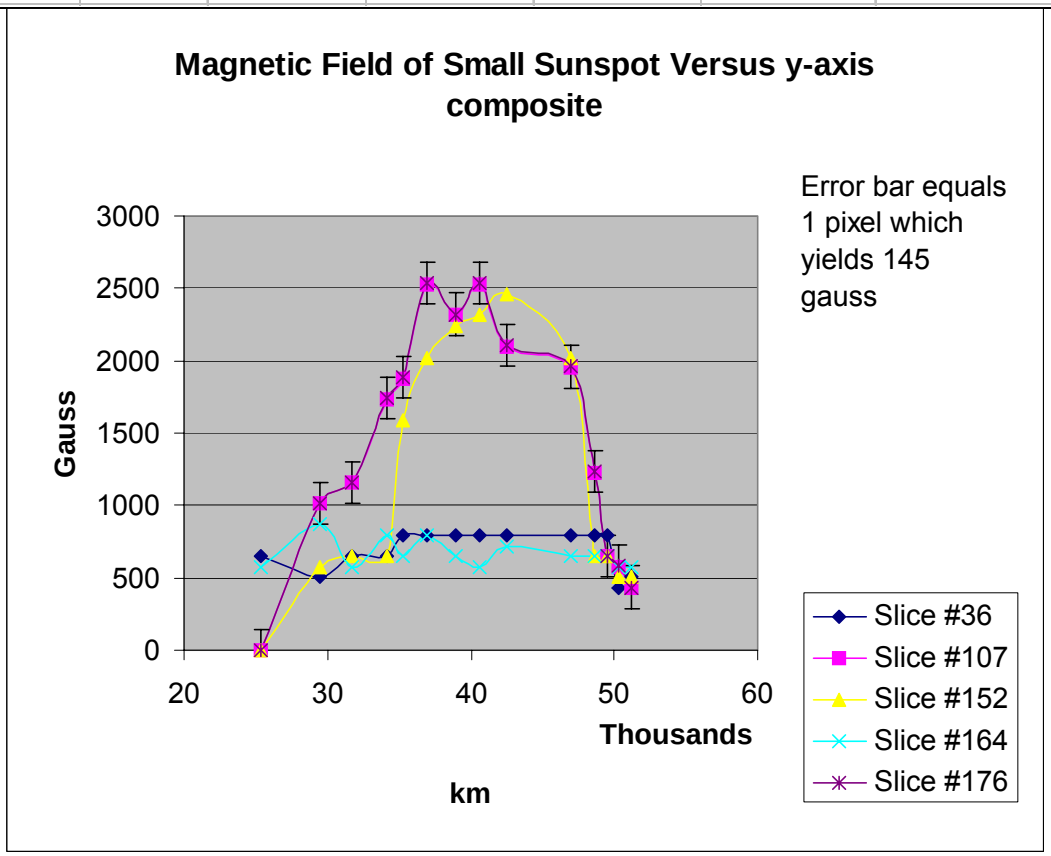

SUNSPOT #1

y-value	km	B value Slice #50	B value Slice #65	B-value Slice #80	B-Value Slice #83
91	25298	5.8024E+02	0.0000E+00	5.8024E+02	7.2221E+02
106	29468	6.5277E+02	2.9012E+02	6.5277E+02	7.2221E+02
114	31692	7.2530E+02	9.4289E+02	5.8024E+02	9.3887E+02
123	34194	1.0879E+03	1.8132E+03	5.8024E+02	9.3887E+02
127	35306	1.7407E+03	1.3781E+03	5.8024E+02	1.3722E+03
133	36974	2.0308E+03	2.4660E+03	6.5277E+02	1.5889E+03
140	38920	2.0308E+03	2.1759E+03	8.7036E+02	1.7333E+03
146	40588	2.0308E+03	2.3935E+03	1.9583E+03	2.3111E+03
153	42534	1.8132E+03	2.1759E+03	2.0308E+03	2.3833E+03
169	46982	1.4506E+03	1.8132E+03	7.9783E+02	1.0111E+03
175	48650	5.0771E+02	1.4506E+03	7.9783E+02	6.4998E+02
178	49484	5.8024E+02	1.6682E+03	7.9783E+02	3.6110E+02
181	50318	5.8024E+02	1.4506E+03	1.3781E+03	3.6110E+02
184	51152	5.8024E+02	7.9783E+02	1.2330E+03	3.6110E+02
				7.9783E+02	
				5.8024E+02	

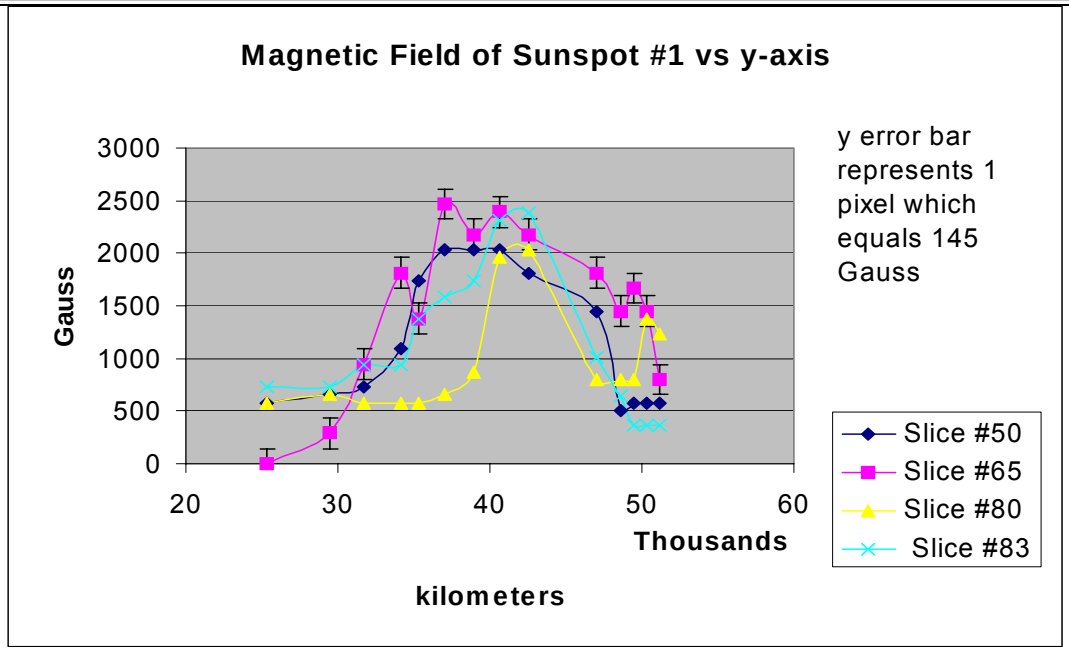

SUNSPOT #2

y-axis	km	Scan # 157	Scan #206	Scan # 218	Scan #227
66	18348	6.4998E+02	3.6110E+02	7.2221E+02	5.7776E+02
72	20016	6.4998E+02	1.0833E+03	7.9443E+02	5.7776E+02
80	22240	8.6665E+02	1.1555E+03	1.0833E+03	5.0554E+02
86	23908	9.3887E+02	1.7333E+03	1.3722E+03	6.4998E+02
91	25298	9.3887E+02	2.1666E+03	1.5166E+03	6.4998E+02
96	26688	1.5889E+03	2.3111E+03	1.8777E+03	6.4998E+02
103	28634	1.6611E+03	2.3111E+03	2.5277E+03	9.3887E+02
109	30302	1.8055E+03	2.3111E+03	1.2277E+03	9.3887E+02
114	31692	2.0944E+03	2.1666E+03	1.0111E+03	7.2221E+02
120	33360	2.0944E+03	1.3722E+03	7.9443E+02	7.2221E+02
125	34750	2.0222E+03	1.3000E+03	7.9443E+02	7.2221E+02
127	35306	1.9500E+03	3.6110E+02	7.2221E+02	5.7776E+02
131	36418	1.8055E+03	3.6110E+02	7.2221E+02	5.7776E+02
138	38364	1.3722E+03	3.6110E+02	5.7776E+02	5.7776E+02
148	41144	7.2221E+02	3.6110E+02	3.6110E+02	5.7776E+02

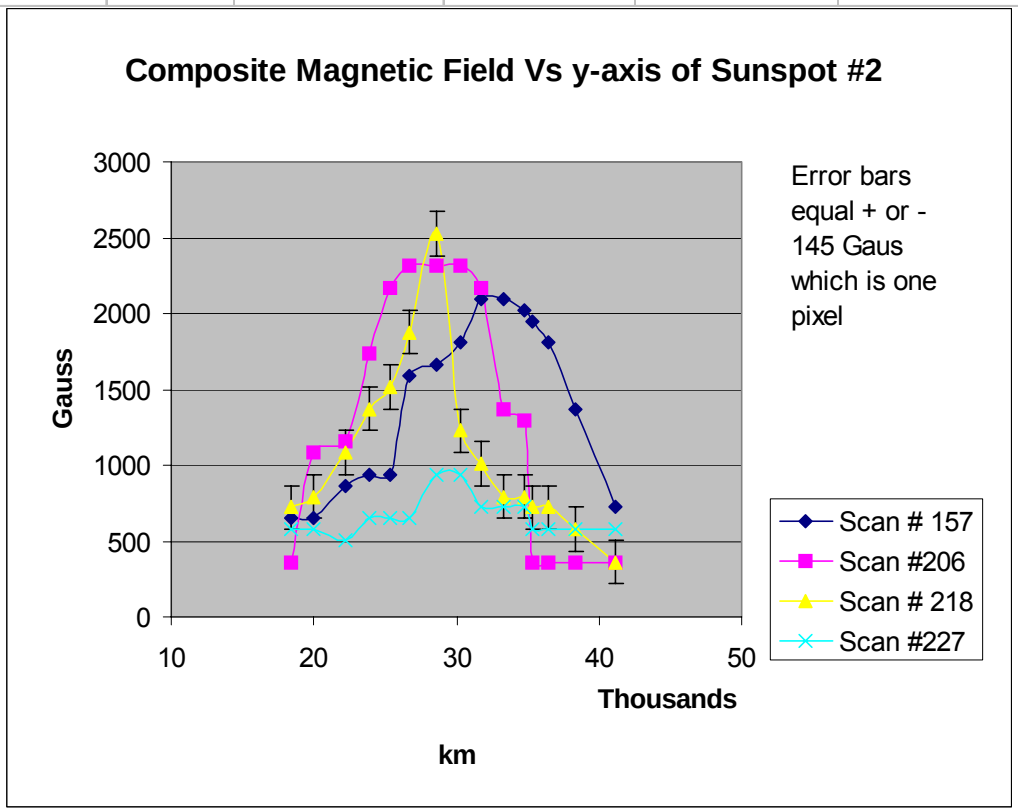

BIG SUNSPOT "A"

	B value	B-Value	B value	B value	B value	y-axis value
km	#55	#144	# 170	# 194	#220	
2505	5.055E+02	5.778E+02	5.0554E+02	4.3332E+02	4.333E+02	9
8073	5.055E+02	5.778E+02	5.7776E+02	5.7776E+02	4.333E+02	29
11136	5.055E+02	5.778E+02	1.0111E+03	5.0554E+02	4.333E+02	40
14198	5.055E+02	5.778E+02	1.7333E+03	5.0554E+02	4.333E+02	51
17260	5.055E+02	1.156E+03	1.7333E+03	7.2221E+02	5.055E+02	62
20601	5.055E+02	1.589E+03	1.8777E+03	1.3000E+03	5.055E+02	74
26447	6.500E+02	1.878E+03	2.5999E+03	1.7333E+03	5.055E+02	95
32293	5.778E+02	1.300E+03	3.0333E+03	1.7333E+03	5.778E+02	116
38139	4.333E+02	1.011E+03	2.7444E+03	1.5889E+03	5.778E+02	137
43985	4.333E+02	5.055E+02	2.3111E+03	1.5889E+03	5.778E+02	158
47604	5.778E+02	3.611E+02	2.4555E+03	1.3000E+03	5.055E+02	171
50945	4.333E+02	3.611E+02	1.4444E+03	8.6665E+02	5.055E+02	183
54286	4.333E+02	3.611E+02	1.0111E+03	5.0554E+02	5.778E+02	195
57626	4.333E+02	3.611E+02	5.0554E+02	5.7776E+02	5.778E+02	207
64864	4.333E+02	3.611E+02	5.0554E+02	4.3332E+02	5.055E+02	233

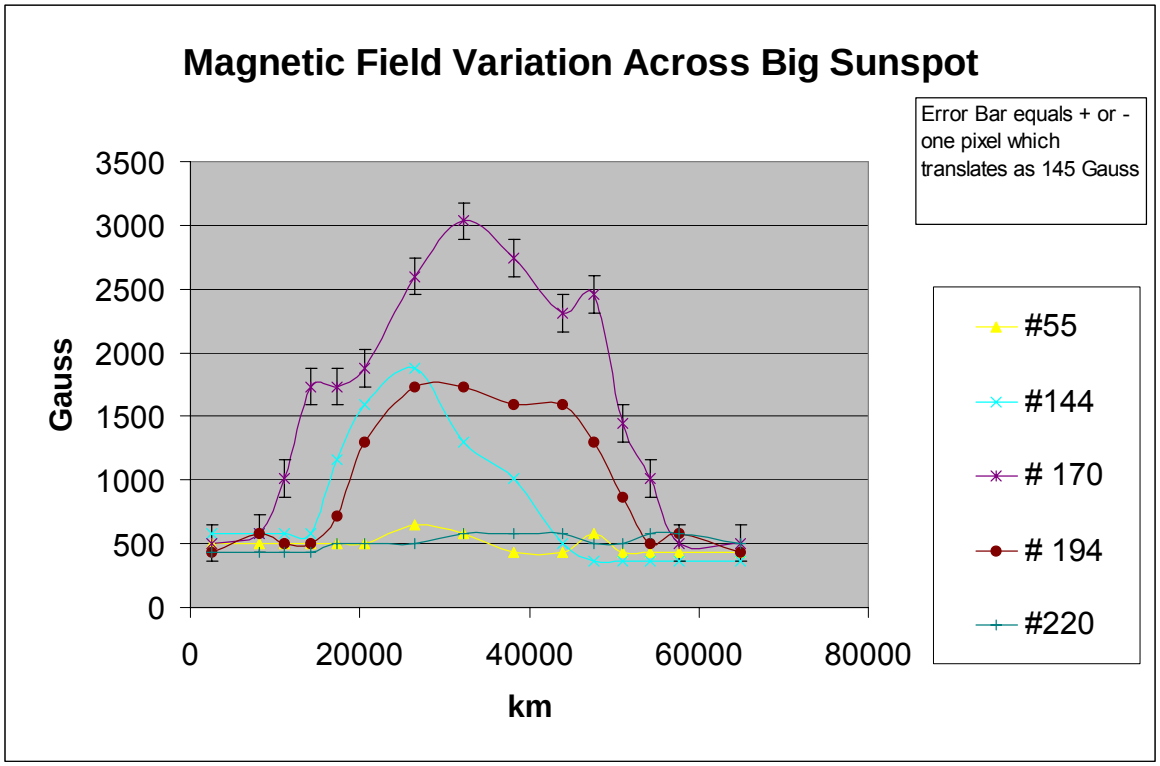

SUNSPOT GROUP D

y-axis	km	B value (Gaus
91	22568	0.0000E+00
106	26288	2.8888E+02
114	28272	1.0833E+03
123	30504	1.8055E+03
127	31496	1.3722E+03
133	32984	2.4555E+03
140	34720	2.1666E+03
146	36208	2.5277E+03
153	37944	2.1666E+03
169	41912	1.8055E+03
175	43400	1.4444E+03
178	44144	1.5166E+03
181	44888	1.4444E+03
184	45632	7.9443E+02

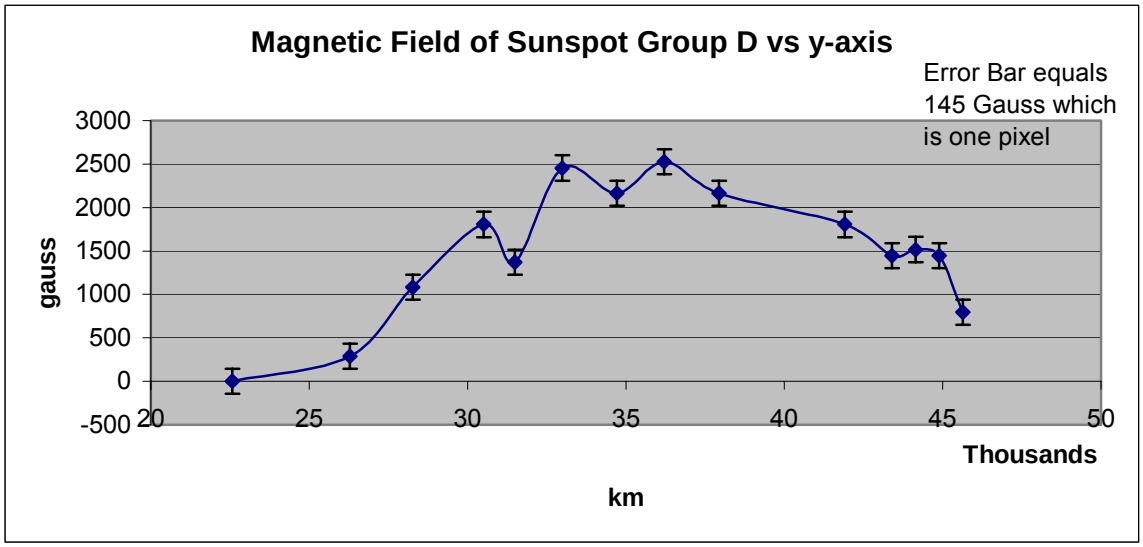

CONCLUSIONS

The graphs show, and the spreadsheets support the notation that the magnetic field strength varies across all the sunspots, increasing from the photosphere to the center of the umbra. This variation is similar in large and small sunspots, and in the diffuse sunspot cluster of Group D.

The strength of the magnetic field increases from the photosphere to a maximum of slightly more than 2500 gauss in the small sunspots and the sunspot cluster and to a maximum of 3033 gauss in the large sunspot. This is more than 17% greater intensity of magnetic field strength.

Measured along the y-axis the smallest sunspot had a diameter of 23,000 kilometers and a maximum B-value of 2528 gauss. The other two sunspots of slightly greater diameters had maximum B-values of equal or slightly less (2466 gauss or 2½ %) intensities. The

large sunspot was more than 2½ times larger with a y-axis diameter of 62,500 kilometers. Since sunspots are not symmetric this is only indicative, but not definitive of the size of the sunspots in the study.

The intensity of the magnetic field does increase in the much larger sunspot but the variation of intensity in sunspots of similar size is inconclusive.

NEXT STEPS

This study suggests several future studies of sunspots' magnetic field. One would be to repeat the experiment in a different wavelength to see if the additional Zeeman split would yield similar values. Since various wavelengths "see" at different depths of the photosphere this would measure magnetic intensity in a vertical direction relative to the sun's surface.

Another study would repeat this experiment in the infrared but to accurately measure the area of the several sunspots to determine a more precise correlation between magnetic intensity and sunspot size. Intense statistical techniques could also be employed to help determine a gauss-to-km^2 ratio.

A study of the magnetic field strength versus the area of the active region in different wavelengths could add to the understanding of the structure of sunspots.

Finally, some "penumbra only" sunspots were found between two "full" sunspots in the "group D cluster". Are these precursors to full sunspots or disruptors between the two companion sunspots?

ACKNOWLEDGEMENT

The researchers would like to acknowledge the National Science Foundation which funded the Teacher Leaders Research Based Science Education project that allowed us to do this research at Kitt Peak. We would also like to acknowledge Connie Walker, Ph.D., Steven Croft, Ph.D., and Stephen Pompea, Ph.D. of the NOAO staff who guided the researchers through the research process. Special thanks and acknowledgement must be given to Claude Plymate and Christoph Keller for operating the McMath-Pierce Solar Telescope on July 3 and July 7.

References

Frank Hill (private communication)

Harry Jones (private communication)

http://www.britannica.com/nobel/micro/653_3.html

A Comparison of the Peak Brightness of Novae to Their Lifespan in the Andromeda Galaxy

Joseph Moore, Katie Boyd, Elisa Woods
Graves County High School, Mayfield, KY
Teacher: Velvet Dowdy, TLRBSE 2003

ABSTRACT

Using images of the Andromeda Galaxy taken at Kitt Peak National Observatory in Arizona, novae in all parts of the galaxy from the past 7 years were analyzed to determine if there is a correlation between the peak brightness of novae and their average lifespan. Out of the total 86 novae found using Scion Image, only 29 were used because all others only appeared in one epoch. Because of the appearance of some novae in only one epoch, there was no way to calculate their lifespan. A correlation, although weak, was found between the peak brightness and lifespan. A nova with a lower initial magnitude does usually have a longer lifespan.

INTRODUCTION

Novae are studied to learn more about the life cycle of stars, particularly white dwarfs. They usually occur in a binary star system. A binary star system consists of two stars that orbit around a common point, called the center of mass (Binary Stars, WWW, 2004). A nova is a faint star that rapidly becomes much brighter, sometimes 10,000 times more intense, and then fades over an extended period of time (Adkins, D., et al, 2003). It is possible for a white dwarf to pull gas from a companion star. Because of the hydrogen build up on the surface of the star, it collapses, heats up, the core ignites and blows off its outer layer of materials, which causes an explosion (Content Background for Nova Research, Rector, T., et al, 2001). As the hydrogen is burned up the nova will fade again. The nova will ultimately reach the end of its life cycle as a star when it becomes white dwarf (Adkins, D., et al, 2003). In another research project, although the students found that the light curves of novae with lower magnitudes decreased more rapidly, they did not compare the magnitudes to the actual lifespans (Camacho, L., et al, 2001).

RESEARCH QUESTION

Is there a correlation between the peak brightness of novae in the Andromeda galaxy and their respective lifespans? From the research presented, our group believes that a nova with a higher initial brightness will have a longer lifespan.

METHODS

Pictures of Andromeda taken by professional astronomers at Kitt Peak National Observatory through the 0.9m telescope were made available through the TLRBSE CD-ROM. Also on this CD was Scion Image, provided by NOAO, which we used to find the novae and measure their magnitude. Because the Andromeda Galaxy is so large, the pictures of the galaxy are divided into 16 subrasters in order to more thoroughly analyze the galaxy. Each observation and subsequent picture of the galaxy is called an epoch. Using Scion Image, we stacked, then blinked every epoch (Cosmic Easter Eggs, Rector, T., et al, 2001) for each subraster to find novae, upon which we used constant stars with previously known magnitudes to compare with the novae and find their magnitude.

Once a nova was found, the subraster in which it appears, along with its magnitude in each epoch in which it appears, and the X and Y coordinates were saved. Then, for each nova, to find the lifespan, this group used the recorded date of the epoch in which the nova first and last appeared to find the total difference in days.

Using Vernier's Graphical Analysis 3.1, each nova's magnitude was plotted against its respective lifespan (provided it appeared in more than one epoch). Then, using a linear regression to find a line of best fit, a finite ratio to the otherwise weak correlation between brightness and lifespan was found.

RESULTS

Nova #	Subraster	X	Y	Magnitude	Lifespan (Days)
1	16	80	182	16.57	43.84
2	16	315	257	15.22	50.69
3	15	171	472	15.01	143.84
4	15	220	360	15.35	89.03
5	15	358	44	16.43	83.43
6	15	59	205	18.38	50.69
7	14	53	471	17.06	27
8	11	298	268	17.04	66.09
9	11	364	405	16.79	105.08
10	11	201	127	15.76	118.11
11	11	405	177	18.66	43.84
12	10	195	347	15.63	235.2
13	10	220	42	15.42	25.63
14	10	470	288	17.11	214.9
15	10	458	88	16.67	92.09
16	7	112	93	17.39	105.08
17	7	411	499	15.98	108.97
18	7	228	473	15.73	81.93
19	7	73	431	16.86	112.92
20	7	437	485	16.19	36.07
21	7	76	350	20.83	19.92
22	7	233	494	16.7	57.69
23	6	119	440	16.4	33.03
24	6	75	350	16.8	235.2
25	6	179	209	17.4	25.63
26	6	43	10	17.4	152.81
27	6	232	494	16.7	112.92
28	6	142	473	17.19	23.88
29	6	184	423	18.57	10.14

29 out of 86 novae used because all others only appeared in one epoch

This table shows each nova, the subraster in which it appeared, its X and Y coordinates, and its lifespan in days (hour and minute measures were converted to decimals). This table made it much easier to import the data into Vernier's Graphical Analysis to be plotted.

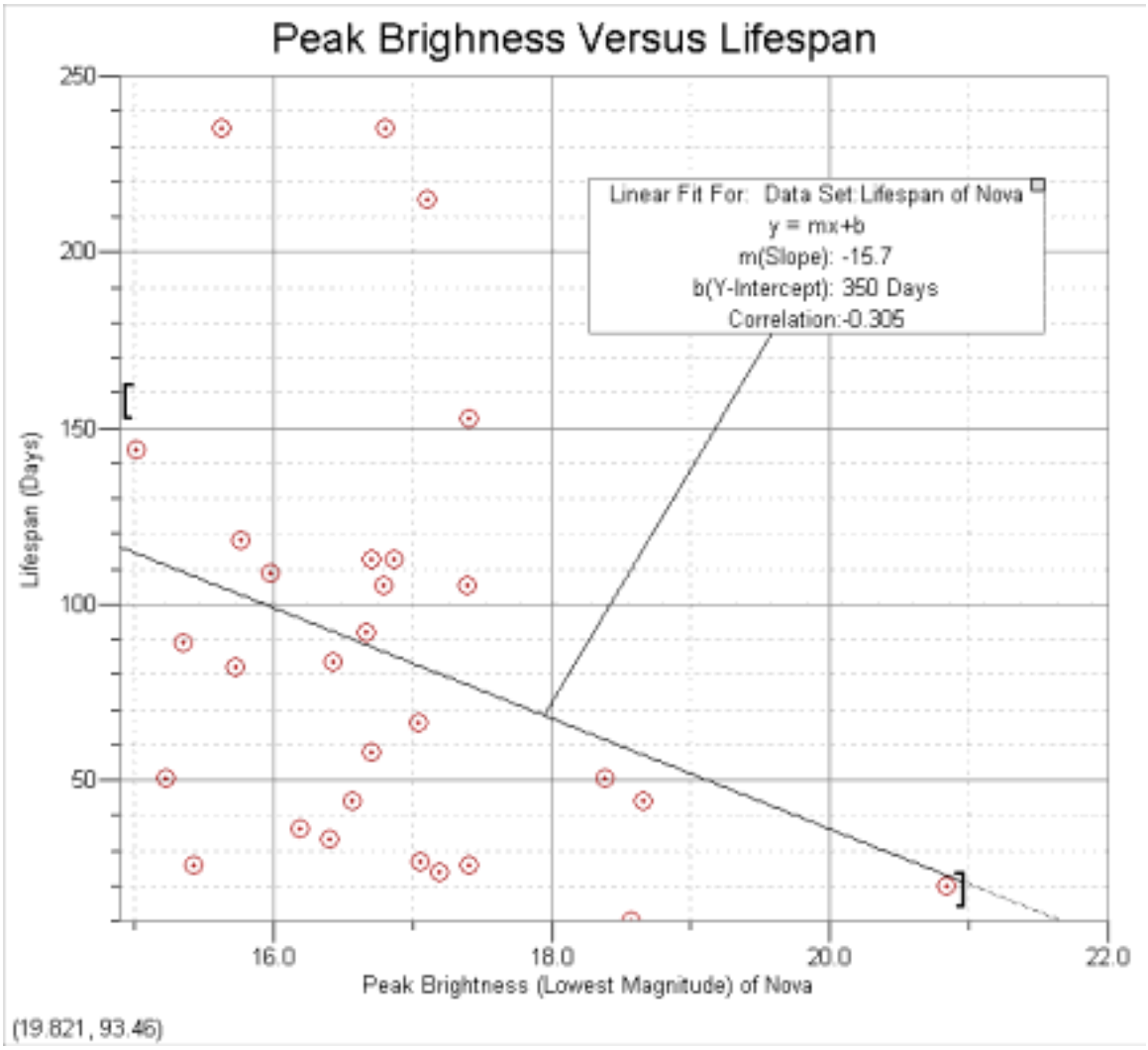

This is the final graph of each nova's brightness plotted against its lifespan. Two extreme outliers (lifespan of more than 500 days) were omitted, because they are most likely variable stars rather than novae. A variable star could easily look much like a nova because it is a star whose brightness changes periodically or irregularly (Grainger Observatory Glossary, WWW, 2004). Interpreting the line of best fit, and going by this present although weak correlation, a nova with magnitude that is one unit higher than another would have a lifespan that is approximately 16 days longer.

CONCLUSION

A weak correlation was found between the lifespans and lowest magnitudes of novae. This correlation is not a very strong one, but it does appear to be a present entity. Although a linear fit may not be the best way to describe the correlation, other types of equations that may at first appear to better fit the data present some problems. An inverse relationship seems at first possible, but all inverse relationships contain a vertical asymptote; therefore, it would not be possible because some magnitude value wouldn't be able to fit the curve, yet all magnitude values are possible for any given nova. Also, a parabolic function may fit that part of the curve best, but parabolic functions first have a negative slope, then turn positive, or vice-versa, where we only want a curve with a negative slope, because that seems to be the general direction of the plot.

Using our current linear fit, though, the results show that a nova with a magnitude that is one unit higher than another would have a lifespan that is approximately 16 days longer.

This research shows different, although not necessarily contradicting evidence from research done by other students. They found that novae with a brighter initial magnitude seemed to have lifespans that decreased more rapidly than those that are not as bright (Camacho, L., et al, 2001). It is possible that both theories could be true, because although the brightness may decrease at a faster rate, the novae that were initially brighter still need a longer period of time to die out because a larger magnitude span must be covered. Because three more years worth of data were available to our group, this could have been a cause of the possibly contradicting results. Also because epochs were not taken in periodic intervals, the novae that only appeared in one epoch could not be analyzed because the lifespan could not be calculated, and lifespan calculations could not be perfectly accurate. This could have affected the results of this project, just as it has affected the outcome of other projects (Clark, N.,2003).

FURTHER STUDY

After more images become available, more research and analysis of novae and their light curves could be completed so that a stronger correlation begins to form. Also, other spiral galaxies' novae could be analyzed to see if they have a larger amount of novae so that a stronger correlation could be found. One could also look into a correlation between magnitude, slope of light curves, and lifespan to see how each affects one another. Data could be kept separate for each subraster to see if the position of the nova in the galaxy affects these three aspects.

REFERENCES

Adkins, Destinee, Begley, M., Farhan, A., Farris, J., Kennedy, C., Kennedy, J., Landis, Z., Osborne, M., and Whisman, D., A Comparison Of M31 Nova Rates to Other Spiral Galaxies, RBSE Journal 2003

Binary Stars, 2004, http://astrosun2.astro.cornell.edu

Camacho, Linda and Miller, R., Magnitudes of Novae in M31, RBSE Journal 2001

Clark, Nick, The Lifespan of Novae in the Andromeda Galaxy, RBSE Journal, 2003

Rector, Travis and Jacoby, G., Nova Search: Cosmic Easter Eggs, TLRBSE website, 2001, www.noao.edu/outreach/tlrbse/

Rector, Travis and Jacoby, G., Nova Search: Content Background for Nova Research, TLRBSE website, 2001, www.noao.edu/outreach/tlrbse/

Locality vs. Maximum Magnitude: Is Location A Factor In A Nova's Maximum Magnitude?

Erin Knoop and Josh Riddle
Franklin Central High School, Indianapolis, IN
Teacher: Jim Hoffman, RBSE 2000

ABSTRACT

There are novae in every galaxy, even the Milky Way. A nova is a star that brightens briefly for a few months or years and then dims. It brightens and dims because it has collected gas from a nearby star; fusion then kicks in and the star uses the hydrogen it has collected to brighten, then dims quickly, once the hydrogen is gone. Sometimes smaller novae are brighter and last longer than larger novae, depending on the amount of hydrogen they have. In this project, a nova's magnitude is compared to its location in the Andromeda Galaxy to see if location affects magnitude. After all of the data was q

QUESTION

Does a nova's position in the Andromeda Galaxy affect its maximum magnitude?

HYPOTHESIS

A nova's location in the Andromeda Galaxy does affect its maximum magnitude. The closer the nova is to the edge of the galaxy, the dimmer the nova is. The closer the nova is to the center, the brighter it is.

PROCEDURE

- Find all of the novae in the galaxy
- Determine the maximum magnitude of each nova found
- Graph the maximum magnitude of each nova
    - **Label the graph in fields dividing each nova into the correct field**
- Determine if the maximum magnitude is affected by locality

PURPOSE

All novae have different maximum magnitudes, and it seems that locality would affect the maximum magnitude.

ANALYSIS

Mr. James Hoffman, advisor, provided all of the data obtained in this project. He provided access to data collected from Kitt Peak through RBSE 2000. That data had been collected on various days throughout the past eight years. To determine the location, as well as the maximum magnitudes of all of the novae, the Scion Image program was used. The graphs and data tables were made using Microsoft Excel. Conclusions were made from observing novae on every side of the galaxy. Novae on the outer edge of the galaxy had a relatively similar maximum magnitude as novae in the center of the galaxy. Thus providing the data used to prove that location is irrelevant.

Andromeda Galaxy Fields And The Novae Found There

1 (0) No Novae	2 (1) 17.04	3 (0) No Novae	4 (0) No Novae
5 (2) 16.74 16.13	6 (4) 15.92 Error twice 16.23	7 (3) 8.03 15.43 15.63	8 (0) No Novae
9 (0) No Novae	10 (1) Error	11 (0) No Novae	12 (0) No Novae
13 (0) No Novae	14 (1) 11.54	15 (1) 15.03	16 (1) 16.47

Error = The nova was too close to the edge of the field to collect it's magnitude

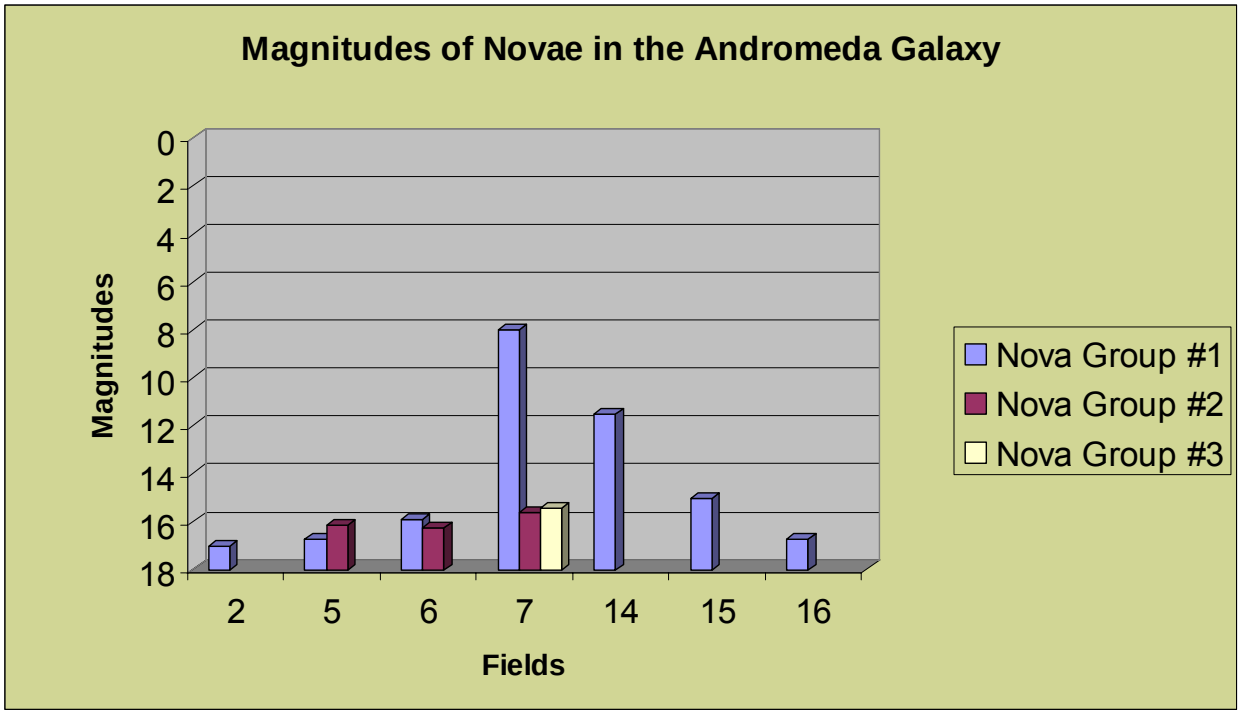

CONCLUSION

It appears that the maximum magnitudes of novae in the Andromeda Galaxy are not affected by their location. From observations of the novae that were found, there seems to be no distinct pattern of magnitudes. A nova in field five had approximately the same maximum magnitude as a nova in field sixteen. Those two fields are on opposite sides of the Andromeda Galaxy. Therefore, it can be concluded that a nova's location does not affect its magnitude.

DATA

Epoch	Field	X	Y	RA	DEC	Mag	r1	r2	r3	A	B
Field 16											
2	**16**	**80.4**	**183.2**	**00:42:08.39**	**+41:08:14.9**	**16.47**	**3**	**7**	**11**	**24.96**	**-2.51**
3	16	80.5	183.0	00:42:08.38	+41:08:14.9	17.30	3	7	11	24.82	-2.51
4	16	80.9	183.0	00:42:08.38	+41:08:14.9	17.35	3	7	11	24.80	-2.51
5	16	80.3	183.0	00:42:08.38	+41:08:14.8	17.35	3	7	11	24.59	-2.51
6	16	80.7	182.9	00:42:08.37	+41:08:14.9	17.51	3	7	11	24.95	-2.51
7	16	80.5	183.1	00:42:08.39	+41:08:14.8	17.60	3	7	11	24.70	-2.51
Field 15											
13	**15**	**172.1**	**473.0**	**00:42:33.77**	**+41:04:57.4**	**15.06**	**3**	**7**	**11**	**24.69**	**-2.51**
14	15	172.2	473.2	00:42:33.77	+41:04:57.3	16.65	3	7	11	24.54	-2.51
15	15	172.4	473.1	00:42:33.76	+41:04:57.3	17.16	3	7	11	24.35	-2.51
16	15	172.3	473.1	00:42:33.77	+41:04:57.3	16.31	3	7	11	23.71	-2.51
17	15	172.6	473.3	00:42:33.75	+41:04:57.2	18.58	3	7	11	24.70	-2.51
18	15	173.1	475.5	00:42:33.72	+41:04:55.8	19.83	3	7	11	24.63	-2.51
Field 14											
3	14	409.8	222.9	00:42:50.33	+41:07:47.8	17.22	3	7	11	24.73	-2.51
4	14	409.9	222.8	00:42:50.32	+41:07:47.8	17.56	3	7	11	24.79	-2.51
5	14	409.8	222.8	00:42:50.31	+41:07:47.7	17.75	3	7	11	24.49	-2.51
6	14	409.7	222.8	00:42:50.33	+41:07:47.7	16.90	3	7	11	24.88	-2.51
7	14	409.5	223.0	00:42:50.34	+41:07:47.7	16.56	3	7	11	24.56	-2.51
8	14	409.8	222.9	00:42:50.32	+41:07:47.6	15.82	3	7	11	23.63	-2.51
9	**14**	**409.5**	**222.7**	**00:42:50.34**	**+41:07:47.7**	**13.54**	**3**	**7**	**11**	**18.14**	**-2.51**
10	14	409.8	222.8	00:42:50.33	+41:07:47.6	17.67	3	7	11	23.62	-2.51
11	14	409.5	222.7	00:42:50.35	+41:07:47.8	17.85	3	7	11	23.93	-2.51
12	14	409.9	222.7	00:42:50.32	+41:07:47.8	13.77	3	7	11	19.85	-2.51

Field 13

There were no novae found in Field Thirteen.

Field 12

There were no novae found in Field Twelve.

Field 11

There were no novae found in Field Eleven.

Epoch	Field	X	Y	RA	DEC	Mag	r1	r2	r3	A	B

Field 10

The nova in epochs 3-7 is too close to the edge of the field to determine its maximum brightness.

Field 9

There were no novae found in Field Nine.

Field 8

There were no novae found in Field Eight.

Field 7

(1)

10	**7**	**229.3**	**474.2**	**00:42:30.32**	**+41:16:33.5**	**13.73**	**3**	**7**	**11**	**22.60**	**-2.51**
11	7	229.3	474.4	00:42:30.31	+41:16:33.4	18.03	3	7	11	17.14	-2.51
12	7	229.4	474.4	00:42:30.31	+41:16:33.4	16.36	3	7	11	24.76	-2.51
13	7	229.4	474.4	00:42:30.32	+41:16:33.4	16.25	3	7	11	24.46	-2.51
14	7	229.2	475.2	00:42:30.33	+41:16:32.9	18.34	3	7	11	24.57	-2.51
15	7	228.3	475.4	00:42:30.39	+41:16:32.6	18.82	3	7	11	24.33	-2.51
16	7	228.1	475.4	00:42:30.39	+41:16:32.7	19.19	3	7	11	24.78	-2.51

Field 7 continued…

(2)

10	7	119.4	441.8	00:42:36.95	+41:16:55.5	16.42	3	7	11	24.57	-2.51
11	**7**	**119.5**	**441.9**	**00:42:36.94**	**+41:16:55.5**	**15.63**	**3**	**7**	**11**	**24.65**	**-2.51**
12	7	120.1	442.3	00:42:36.91	+41:16:55.2	18.25	3	7	11	24.76	-2.51

(3)

32	7	74.9	432.0	00:42:39.62	+41:17:02.4	16.90	3	7	11	24.63	-2.51
33	7	74.2	432.0	00:42:39.67	+41:17:02.5	17.17	3	7	11	24.64	-2.51
34	7	74.5	432.0	00:42:40.54	+41:17:02.8	18.27	3	7	11	24.63	-2.51
35	7	74.1	432.0	00:42:39.67	+41:17:02.4	16.79	3	7	11	23.55	-2.51
36	**7**	**74.4**	**432.1**	**00:42:39.68**	**+41:17:02.3**	**15.43**	**3**	**7**	**11**	**22.33**	**-2.51**
37	7	74.1	432.0	00:42:39.67	+41:17:02.5	17.80	3	7	11	24.72	-2.51
38	7	74.2	432.9	00:42:39.66	+41:17:01.8	18.87	3	7	11	24.65	-2.51
39	7	74.5	433.7	00:42:39.65	+41:17:01.3	19.08	3	7	11	24.64	-2.51

Field 6:
(1)
The nova in epochs 2-7 is to close to the edge of the field to determine its maximum brightness.

Epoch	Field	X	Y	RA	DEC	Mag	r1	r2	r3	A	B

Field 6 continued…
(2)

10	**6**	**135.9**	**333.2**	**00:43:06.86**	**+41:18:09.4**	**15.92**	**3**	**7**	**11**	**24.58**	**-2.51**
11	6	136.0	333.4	00:43:06.86	+41:18:09.3	16.11	3	7	11	24.72	-2.51
12	6	135.8	333.4	00:43:06.87	+41:18:09.4	16.08	3	7	11	24.82	-2.51
13	6	135.9	333.4	00:43:06.86	+41:18:09.3	16.50	3	7	11	24.76	-2.51
14	6	136.0	333.4	00:43:06.86	+41:18:09.4	17.13	3	7	11	24.59	-2.51
15	6	136.1	333.5	00:43:06.86	+41:18:09.2	17.38	3	7	11	24.35	-2.51
16	6	135.9	333.5	00:43:06.87	+41:18:09.3	17.61	3	7	11	24.83	-2.51

(3)

The nova in epochs 21-25 is too close to the edge of the field to determine its maximum brightness.

(4)

32	**6**	**233.2**	**495.1**	**00:43:00.97**	**+41:16:19.5**	**16.28**	**3**	**7**	**11**	**24.70**	**-2.51**
33	6	233.0	495.2	00:43:00.99	+41:16:19.4	17.58	3	7	11	24.72	-2.51
34	6	233.3	494.9	00:43:00.98	+41:16:19.5	18.15	3	7	11	24.59	-2.51
35	6	233.5	495.0	00:43:00.99	+41:16:19.5	18.36	3	7	11	24.68	-2.51

Field 5:
(1)

2	**5**	**372.4**	**25.5**	**00:43:23.47**	**+41:21:39.0**	**16.74**	**3**	**7**	**11**	**25.14**	**-2.51**
3	5	372.5	25.2	00:43:23.48	+41:21:39.1	16.96	3	7	11	25.00	-2.51
4	5	372.3	25.1	00:43:23.49	+41:21:39.2	16.98	3	7	11	25.09	-2.51
5	5	372.5	25.3	00:43:23.49	+41:21:39.1	16.92	3	7	11	24.94	-2.51
6	5	372.4	25.2	00:43:23.49	+41:21:39.1	17.10	3	7	11	25.31	-2.51

(2)

9	5	288.0	20.2	00:43:28.58	+41:21:42.5	16.39	3	7	11	24.67	-2.51
10	5	287.6	20.1	00:43:28.62	+41:21:42.6	16.67	3	7	11	24.65	-2.51
11	**5**	**287.8**	**20.4**	**00:43:28.60**	**+41:21:42.3**	**16.13**	**3**	**7**	**11**	**23.95**	**-2.51**
12	5	287.6	20.3	00:43:28.61	+41:21:42.4	16.21	3	7	11	24.66	-2.51
13	5	287.6	20.2	00:43:28.61	+41:21:42.5	16.44	3	7	11	24.64	-2.51

14	5	287.6	20.2	00:43:28.62	+41:21:42.5	16.95	3	7	11	24.66	-2.51
15	5	287.6	20.4	00:43:28.61	+41:21:42.3	17.27	3	7	11	24.32	-2.51
16	5	287.6	20.3	00:43:28.62	+41:21:42.5	17.40	3	7	11	24.80	-2.51

Epoch	Field	X	Y	RA	DEC	Mag	r1	r2	r3	A	B

Field 4:

There were no novae found in Field Four.

Field 3:

There were no novae found in Field Three.

Field 2:

31	2	398.9	313.1	00:42:50.97	+41:24:12.8	17.04	3	7	11	24.56	-2.51
32	2	400.9	312.2	00:42:50.84	+41:24:12.5	17.20	3	7	11	24.68	-2.51
33	2	399.9	313.2	00:42:50.91	+41:24:12.4	17.86	3	7	11	24.75	-2.51
34	2	400.2	313.1	00:42:50.90	+41:24:12.3	18.01	3	7	11	24.65	-2.51
35	2	400.5	312.2	00:42:50.89	+41:24:12.5	18.18	3	7	11	24.67	-2.51
36	2	401.1	312.5	00:42:50.88	+41:24:12.3	18.25	3	7	11	24.50	-2.51
37	2	400.1	313.0	00:42:50.91	+41:24:12.5	17.95	3	7	11	24.73	-2.51
38	2	400.3	312.7	00:42:50.89	+41:24:12.3	18.06	3	7	11	24.73	-2.51
39	2	400.2	312.3	00:42:50.90	+41:24:12.5	18.07	3	7	11	24.66	-2.51

Field 1:

There were no novae found in Field One.

Patterns in the Distribution of Novae in M31

Derek Dudley
Wauwatosa East High School, Wauwatosa WI
Teacher: Gary Sampson, TLRBSE 2003

ABSTRACT

The purpose of this research paper was to locate new novae in the Andromeda Galaxy, M31, and to find patterns in their placement across the bulge of the galaxy.

To do this task, images from the Kitt Peak National Observatory were "blinked" to show the locations of novae in M31. The locations of the novae were plotted on an image of Andromeda and then spiral arms were superimposed on these images.

The data show that there is a pattern in the distribution of novae in M31. When the novae are traced, they show a normal spiral structure in the bulge. Another possible pattern of distribution of novae is consistent with a barred spiral pattern.

BACKGROUND

M31, the Andromeda Galaxy, is the closest large spiral galaxy to our own galaxy. It is 150,000 light years across, making it 1 ½ times the size of the Milky Way. It is generally thought to be a normal spiral galaxy. However, Hubble Space Telescope images showed a double nucleus at the core of the galaxy. This could mean that M31 devoured another galaxy, or that there is matter blocking our view of the whole nucleus.

Most spiral galaxies have novae, and M31 is one of them. A nova is a star that expels the outer layers of itself in an abrupt blast. These layers are composed of hydrogen that is transferred from one star to a nearby star in a binary system. The companion star, which gives off the hydrogen, is usually a giant main sequence star. The star that collects the matter is an old white dwarf. As the hydrogen collects, the temperature on the surface of the white dwarf increases, and eventually nuclear fusion occurs, creating the Latin for "new star," a nova.

HYPOTHESIS

The researcher believes that there is a pattern in the distribution of novae in M31, and it will be related to the spiral arms.

PROCEDURE

The first step was to collect data. All of the images that were used came from the Kitt Peak Observatory using one of three telescopes: the MDM 1.3m, the KPNO .9m, or the KPNO 2.1m. The images were taken using a hydrogen-alpha filter in order to be able to see the novae better. Epochs 1-39 were imaged over the past 8 years, and epochs 40-61 were imaged in the summer of 2003 by the TLRBSE team.

After the data were collected, the new and old images were viewed with Scion Image through a process called "blinking." During this process, two or more images would be stacked on top of each other and then flipped back and forth. If a star is in one image,

and not in the other, it is a possible nova. All 61 epochs, in 16 subrasters, were viewed. The next step narrowed down the nova candidates.

When all of the magnitudes for a candidate had been recorded, a light curve was made using Microsoft Excel. If the curve looks like the curve of a nova, then it is labeled as one. However, if it did not look like a normal nova light curve, the data were scrapped (See Fig. I as an example of a typical nova light curve). The times and dates of the epochs were taken into consideration as well. Not all of the light curves were smooth because of missing data between epochs. This was done for all of the possible novae, and the field was narrowed.

In order to plot the novae and find patterns in their locations, the finder charts that were used to determine magnitudes were cut out and taped together to make one large picture of the center of M31. The XY coordinates were used to plot the locations of the novae on the chart. Once this was done, a computer image of the galaxy was brought up in the Windows program Paint, and the locations from the chart were placed on the image in Paint. Spiral arms were superimposed over areas of high nova density

RESULTS

Thirty-two possible novae were discovered, and after the narrowing process, 29 novae were left. These final novae were plotted on the finder charts using their XY coordinates. After this, an image of M31 was brought up in Paint, and the locations from the finder chart were put on the image in Paint. The images, Fig. II and Fig. III, were the results. Chart 1 is the data from the first to last appearance of each of the 29 novae.

Field	Epoch	X	Y	RA	Dec
2	31-43	398.9	313.1	00:42:50:97	+41:24:12.8
5	2-7	372.4	25.2	00:43:23.47	+41:21:39.2
5	9-17	288	20.2	00:43:28.58	+41:21:42.5
6	10-17	135.9	333.2	00:43:06.86	+41:18:09.4
6	32-35	233.2	495.1	00:43:00.97	+41:16:19.5
6	47-61	497.2	357.2	00:42:45.04	+41:17:53.5
6	55-61	422.5	345.8	00:42:49.51	+41:18:00.9
7	3-9	412.5	500.2	00:42:19.25	+41:16:15.9
7	10-12	119.4	441.8	00:42:36.95	+41:16:55.5
7	10-15	229.3	474.2	00:42:30.32	+41:16:33.5
7	14-17	113.5	94.4	00:42:37.31	+41:20:52.0
10	8-10	162.2	101.3	00:42:05.27	+41:14:58.8
10	18-19	220.8	44.2	00:43:01.75	+41:15:37.9
10	14-17	473.1	116.3	00:42:46.51	+41:14:48.6
10	28-34	196.3	347.9	00:43:03:24	+41:12:11.0
10	40-61	379.4	197.1	00:42:52:15	+41:13:53.8
11	1-8	276.3	319.9	00:42:27:47	+41:12:30.2
11	3-8	201.7	127.2	00:42:31:98	+41:14:41.3
11	14-17	365.6	407	00:42:22:10	+41:11:30.8
11	53-61	470.4	364.9	00:42:15.74	+41:11:59.5

12	55-61	170	113.1	00:42:02.97	+41:14:50.8
14	25-27	298.8	269.3	00:42:57.06	+41:07:16.2
15	13-17	172.1	473	00:42:33.77	+41:04:57.4
15	31-34	359	45.3	00:42:22.48	+41:09:48.5
15	33-39	221.2	361.2	00:42:30.79	+41:06:12.9
16	2-7	80.4	183.2	00:42:08.39	+41:08:14.9
16	28-30	316.9	258.1	00:41:54.04	+41:07:23.6
16	31-39	283.9	157.8	00:41:56.11	+41:08:31.9
16	38-39	254.3	138.1	00:41:57.85	+41:08:45.3

Chart 1

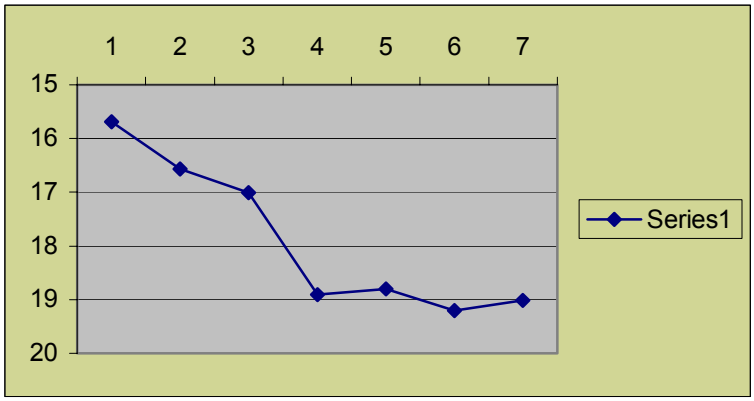

Fig. I
Light Curve For Nova 4 In Subraster 10

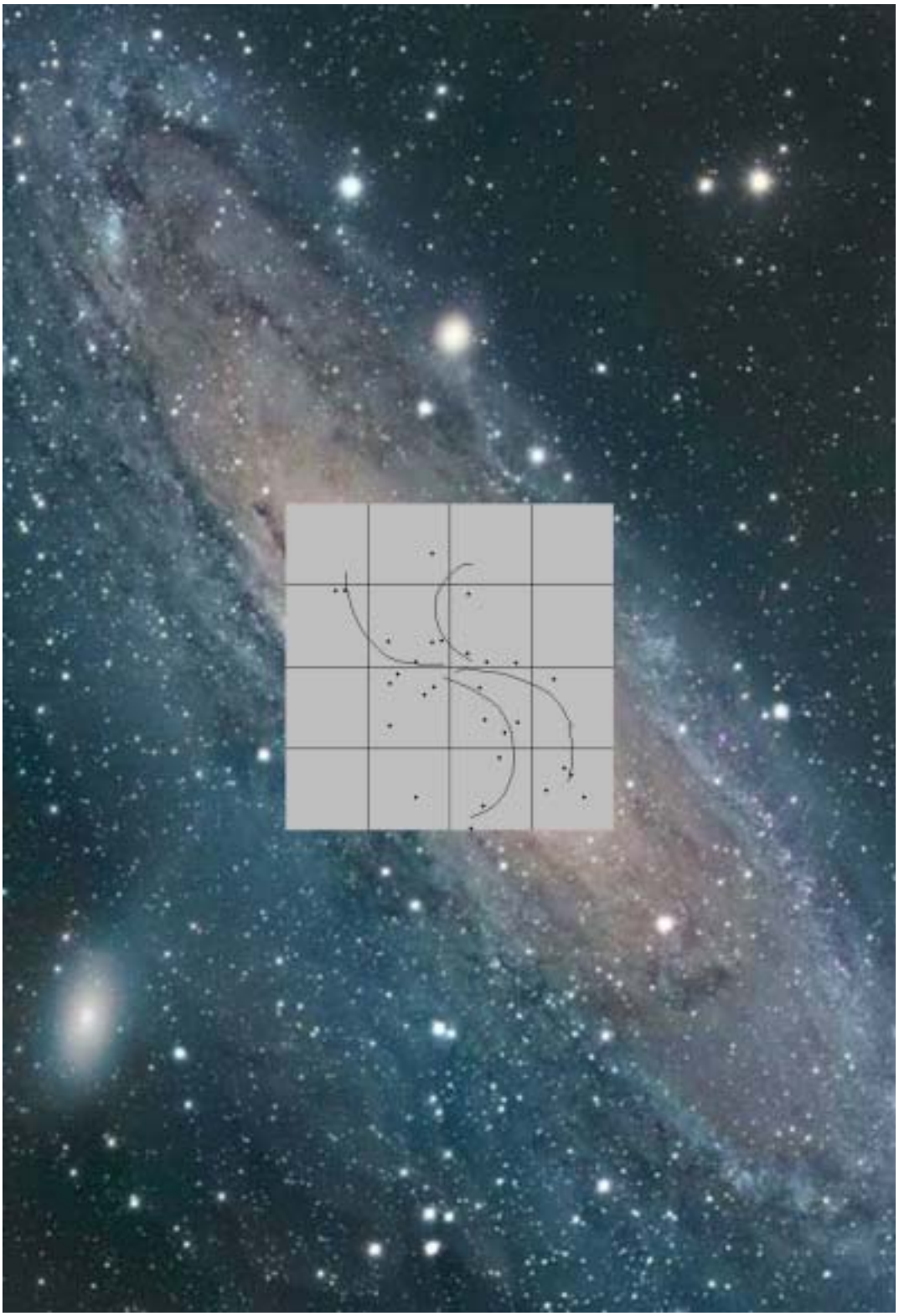

Fig. II
M31 Image With Possible Normal Spiral Structure In The Central Bulge

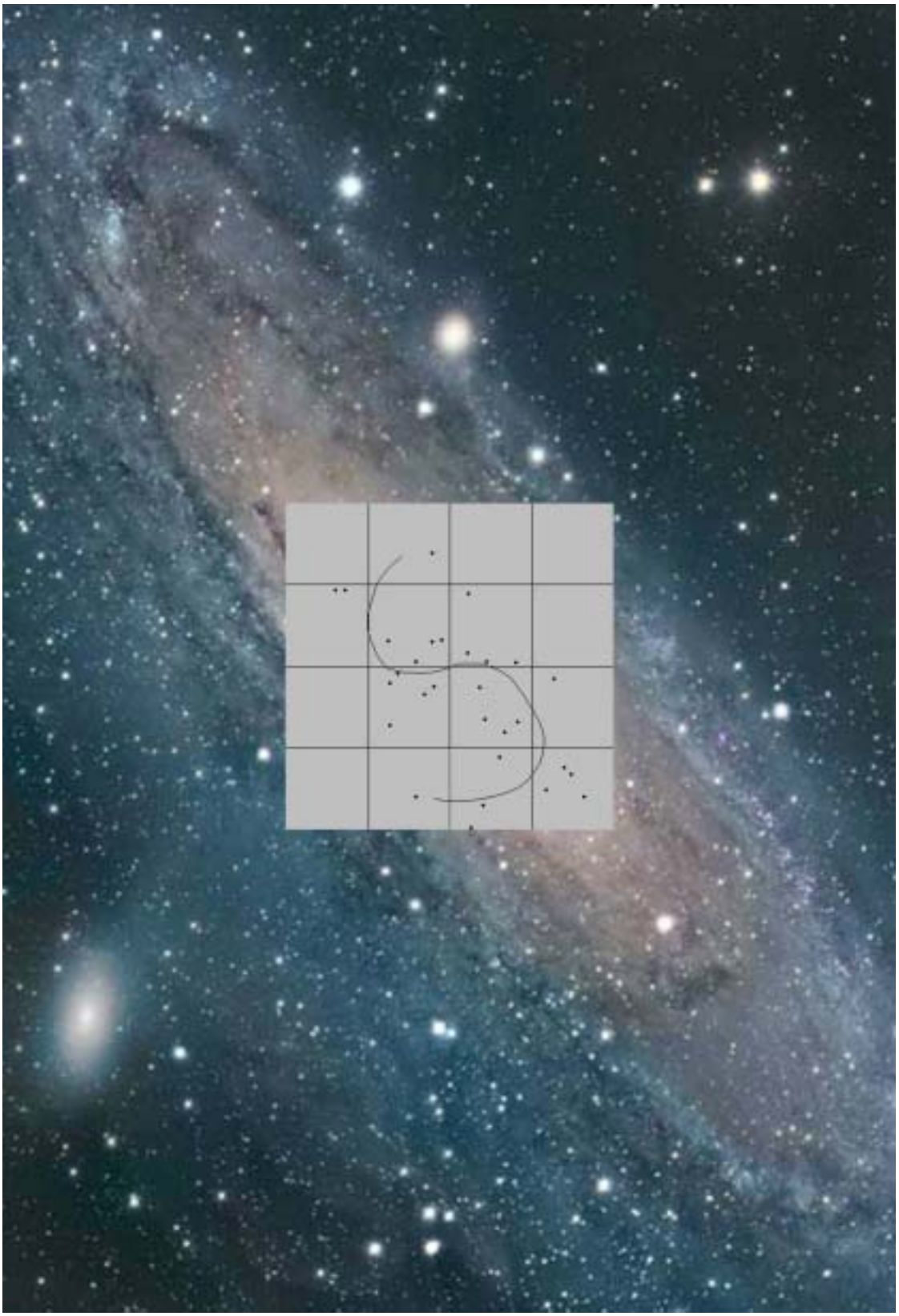

Fig. III
M31 Image With Possible Barred Spiral Structure In The Central Bulge

CONCLUSION

Fig. II shows a pattern that resembles spiral arms radiating from the center of the bulge of M31. Lines have been drawn on Fig. II that show a normal spiral pattern emanating from the bulge.

POSSIBLE NEXT STEPS

Fig. III shows a possible barred spiral structure leading from the center of the M31. Andromeda is not a barred spiral galaxy, but it is possible that it was a barred before becoming a regular spiral galaxy. This could be related to the merging of Andromeda and another galaxy, but other research will need to be done.

The next step will be to wait until next year's data comes in, and then plot the locations of the new novae. The more novae that are found and plotted, the clearer the pattern of novae distribution will become.

REFERENCES

Atlas of the Andromeda Galaxy. Ed. Paul W. Hodge. University of Washington Press. 1981 <http://nedwww.ipac.caltech.edu/level5/ANDROMEDA_Atlas/Hodge_contents.html>.

Ciardullo, Robin, et al. "The Hα Light Curves of Novae in M31." The Astrophysical Journal 356 (1990): 472-482.

Feidler, Josh, and Brett Shaw. "Patterns in the Occurrence of Novae." The RBSE Journal (2003):19-20.

Hatano, Kazuhito, and David Branch and Adam Fisher. "New Insight Into the Spatial Distribution of Novae in M31." The Astrophysical Journal 487 (1997): L45-L48.

Hubbell, Alex, et al. "Extrinsic Triggers for Nova Formation in the Andromeda Galaxy." The RBSE Journal (2003): 8-13.

McGee, Joel. "The Use of Novae to Determine the Spiral Structure Near the Core of the Andromeda Galaxy." The RBSE Journal (2001): 16-18.

Mass Distribution Of White Dwarfs Within The Bulge Of The Andromeda Galaxy (M31)

Harlan Devore, Cape Fear High School, Fayetteville, NC – TLRBSE 2003
Velvet Dowdy, Graves County High School, Mayfield, KY – TLRBSE 2003
Kathy Malone, Shady Side Academy, Pittsburgh, PA – TLRBSE 2003
Thomas Morin, Belmont High School, Belmont, NH – TLRBSE 2003
Gary Sampson, Wauwatosa East High School, Wauwatosa, WI – TLRBSE 2003

ABSTRACT

A total of 83 novae occurring over 61 epochs were studied to determine the distribution of high and low mass white dwarfs in the bulge of the Andromeda Galaxy (M31). Fast-decaying novae (45 days/magnitude or less) were classifies as originating from high mass white dwarfs; those that decayed in more than 45 days/magnitude were considered as having low mass white dwarf origins. The study shows that both high and low mass white dwarfs follow an inverse square pattern of distribution with respect to radial distance from the center. Scatter plots of these white dwarfs show that most are not randomly distributed, but tend to group together in curved bands or chains. There appears to be a slight tendency for high mass white dwarf to be located in clusters and chains nearer the center, while the low mass white dwarfs tend to be more uniformly distributed farther from the center. The distribution pattern also suggests the extension of spiral arms from the disk into the bulge of M31.

BACKGROUND

M31, commonly referred to as the Andromeda Galaxy, is the closest spiral galaxy to the Milky Way. Andromeda has been of particular interest to astronomers throughout history for many reasons. Initially, M31 was believed to be the closest nebula to us. It was William Huggins, the pioneer of spectroscopy, who in 1864 noted the continuous spectra produced by M31,not the line spectra noted for nebulae, and Isaac Roberts in 1887 whose photograph of Andromeda showed its obvious spiral structure. M31 continues to be of interest to astronomers because it provides a look into the structure of a spiral galaxy, similar to that of our own. In addition, Andromeda is approximately 2.2 million light years from us and lies within a local group of galaxies that includes the Milky Way. It is approximately twice the size of the Milky Way and has been shown to possess a double nucleus.

Interestingly enough, the term nova means "new star". The ancients perceived novae as the birth of a new stars, when in fact, they are events caused by the interaction of stars near the end of their lives. It is now believed that novae are the result of white dwarfs accreting hydrogen from the surface of red giant companion stars. The hydrogen pulled off the larger binary companion accumulates and heats up the surface of the degenerate white dwarf star. This new layer of hydrogen eventually reaches a temperature that causes fusion to begin in a sudden, explosive way. In this cataclysmic event, mass is ejected from the surface of the white dwarf and the brightness of this star increases, often by several magnitudes. Photometric techniques are used to observe the nova's maximum brightness and eventual decline.

To date, hundreds of novae have been observed and documented in the galaxy of Andromeda. Numerous studies have attempted to define the distribution of these events, and relate their light curves to characteristics of the white dwarfs that produce these eruptions.

Initially, an attempt was made to use the novae in M31 as distance indicators, much like Cepheid variables. However, the lack of understanding of how the properties of novae may vary from one galaxy to another has made this impractical. (Shafter, 2001) In addition, the lack of reliably known properties of novae, and the inconsistencies of reported results, limit their usefulness.

In 1987, Ciardullo and collaborators used images of the inner bulge of M31 using narrow band H alpha filters. This imaging technique provided a distinct advantage. H alpha emission of novae becomes bright and remains so, days or even weeks after the brightness on the visible spectrum has faded. This allowed the identification of many more novae and the construction of reliable light curves for many more novae, even without consecutive nights of observing time. This survey of novae in M31 identified the distribution of novae within the bulge population. (Ciardullo, et al 1983) In 1997, Hatano and collaborators identified the novae in M 31 with the disk population, citing sampling biases and the presence of interstellar dust as the reason why nova were association with the bulge population. Finally in 2001, Shafter and Irby published findings consistent with the distribution of novae associated with the bulge population of M 31.

Other researchers have correlated the mass of white dwarf with the time required for the magnitude of its nova event to decay 3 magnitudes (Rector, 2003), and the mass of the white dwarf in relation to the progenitor star (Rector, 2003).

This leads us to the research question investigated here: What is the distribution of high and low mass white dwarfs in M 31?

STATE PROBLEM

The major research question investigated was to determine the pattern of distribution of high and low mass white dwarfs in the bulge of M31.

PROCEDURE

The M31 images used for this study were taken with the MDM 1.3-meter, KPNO 0.9-meter, and the KPNO 2.1-meter telescopes at Kit Peak National Observatory. All images were taken using H-alpha filters to provide maximum contrast between novae and the brightness of the M31 bulge. 39 image epochs were used. The first epoch, taken 3 Sep 95, served as a reference image. The remaining 38 epochs were taken between 18 Jun 97 and 11 Nov 02. (Appendix 1) The images were generally taken at one-month intervals during the July - January period when M31 is visible from Earth. Some months contain multiple epochs. Gaps in coverage also exist when the telescopes were not available. The original images were quite large - 2048 x 2048 pixels. For ease of use, each image was divided into 16 subrasters or fields, each 512 x 512 pixels. (App 2) For ease of identifying images, the image file name contained the epoch number (characters 4-6) and the field (characters 7-9).

Image analysis was done primarily using Scion Image. After opening Scion Image, nova search macros were loaded. This allowed all 39 epochs of a given field to be loaded as a stack. Using Scion Image's animation feature, the images were blinked, allowing novae to be identified as they appeared, brightened or dimmed, then disappeared as successive epochs were viewed. As each nova was located, its epoch numbers and coordinates were entered into an Excel spreadsheet.

After all novae were logged, Scion Images' photometry tool was used to determine the apparent H-alpha magnitude of each nova for each epoch in which it appeared. To calibrate the photometry tool, at least three standard stars were measured in each epoch before measuring the unknown nova magnitude. Several novae were located near the edge of images, and Scion Image's photometry tool was often not successful in measuring their magnitudes. For these stars, Software Bisque's CCD Soft program was used to measure magnitudes.

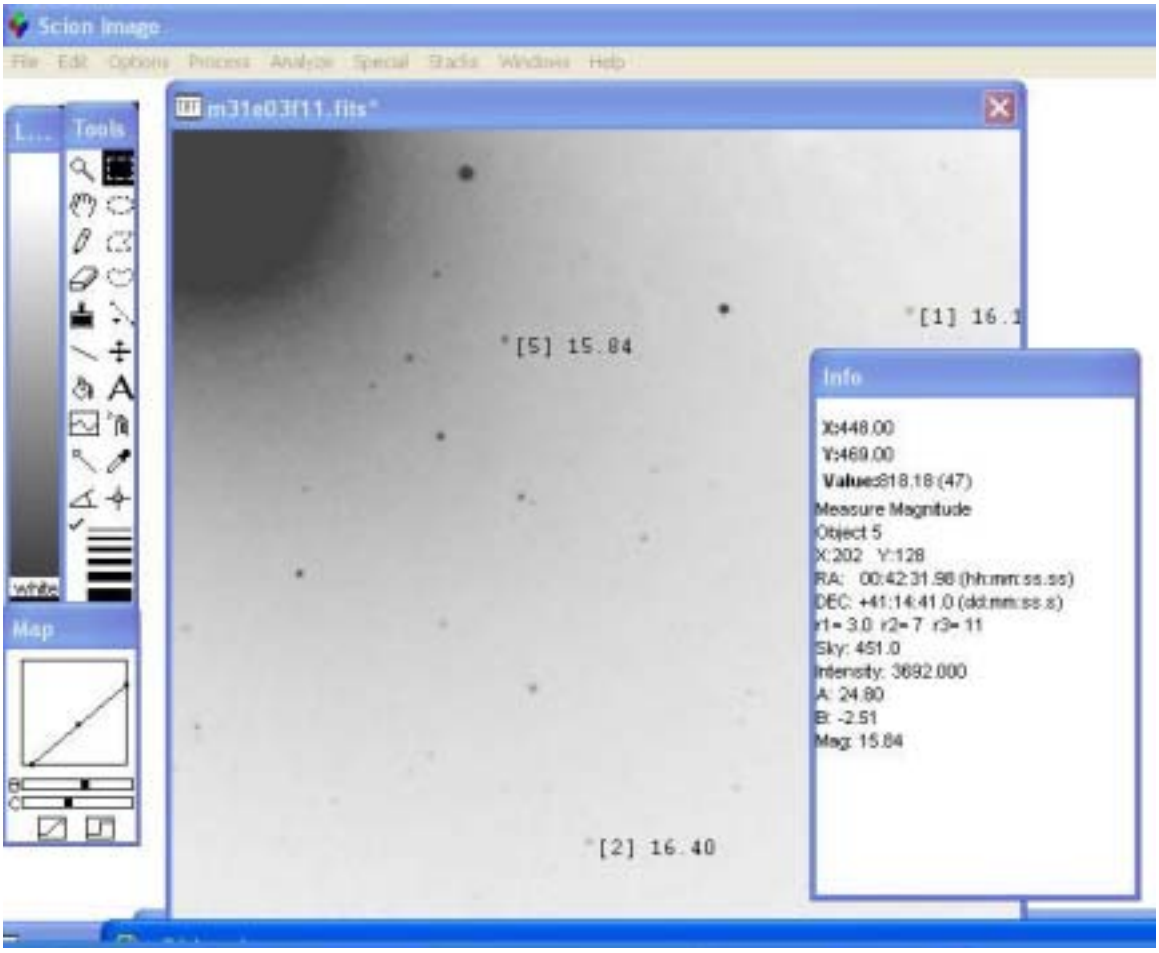

Measuremag

Next, an Excel table was created that matched epoch numbers to the dates and times the images were made. (App 1) An Excel VLOOKUP function was then used to correlate dates and times to each epoch in the data log. This allowed calculation of elapsed time for each nova relative to the first epoch in which it appeared.

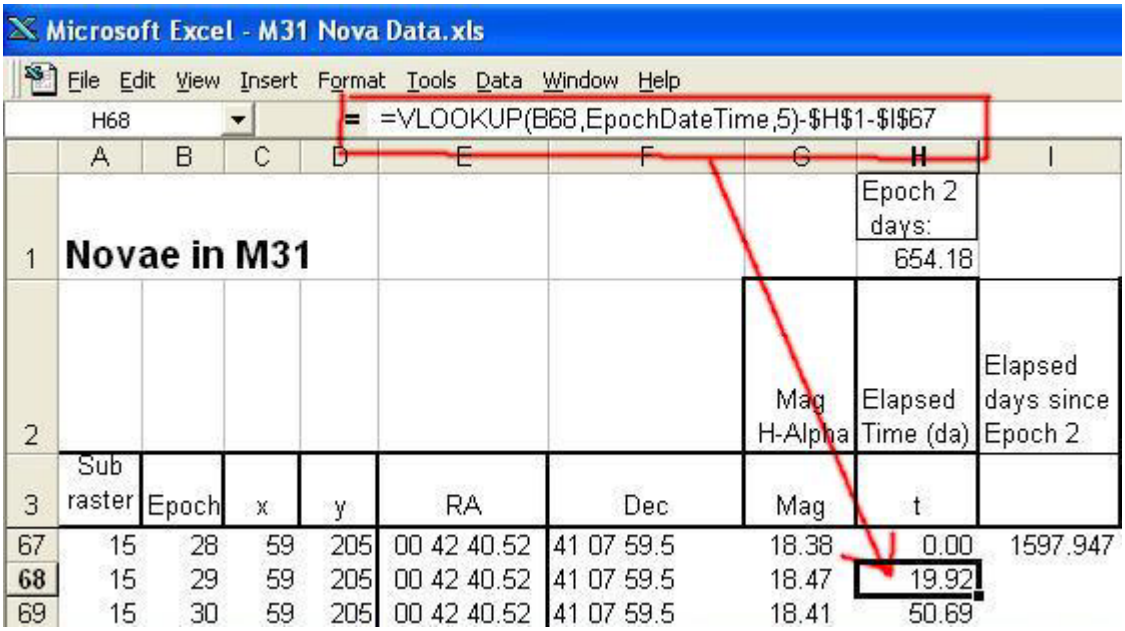

Timecalc

Excel's SLOPE function was then used to calculate the rate of decay of the nova's magnitude in days/magnitude. In a few novae, the light curves included both brightening and decay. For these novae, only data points that were in the decay portion of the curve were included in the slope calculation. USAVSO classifies novae into two categories: fast novae are those that decay by 3 magnitudes in less than 50 days, and slow novae, those that require more than 50 days to decay 3 magnitudes. By multiplying the calculated slope by 3, the novae in our study could now be classified as slow or fast novae.

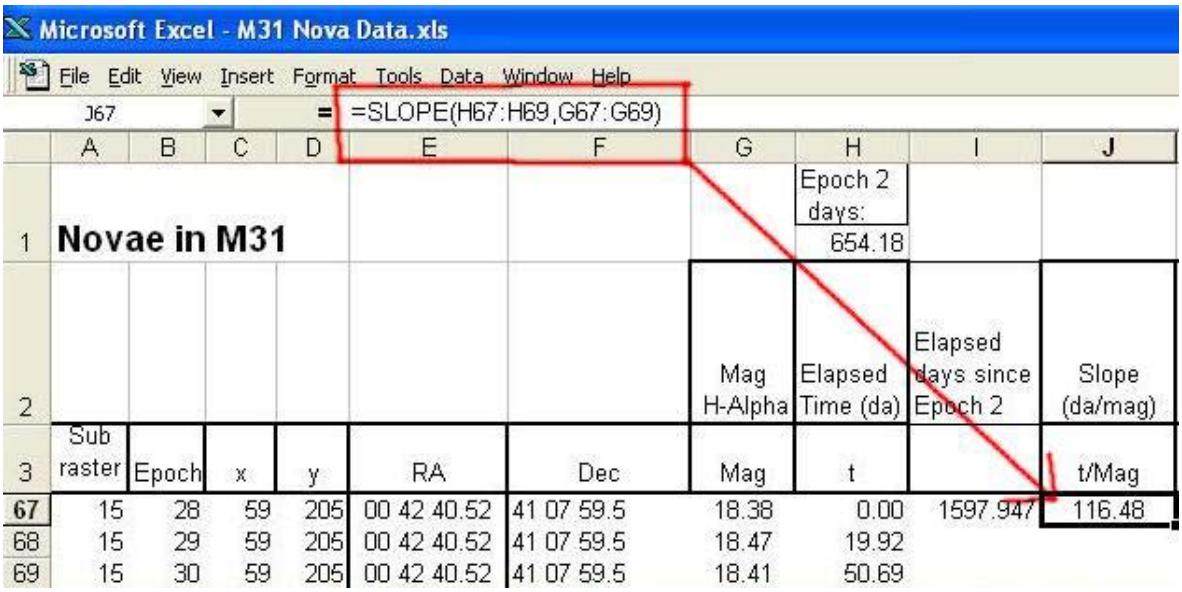

Slopecalc

Before distances from the galactic center could be assigned to each nova, three coordinate transformations had to be made. First, pixel coordinates for each subraster had to be converted to a galactic coordinate system. Secondly, these galactic coordinates must be rotated so that the long axis of the galaxy was horizontal. Finally, the plane of the galaxy had to de-projected to correct for its tilt.

The original 2048 x 2048 pixel images used in this study had been sectioned so that the intersection of subrasters 6, 7, 10, and 11 coincided with the center of M31's bulge. This intersection was chosen to be the origin (0,0) in the galactic coordinate system.

To convert each subraster's coordinates into galactic coordinates, an Excel table was created with the value (j) that must be added to each subraster x value to convert it into a galactic x' value. A second value (k) was included in the table which would convert a subraster's y value into a galactic y' value.

Coordinate Conversion

Subraster Numbering System

1	2	3	4
5	6	7	8
9	10	11	12
13	14	15	16

Pixel Coord on Subrasters

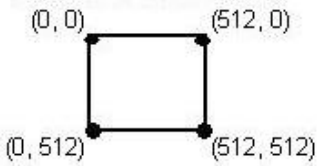

Tranformation to Galactic Coordinates

Subraster	j (x' = x + j)	k (y' = k - y)
1	-1024	1024
2	-512	1024
3	0	1024
4	512	1024
5	-1024	512
6	-512	512
7	0	512
8	512	512
9	-1024	0
10	-512	0
11	0	0
12	512	0
13	-1024	-512
14	-512	-512
15	0	-512
16	512	-512

GalacticCoordLookup

Excel's VLOOKUP function was then used to extract the j and k values from this table to convert all novae pixel coordinates in the data log into galactic coordinates.

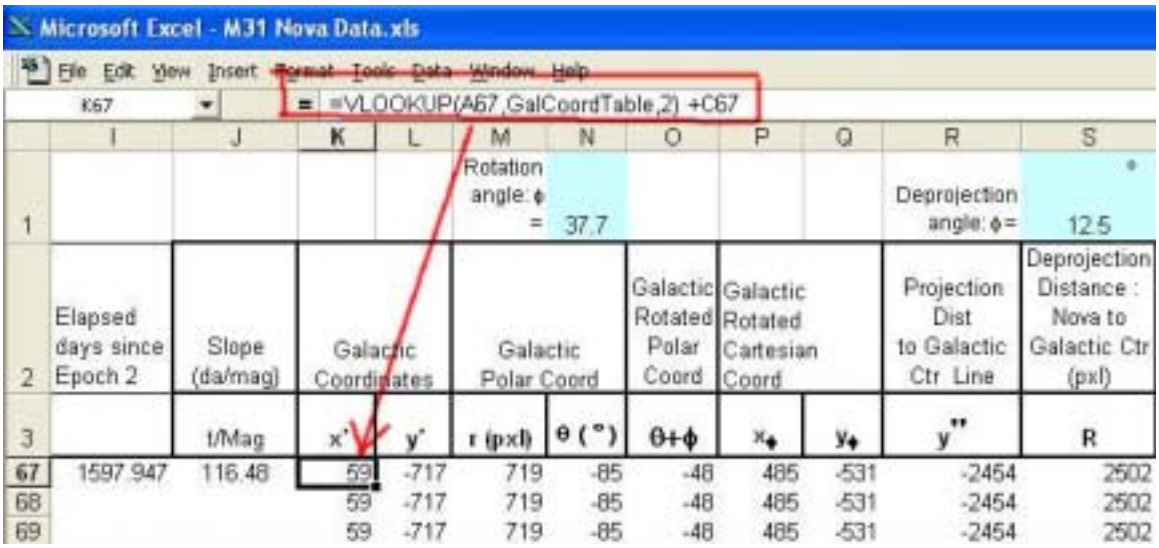

GalacticCoordConv

The major axis of M31 is tilted by 37.7° with respect to the ecliptic. In the images used in this study, the ecliptic is parallel to the x-axis of the image. To de-rotate the M31 images, then, the galactic coordinates had to be rotated by 37.7°. This was achieved by first converting the galactic coordinates of each nova into polar coordinates, where r = v(X'2 +Y'2) and = tan-1 (Y'/X')., then adding the rotation angle to the angular coordinate: ϕ = θ + 37.7°. Finally, the rotated polar coordinate system (r,ϕ)was converted back to Cartesian coordinates to produce a rotated galactic coordinate system: xϕ = r cos ϕ and yϕ = r sin ϕ.

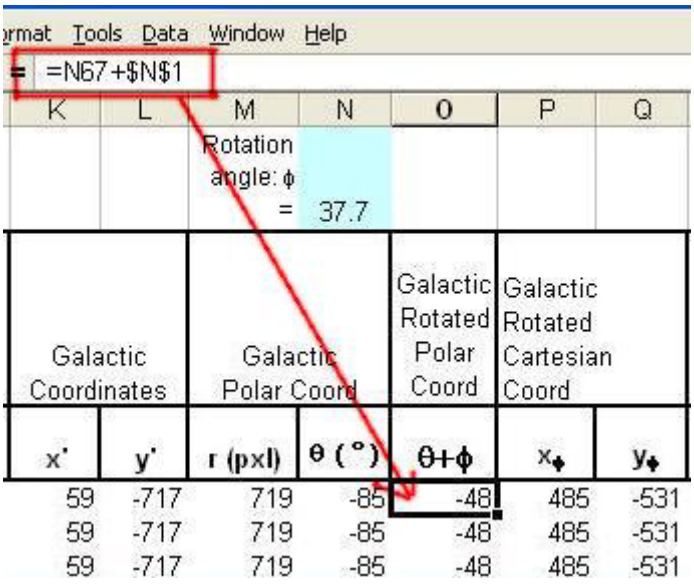

CoordRotJPG

Before White Dwarf distribution as a function of radial distance can be analyzed, a final coordinate transformation must be made. As seen from Earth, the plane of M31 is tilted by 12.5°. This means that M31 is not quite an edge-on spiral galaxy to the Earth observer. Instead, the galactic plane forms a 12.5° angle to a line from the Earth to M31's center. This makes the yϕ pixel distances smaller that they would be if M31 were viewed face-on. To correct for this effect, all yϕ coordinate values must be de-projected by dividing by sin 12.5°: y" = yϕ /sin (12.5°) and x" = xϕ.

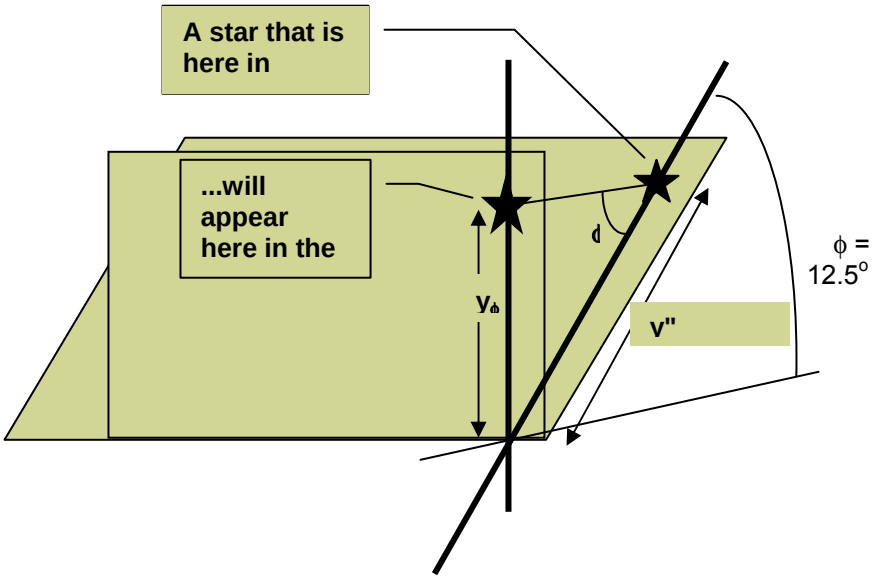

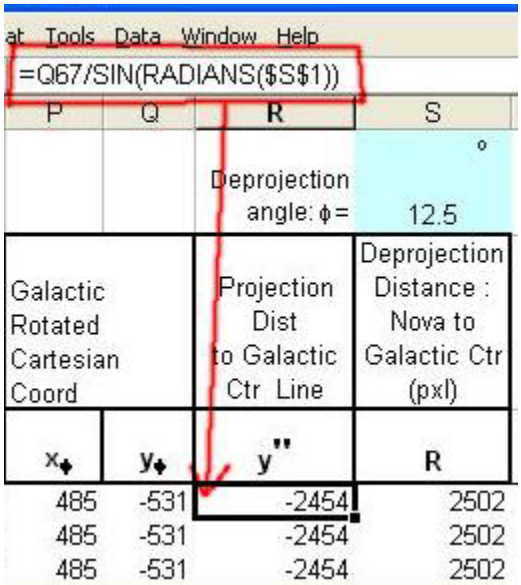
at Tools Data Window Help

=Q67/SIN(RADIANS(S1))

P	Q	R	S
		Deprojection angle: ϕ =	12.5
Galactic Rotated Cartesian Coord		Projection Dist to Galactic Ctr Line	Deprojection Distance : Nova to Galactic Ctr (pxl)
x_ϕ	y_ϕ	y"	R
485	-531	-2454	2502
485	-531	-2454	2502
485	-531	-2454	2502

Galacproj]

With this final coordinate conversion, nova image coordinates have been converted into galactic coordinates that have been rotated and de-projected. It is now possible to determine the distance of each nova from the galaxy center by using the distance formula: d = v(x”2 +y”2). (Appendix 5)

RESULTS

A total of 83 novae were identified in the bulge of M31 from the 61 epochs that were analyzed. Using galactic coordinates, their locations within the bulge were plotted as shown.

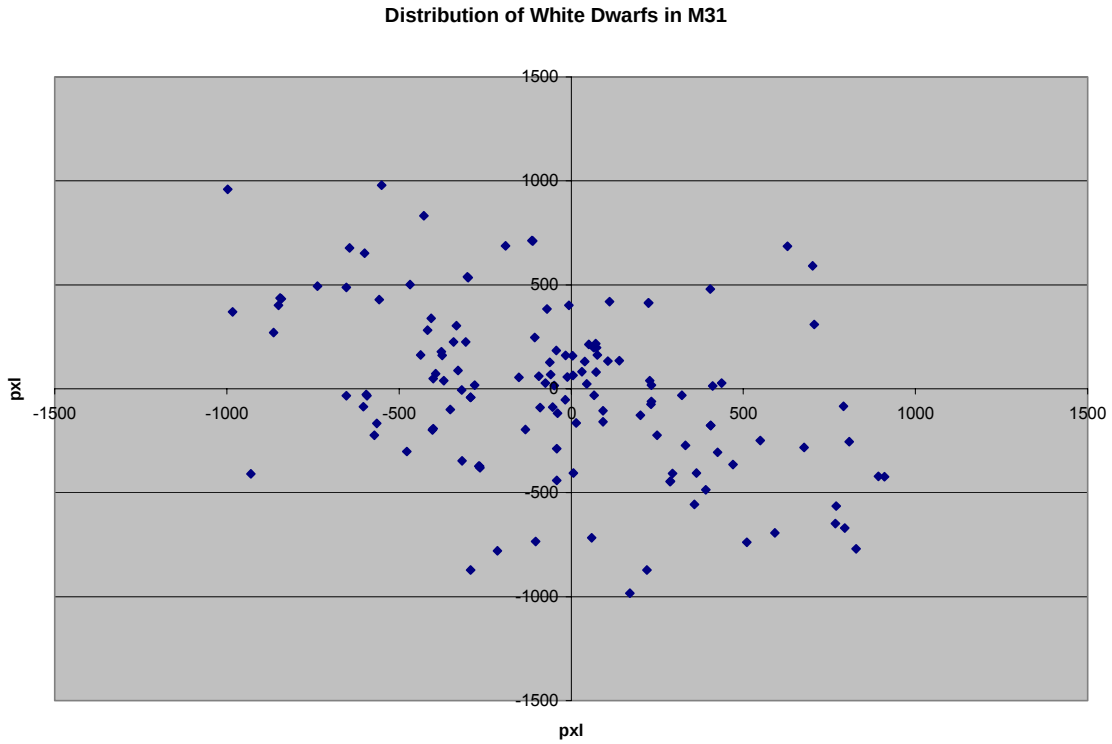

As might be expected, their population was denser near the center of the bulge where the star population was denser.

After analysis, only 62 of the novae produced light curves that would allow them to be classified as fast or slow novae. These were stars that appeared in at least 3 epochs, and produced decaying light curves. (Appendix 2)

Another 3 novae were found in only two epochs, thus only a two-point slope would have been possible for the light curve. With just two points, it could not be determined where on the light curve the points fell. These novae could not be used for estimation of White Dwarf masses. Four stars had negative slopes, indicating that the images were captured while the novae were still brightening. (Appendix 2)

Another 63 novae candidates appeared only in one epoch. Most are probably short-term novae, but many may be long term novae for which there are gaps in image coverage of

M31. Several dimmer candidates might also have been variable stars that were dimming below the magnitude limit for the telescope. A few might be cosmic ray artifacts that were incorrectly classified as stars. (Appendix 3)

An additional 29 objects were classified as either cosmic rays or hot pixels. A few of these might have been novae, but it is unlikely. (Appendix 4)

Finally, one star in Field 5 (RA 00:43:30.27, Dec +41:16:35.0) was almost certainly a variable star. Its magnitude fluctuated, sometimes disappearing completely, with no obvious decay trend.

To separate the fast novae - produced by high mass white dwarfs, from the slow novae - produced by low mass white dwarfs, the data table was sorted using the light curve slope as the sort key. After sorting, it was determined that only 8 novae met the AAVSO criteria (less than 50 days to decay 3 magnitudes) for high mass white dwarfs.

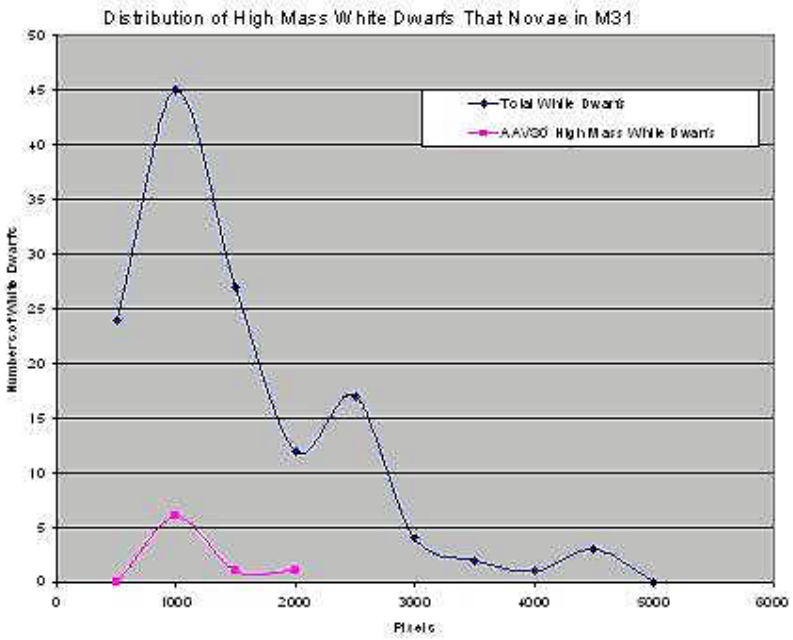

Highmassdist

Although the sample was small, the above graph shows that the AAVSO-defined high mass dwarfs generally followed the same distribution pattern as the total white dwarf pattern for M31. (For graphing purposes, white dwarf distances from the galactic center are binned in groups 500 pixels wide). However, there were no high mass white dwarfs beyond 2000 pixels from the galactic center. (Note that the total white dwarf plot line above includes those novae for which no slope could be obtained.)

In order to obtain a more statistically significant determination of whether differences by mass exist in the distribution of M31 white dwarfs, a redefinition of high and low mass white dwarfs was made. Thirty-one novae that had decay curves less than or equal to 45 days/magnitude. These were defined to be produced by high mass white dwarfs. Thirty-

one had decay curves greater than 45 days/magnitude and were defined to be produced by low mass white dwarfs. Based on this criterion, the white dwarf distribution showed a slight tendency for high mass white dwarfs near the center of the galaxy, with lower mass dwarfs slightly favored in the range from 2000-3000 pixels from the center. However, these slight differences may not be statistically significant.

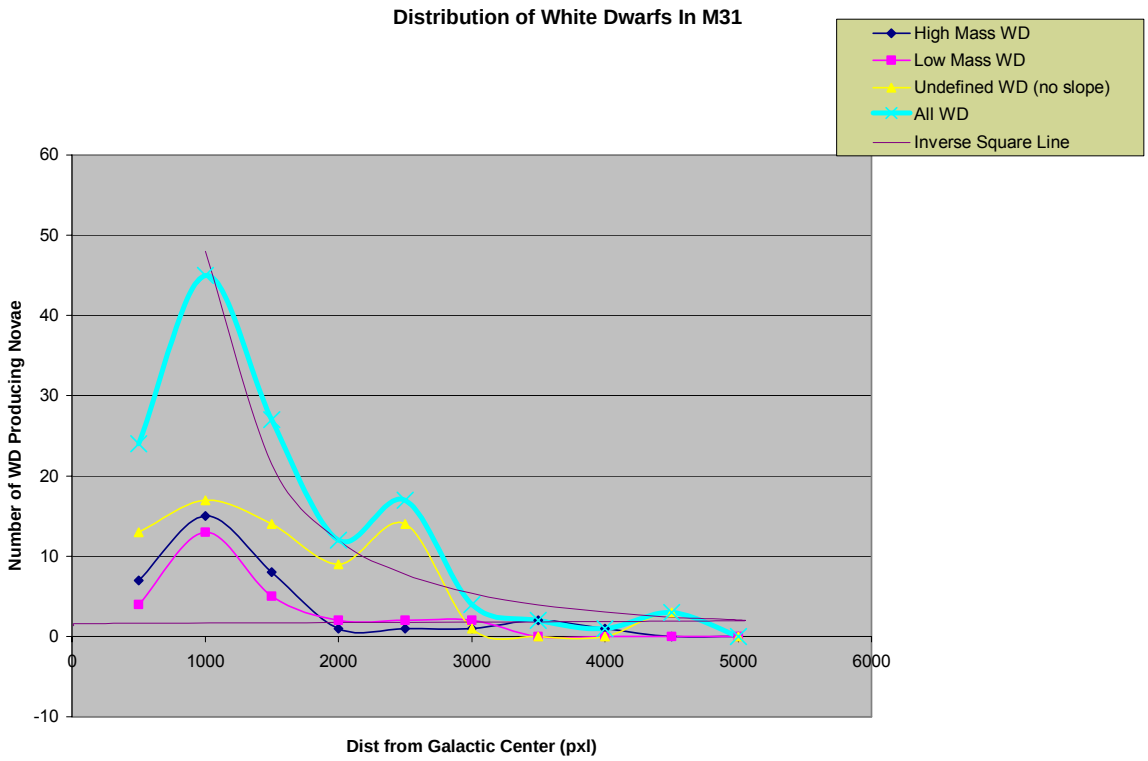

The overall pattern of distribution for both the high and low mass white dwarfs followed an inverse square relationship. When the white dwarfs for which no slope could be determined were added to the graph, an unexpected peak in the number of white dwarfs occurred between 2000 and 2500 pixels. To understand the reason for this, a series of scatter plots were made using the de-rotated and de-projected novae coordinates. The follow graph shows only those novae that had a light curve slope:

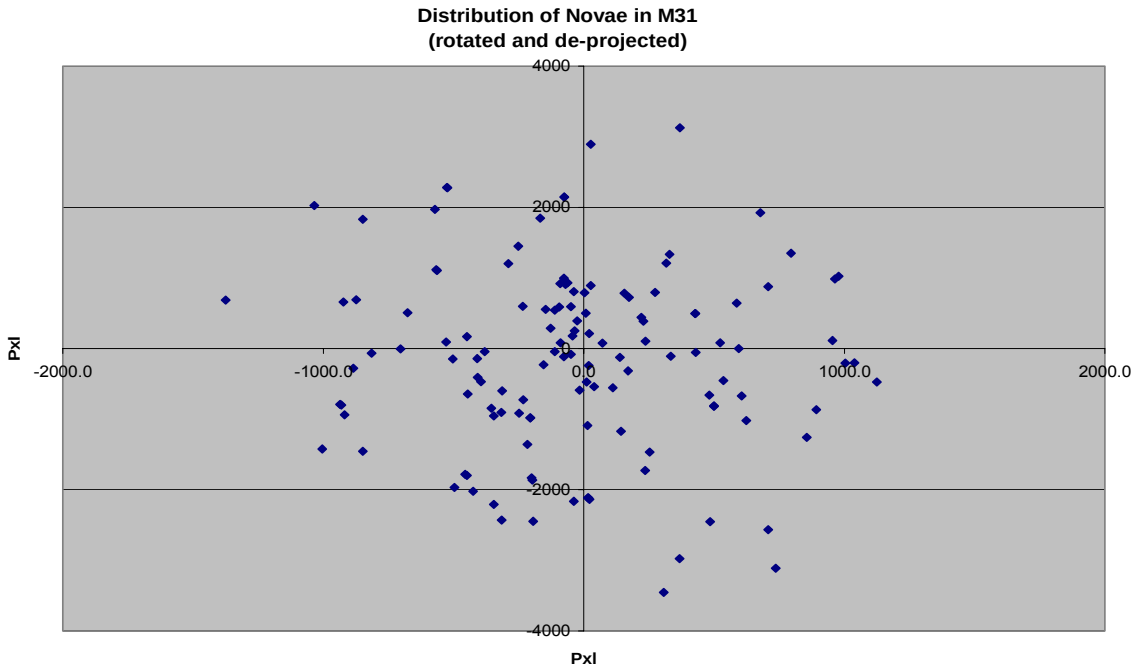

The scatter plot shows that the distribution of novae producing white dwarfs in the bulge of M31 is not completely random. Rather, there are large areas that have no novae at all. The novae themselves tend to be clustered into local groupings and chains that are elongated and curved. This suggests that the bulge contains star populations distributed in various age groupings. Perhaps the areas with no novae are areas with stars that are too old or too young to produce novae. Further, the shape of the groupings is somewhat suggestive of an underlying spiral arm structure within the bulge.

The scatter plot below shows the distribution of high and low mass white dwarfs, as well as those for which no light curve slope could be made:

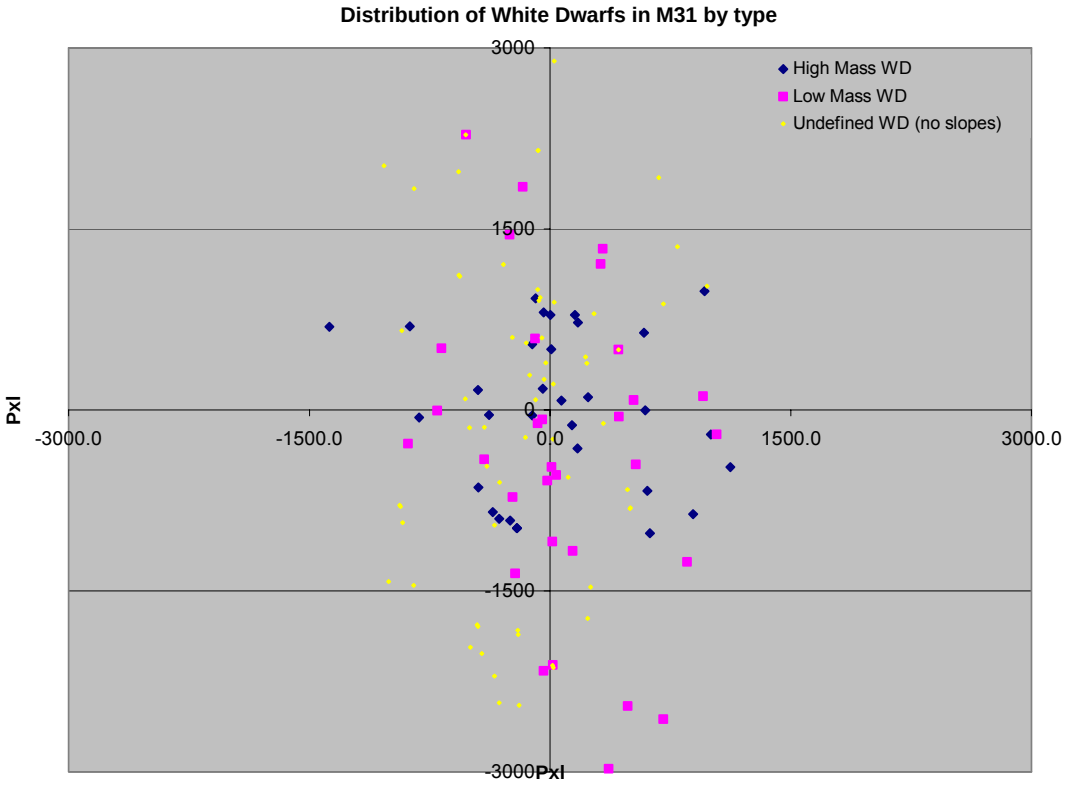

This plot shows the reason for the peak between 2000-3000 pixels in the distribution curve. The peak is due to groupings of low mass and undefined slope white dwarfs that cross the Y-axis at distances between 1600 and 3000 pixels above and below the galactic center. While the existence of the undefined slope white dwarfs cannot be proven, if they are real, then the distribution of novae above and below the galactic center is quite different than the distribution to the left and right of the center. The distribution pattern above and below the center seems to suggest spiral arms extending into the bulge from the disk.

The scatter plot also seems to indicate a tendency for high mass dwarfs to be located in clusters and chains near the galactic center, with lower mass dwarfs more uniformly distributed and farther from the center. This likely reflects differences in the ages of stars groupings.

CONCLUSION

An analysis of the data indicates that the distribution of white dwarfs that nova in the bulge of M31 follows an inverse square relationship. Both high and low mass white dwarfs follow this inverse square pattern. There does appear to be a slight preference for high mass dwarfs near the galactic center and a slight preference for low mass dwarfs farther away from the center. Scatter plots of these white dwarfs show that they are not randomly distributed, but tend to form local groupings of novae in the shape of curved bands or chains. Some of the groupings show predominance for either low or high mass white dwarfs

NEXT STEPS

Ten possible next steps were identified:

1) To determine the correlation of white dwarf masses with the percentage of possible progenitors on the main sequence.
2) To determine the distribution of white dwarfs within the disk of M31.
3) To compare the distribution of white dwarfs within the disk of M31 to the white dwarf distribution in other galaxies.
4) To determine the relative ages of stellar populations in M31 from the distribution of white dwarf progenitors.
5) One of the negative slope nova candidates needs further observation and analysis. It is located in Field 1 (00:43:20.37 +41:23:33.0) and first appears in Epoch 31. It continued to brighten for 637 days through Epoch 61, the last one in the study. This is an extremely long brightening period. Most novae brighten for only a few days or weeks. Is this really a nova? If so, will it have a similarly long-term decay? The star also exhibits several sharp spikes in brightness that look almost periodic. One possible explanation could be that it is an eclipsing binary.

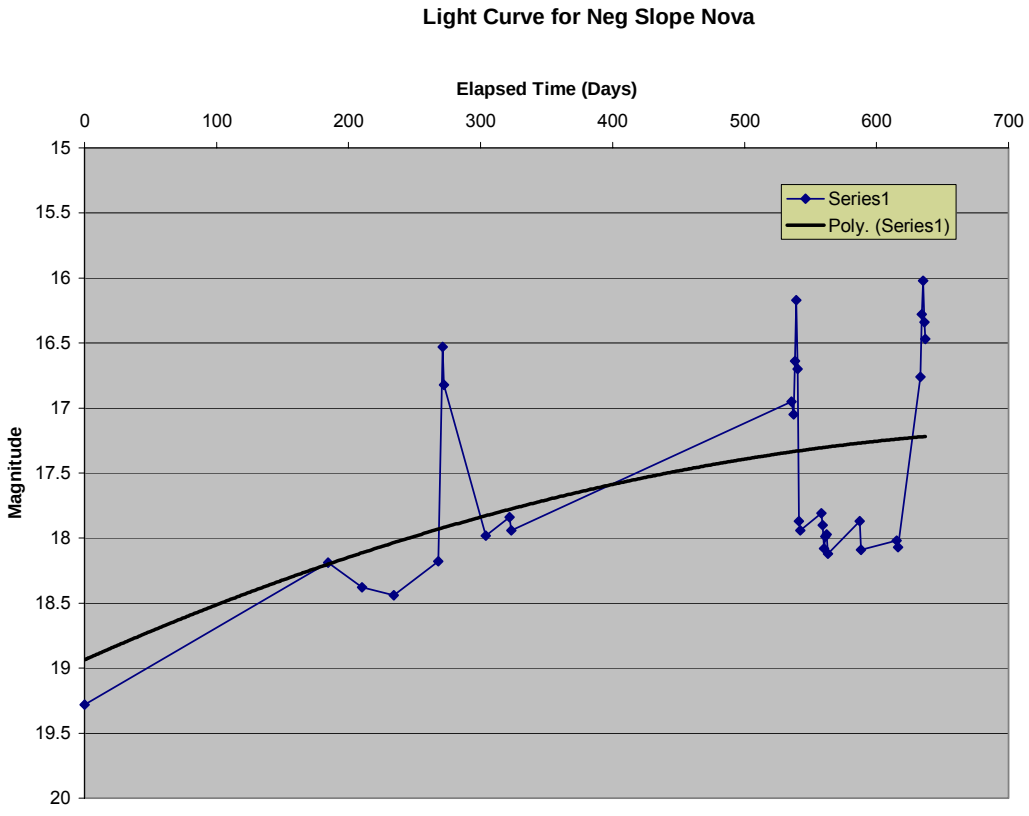

6) X-ray images of M31 covering the period of this study are available. Can the novae identified in the Kitt Peak images be correlated with X-ray events in the

Chandra files? Can additional novae be found in the X-ray files, perhaps from deeper into the bulge? Can decay slopes be determined from the X-ray events that can be correlated to the optical decay slopes?

7) As the M31 database continues to grow, can eclipsing binary pairs be identified from dips in the light curve of long-term novae? If so, could they be used to validate WD mass vs. light curve decay relationships?

8) As additional epochs are imaged and analyzed, can the hypothesis that distribution patterns of novae reflect the underlying spiral structure of the bulge be supported or refuted?

9) Can the indications that there is a slight preference for high mass white dwarfs nearer the galactic center be supported or falsified?

10) The literature suggests that M31 has a double nucleus. Will the pattern of novae also show this? One of the arc shaped groupings of novae appears to spiral in the opposite direction from other groupings - is this an indication that the nuclei rotate in different directions?

ACKNOWLEGEMENTS

Special thanks are due to Travis Rector, our mentor, and to Jeff Lockwood, our PI, who helped us through the research and report process.

Also, thanks also to Pat Knezek for her assistance and support at the 0.9m WIYN telescope.

In addition, thanks to the TLRBSE/NOAO staff, including Steve Pompea, Steve Croft, Connie Walker, Don McCarthy, Steve Howell, and Kathie Coil.

Finally, sincere thanks to the KPNO staff who accommodated us during our stay at Kitt Peak.

REFERENCES

Ciardullo, R., Ford, H. and Jacoby, G., *Ap. J.*, 272:92, 1983

Ciardullo, R., Ford,H.C., Neill, J.D., Jacoby, G. H., and Shafter,A.W.,*Ap. J.*, 318:520, 1987

Dopita, Jacoby, and Vassaliadis, *Ap. J.,* 389:27, 1992

Fraknoi, A., Morrison, D. and Wolff, S, *Voyages through the Universe,* 2nd Edition, 2000.

Hatano, K., Branch,D.,Fisher, A. and Starrfield, S., *Ap. J.*, 487:L45-L48, 1997

Rector, T., and Jacoby, G., "Nova Search: Cosmic Easter Eggs,*TLRBSE*, 2001.

Rector, T., personal communication, 6/30/03

Shafter, A.W., and Irby, *Ap .J.,* 563:749, 2001.

Weidemann, V. *Astronomy and Astrophysics,* 363:647, 2000.

APPENDICES

Appendix 1

IMAGE EPOCHS AND DATES

EpochDateTime13-Sep-956:13:56218-Jun-9710:38:22323-Jul-977:46:23424-Jul-978:49:12525-Jul-976:30:01631-Jul-977:44:2971-Aug-978:16:48818-Nov-978:10:1396-Jun-9810:35:051024-Jul-988:39:491125-Jul-987:19:571226-Aug-986:08:58135-Sep-988:21:211414-Oct-984:46:251530-Oct-985:29:471611-Nov-984:04:461727-Jan-992:30:091824-Jun-999:42:541920-Jul-997:57:522014-Jun-009:54:222117-Jul-009:05:342213-Sep-004:52:182314-Sep-008:55:422415-Oct-005:48:012510-Nov-003:11:112612-Jan-012:08:382715-Jan-011:47:55282-Nov-014:56:062922-Nov-016:12:133023-Dec-011:54:253125-Jun-029:45:343221-Jul-0211:23:383314-Aug-0210:12:503417-Sep-024:25:343520-Sep-026:32:473621-Sep-028:10:023723-Oct-023:58:213810-Nov-021:53:183911-Nov-021:31:55

40	11-Jun-03	10:27:09
41	13-Jun-03	10:27:15
42	14-Jun-03	10:01:44
43	15-Jun-03	10:33:40
44	16-Jun-03	10:16:52
45	17-Jun-03	10:43:08
46	18-Jun-03	10:37:19
47	4-Jul-03	10:08:18
48	5-Jul-03	9:30:54
49	6-Jul-03	8:28:09
50	7-Jul-03	8:31:30
51	8-Jul-03	8:27:06
52	9-Jul-03	11:09:51
53	2-Aug-03	8:46:38
54	3-Aug-03	8:05:31
55	30-Aug-03	8:13:59
56	31-Aug-03	6:47:56
57	17-Sep-03	7:32:52
58	18-Sep-03	6:48:34
59	19-Sep-03	7:26:13
60	20-Sep-03	9:01:27
61	21-Sep-03	6:24:40

Appendix 2

Novae in M31Mag H-AlphaElapsed Time (da)Slope (da/mag)FldEpochxyRADecMagtt/Mag632-3314247300 43 6.5341 16 33.217.19-17.1923.90.00135-362765 00:43:44.65 +41:27:00.815.92-16.441.01.88103-61945 00:43:03.41 +41:16:03.815.94-16.708.27.01122-737249 00:42:11.01 +41:13:18.417.94-18.0243.88.29162-78018200 42 08+41:08:14.7 16.57-20.1543.811.86610-1211944000 42 36.9441 16 55.516.40-18.2533.013.151111-12391486 00:42:20.56 +41:10;36.817.75-19.7532.016.00722-23107379 00:42:37.64 +41:17:38.517.59-17.671.316.811628-30315257 00:41:54.04 +41:07:23.6 15.22-18.1950.717.131018-192204200 43 01.7541 15 37.915.42-16.9025.617.321011-1249553 00:42:45.09 +41:15:31.015.87-17.5332.019.28732-397343100 42 39.6241 17 02.416.86-19.04112.921.28113-820112742:32.0+41:14:41.015.76-16.14118.123.571531-343584400 42 22.4841 09 48.516.43-19.7583.425.001118-1993159 00:42:38.54 +41:14:18.415.67-16.6325.626.69122-7381421 00:41:50:13 +41:11:20.719.02-19.8143.827.341153-61470364 00:42:15.74 +41:11:59.517.03-18.7450.027.53747-6151299 00:42:41.07 +41:18:31.717.41-17.7678.927.61628-317535000 43 17.21+41 17 56.816.8-18.17235.228.41710-16228473 00:42:30.39 +41:16:32.615.73-19.14110.029.57112-76731 00:42:40.10 +41:15:46.915.70-17.1343.830.201425-2729826800 42 57.06 +41 07 16.217.04-19.0766.131.98655-61496351 00:42:45.02 +41:17:52.616.79-17.4521.932.4652-837125 00:43:23.47 +41:21:39.217.33-18.89152.835.03614-16418452 00:42:49.82 +41:16.47.616.39-17.0428.138.771118-1993106 00:42:38.66 +41:14:57.818.14-18.7825.640.041513-1717147200 42 33.7741 04 57.415.01-18.41143.841.1461-820628700 43 02.5941 18 40.618.03-18.87807.042.28732-3423349400 43 00.9941 16 19.616.70-18.0557.742.5762-8501455 00:42:44.87 +41:16:48.817.10-18.83152.844.371031-32246373 00:43:00.19 +41:11:53.418.96-19.5325.745.16621-25505110 00:42:44.65 +41:20:42.116.14-18.62115.946.351433-39220360 00:42:30.80 +41:06:12.815.31-17.1989.047.831533-3922036000 42 30.7941 06 12.715.35-17.2389.048.2473-8411499 00:42:19.29 +41:16:12.615.71-18.18118.149.04632-3923249400 43 00.9941 16 19.616.70-18.64112.957.331631-39283158 00:41:56.1 +41:08:31.917.39-19.66138.757.911114-1736440500:42:28.4+41:11:07.116.79-18.56105.158.4669-1813533300 43 13.53+41 18 09.818.62-19.52383.258.661014-17472117 00:42:45.54 +41:14:48.616.01-17.790.059.621020-27470288 00:42:46.68 +41:12:51.417.11-18.76214.965.131040-61379196 00:42:52.14 +41:13:53.615.63-16.62101.565.601020-234588800 42 47.37+41 15 07.316.67-18.1692.166.301512-17510227 00 42 13.38 +41:07:41.416.03-18.26154.067.75734-3743748500 42 57.7241 16 25.616.19-16.6936.168.34108-10161100 00:43:05.27 +41:14:58.615.21-18.99247.970.08628-30463496 00:42:47.11 +41:16:17.716.27-16.9550.774.711128-30425306 00:42:18.41 +41:12:39.118.04-18.6750.786.6262-84411 00:43:12.39 +41:21:49.216.91-18.65152.887.21634-46437485 00:42:49.82 +41:16:47.616.13-19.85274.288.2259-1928719 00:43:28.58 +41:21:42.116.24-19.20408.891.051028-31195347 00:43:03.24 +41:12:10.715.63-18.03235.298.1858-1646783 00:43:17.71 +41:20:59.517.23-20.73357.9100.78722-264354 00:42:43.92 +41:17:55.517.37-18.83479.0103.91714-171129300 42 37.31+41 20 52.017.39-17.97105.1108.591528-305920500 42 40.5241 07 59.518.38-18.4150.7116.48143-1740922200 42 50.33 +41 07 47.817.22-19.29553.1156.041019-

214229100 42 49.59+41 15 05.016.58-17.95363.0161.541628-5625852
00:41:57.48+41:09:43.9 18.09-19.84666.8201.46231-61400314 00:42:50.93
+41:24:11.216.48-18.40452.6274.68112-10332272 00:42:24.05 +41:13:02.518.57-
19.35400.7299.51112-940517700:42:20.0 +41:13:58.718.66-19.40352.9446.52

Light Decay Curves with Negative Slopes

618-1917920900 43 09 91+41 19 38.217.40-17.2625.6-183.05130-61424371 00:43:20.37
+41:23:33.019.28-16.47637.1-100.95728-297635000 42 39.4041 17 56.120.83-
18.8019.9-9.811638-39255137 00:41:57.85 +41:08:45.318.29-16.981.1-1.22

Novae Appearing in Only Two Epochs (no slope)

Appendix 3

Probable Cosmic Rays, Hot Pixels and Artifacts

Appendix 5

De-projection Distances to Galactic Center for M31 Novae
Novae in M31?12.5Slope (da/mag)Galactic Rotated Cartesian CoordProjection Dist to Galactic Ctr LineDeproj Dist : Nova to Galactic Ctr (pxl)FldEpochxyRADect/Mag
x??x"y"R618-1917920900 43 09 91+41 19 38.2-183.05-448.8167479130-61424371
00:43:20.37+41:23:33.0-100.95-874.16921115728-297635000 42 39.4041 17 56.1-9.81-
38.98078081638-39255137 00:41:57.85+41:08:45.3-1.221003.7-2051025632-
3314247300 43 6.5341 16 33.20.00-316.6-903957135-362765 00:43:44.65
+41:27:00.81.88-1375.36891538103-61945 00:43:03.41+41:16:03.87.01-248.6-
917950122-737249 00:42:11.01+41:13:18.48.29586.7641869162-78018200 42
08+41:08:14.7 11.86892.8-8641243610-1211944000 42 36.9441 16 55.513.15-355.0-
8479191111-12391486 00:42:20.56+41:10;36.816.00606.6-672905722-23107379
00:42:37.64+41:17:38.516.813.37897891628-30315257 00:41:54.04 +41:07:23.6
17.131124.6-47512211018-192204200 43 01.7541 15 37.917.32-205.4-97910001011-
1249553 00:42:45.09+41:15:31.019.28-205.4-9791000732-397343100 42 39.6241 17
02.421.288.2502502113-820112742:32.0+41:14:41.023.57236.71042581531-343584400
42 22.4841 09 48.525.00623.3-102111961118-1993159
00:42:38.54+41:14:18.426.69170.8-318361122-7381421
00:41:50:13+41:11:20.727.34964.098413781153-61470364
00:42:15.74+41:11:59.527.53594.5-3594747-6151299 00:42:41.07+41:18:31.727.61-
89.9923927628-317535000 43 17.21+41 17 56.828.41-444.8-642781710-16228473
00:42:30.39+41:16:32.629.57156.5787802112-76731
00:42:40.10+41:15:46.930.2072.0761051425-2729826800 42 57.06+41 07
16.231.98307.7-34563470655-61496351 00:42:45.02+41:17:52.632.46-111.154355552-
837125 00:43:23.47+41:21:39.235.03-814.5-65817614-16418452
00:42:49.82+41:16.47.638.77-111.1-461201118-1993106
00:42:38.66+41:14:57.840.04138.4-1251861513-1717147200 42 33.7741 04
57.441.14737.0-3114320061-820628700 43 02.5941 18 40.642.28-379.7-42382732-
3423349400 43 00.9941 16 19.642.57173.372474562-8501455
00:42:44.87+41:16:48.844.37-43.61771831031-32246373
00:43:00.19+41:11:53.445.1617.6-21152115621-25505110

00:42:44.65+41:20:42.146.35-251.4145014711433-39220360
00:42:30.80+41:06:12.847.83302.2-401340241533-3922036000 42 30.7941 06
12.748.24707.3-2566266273-8411499 00:42:19.29+41:16:12.649.04317.212091250632-
3923249400 43 00.9941 16 19.657.33-232.6-7257621631-39283158
00:41:56.1+41:08:31.957.911038.7-20310581114-
1736440500:42:28.4+41:11:07.158.46535.7-45270169-1813533300 43 13.53+41 18
09.858.66-407.8-4115791014-17472117 00:42:45.54+41:14:48.659.6239.9-5415421020-
27470288 00:42:46.68+41:12:51.465.13142.9-117111801040-61379196
00:42:52.14+41:13:53.665.6014.6-109210921020-234588800 42 47.37+41 15
07.366.3011.1-4744741512-17510227 00 42 13.38+41:07:41.467.75855.4-12611523734-
3743748500 42 57.7241 16 25.668.34329.313331373108-10161100
00:43:05.27+41:14:58.670.08-216.6-13571374628-30463496
00:42:47.11+41:16:17.774.71-48.6-80941128-30425306
00:42:18.41+41:12:39.186.62523.48253062-84411 00:43:12.39+41:21:49.287.21-
676.7509847634-46437485 00:42:49.82+41:16:47.688.22-75.9-11313659-1928719
00:43:28.58+41:21:42.191.05-884.6-2809281028-31195347
00:43:03.24+41:12:10.798.18-38.6-2164216458-1646783
00:43:17.71+41:20:59.5100.78-703.1-5703722-264354 00:42:43.92+41:17:55.5103.91-
93.5589596714-171129300 42 37.31+41 20 52.0108.59-167.6184818561528-305920500
42 40.5241 07 59.5116.48485.1-24542502143-1740922200 42 50.33+41 07
47.8156.04367.4-297429971019-214229100 42 49.59+41 15 05.0161.54-15.6-
5875871628-5625852 00:41:57.48+41:09:43.9 201.46954.1114961231-61400314
00:42:50.93+41:24:11.2274.68-522.822792338112-10332272
00:42:24.05+41:13:02.5299.51429.0-56433112-
940517700:42:20.0+41:13:58.7446.52428.74976571244164282
00:42:03.28+41:12:54.7707.38791128128296255
00:41:55.38+41:13:11.5795.213511567128398423
00:41:49.22+41:11:17.8978.71025141712827985
00:41:56.34+41:15:08.6677.819242040111249223 00:42:29.04+41:13:35.4333.4-
112352112023360 00:42:30.05+41:15:26.8221.0439491112532231
00:42:24.70+41:15.45.8273.779684211133338
00:42:42.0441:12:12.2.428.7497657111123274
00:42:30.21+41:15:19.2228.838544811815164 00:42:43.22+41:14:15.3112.2-
55756811176406 00:42:43.80+41:11:29.4253.0-146714891131294408
00:42:26.35+41:11:29.4482.1-661818101470440 00:42:46.67+41:11:06.5235.8-
17271743109109198 00:43:18.63+41:18:23.9-197.8-186218731011287140
00:42:57.68+41:14:37.919.0-242243103135301 00:43:12.80+41:12:42.3-193.3-
244824561032247379 00:43:00.13+41:11:50.022.1-213421341019112191
00:42:03.41+41:16:03.8-199.7-182818391054244372 00:43:00.20+41:11:53.315.4-
2117211791137133 00:43:23.51+41:15:44.4-496.5-1966202791194409
00:43:40.23+41:11:28.7-485.7-41234151911453223 00:43:18.56+41:13:34.7-315.4-
24292449911459167 00:43:18.19+41:14:13.1-344.9-2207223493142927
00:43:20.00+41:15:48.4-454.3-1780183793142086 00:43:20:55+41:15:09.0-425.3-
2021206593243133 00:43:19:90+41:15:44.8-449.0-1796185181194202
00:42:01.49+41:19:38.2369.03128315073131429 00:42:42.26+41:17:03.6-
26.239139273140380 00:42:41.71+41:17:37.5-49.159659873165314

00:42:40.19+41:18:21.8-69.790791073174315 00:42:39.69+41:18:21.0-61.9929931731140376 00:42:35.65+41:17:39.927.689389373171294 00:42:39.81+41:18:35.9-77.1998100171922598 00:42:30.55+41:20:49.3-75.121492150715447 00:42:43.84+41:16:50.8-35.825225472822598 00:42:30.55+41:19:25.1-75.12149215073045488 00:42:41.43+41:16:20.220.921521671140433 00:42:19.69+41:21:30.826.728932893517174111 00:43:35.40+41:20:38.9-917.8-936131152160242 00:43:36.21+41:19:11.1-848.7-1454168453117975 00:13:35.14+41:21:05.5-935.8-790122553218280 00:43:34.9+41:21:01.3-930.4-800122751141141 00:43:43.47+41:20:20.0-1004.6-14211740631360457 00:42:53.27+41:16:44.5-153.9-22827561112464 00:43:08.24+41:16:39.7-345.8-955101562106173 00:43:08.62+41:19:57.7-528.59253762450385 00:42:47.88+41:17:32.5-126.728931661195230 00:43:09.33+41:19:19.7-502.4-147524611138351 00:43:06.72+41:17:57.6-394.4-468612611170287 00:43:04.79+41:18:40.8-408.2-144433611406266 00:42:50.59+41:18:55.8-234.3600644611442128 00:43:08.24+41:16:39.7-290.212061240611452443 00:42:47.69+41:16:53.9-89.783122611469327 00:42:46.66+41:18:13.6-147.2555574612-1318442300 43 03.9341 17 07.7-313.9-60167842116339 00:42:06.19+41:23:53.178.042784279428189433 00:42:01.68+41:22:49.4193.2414141462184192 00:43:09.91+41:25:33.5-847.418322019231211486 00:43:02.29+41:22:14.6-567.211161252231213490 00:43:02.17+41:22:11.0-563.111071242231322337 00:42:55.51+41:23:55.5-570.519752055231398312 00:42:50.97+41:24:12.8-525.62281234011147445 00:43:17.29+41:27:13.4-1033.920252274132381347 00:43:22.83+41:23:48.1-922.86581133118-9371339 00:42:21.73+41:12:16.2500.9-19153672-330282 00:42:42.48+41:18:40.7-116.9926933612-1318442300 43 03.9341 17 07.7-313.9-601678

Distribution Of Rapidly And Slowly Decaying Novae In M31

Jeff Adkins, Deer Valley High School, Antioch, CA – TLRBSE 2002
Robert Carroll, Lexington High School, Lexington, SC – TLRBSE 2002
Anthony Maranto, Phillips Exeter Academy, Exeter, NH – TLRBSE 2002
Joy Martin, St. Mary's School, Fullerton, CA – TLRBSE 2002
Debbie Michael, North Lincolnton High School, Lincolnton, NC – TLRBSE 2002
Betty Paulsell, Pioneer Ridge Science Ed Center, Independence, MO – TLRBSE 2002
Robert Quackenbush, Riverside High School, Durham, SC – TLRBSE 2002
Steve Rapp, Linwood Holton Governor's School, Abingdon, VA – TLRBSE 2002
Jeff Sayers, Northview High School, Brazil, IN – TLRBSE 2002

ABSTRACT

Images of M31 taken over time reveal the presence of frequent novae distributed over the entire area of the galaxy. When a nova explodes, it gets brighter quickly and then dims slowly over time. The rate of dimming is referred to as the decay rate and is the variable investigated in this study. It was hypothesized that the position of the novae from the center of the galaxy may have an effect on the rate of decay of the light curve of the novae. Decay curves may be affected by the composition, age, and hence position of the novae within the galaxy since the core of the galaxy is composed of older stars than the disk.

Novae found in images from five years of observations of M31 were analyzed for novae decay rates. The position of the novae in the galaxy was measured. These variables were plotted against each other to determine if a correlation between them existed.

No relationship was found in the sample measured. Possible explanations and next steps are discussed.

BACKGROUND

M31

The Andromeda Galaxy, also referred to as M31, is approximately 2.2 million light years away. It is the closest large spiral galaxy to our Milky Way Galaxy. The Hubble Space Telescope has revealed that M31 has a double nucleus.

Novae

"Nova," the Latin word, means "new star". This came from ancient civilizations that thought of this event as the creation of a new star, which was thought of as an omen. A nova which occurred in 134 BC was the first known new star (nova).

Stars near the end of their lives cause novae. A nova can occur in a binary system in which a main sequence or red giant star has a close white dwarf companion. The strong gravitational field of the white dwarf pulls gas from the atmosphere of the companion star. As material builds up on the outer surface of the white dwarf, the pressure and temperature increase at the base of the deposited layer. The temperature increases to the point at which nuclear reactions ignite explosively, ejecting much of the deposited material. The brightness of the star increases dramatically by 8-15 magnitudes during a short time interval. After peak brightness is reached the nova declines to near its original

brightness over a few days to a few months. A slow nova may take 150 days or more before experiencing a decline in brightness. The fast nova displays a brightness that lasts only a few days and shows a steep decline in brightness (as shown by slope in a graph of magnitude vs. time). A very slow nova may take years to fade. The AAVSO (American Association of Variable Star Observers) defines the division between fast and slow novae as thirty-seven days per magnitude.

Up until 1900, a total of 161 novae were discovered. Due to new technology, the number has more than doubled in the years since 1900. With new advanced techniques, the number of novae will continue to increase significantly. For example, more than 300 novae have been discovered since 1917 in M31.

Differences In Novae By Location

There have been many views as to where the most novae develop in a galaxy. According to Hatano, Branch and Fisher (1997) most M31 novae come from the disk population, rather than the bulge population. Their results indicate that the M31 bulge-to-disk nova ration is as low as, or lower than, the M31 bulge-to disk mass ratio. Based on observation, Della Valle et al. (1994) concluded that bulge-dominated galaxies such as M31 have a nova rate per unit *H*-band luminosity that is more than a factor of 3 lower than that of nearly bulgeless galaxies such as M33. Both of these cited papers has led to a point of view that young populations produce more novae than old populations.

The other view of Sharov, Alksnis, Zharova and Shokin (1999) indicated that more novae are produced in the bulge of M31 than the arms. Exploiting the ability of CCDs to detect novae against the bright nuclear background, Ciardullo and collaborators (Ciardullo et al, 1990) established that the radial distribution of novae follows that of the buldge light to the center of the M31 Galaxy. Shafter and Irby (2001) suggest that ~70% of the novae arise from the bulge.

Hypothesis

Based on the differences in stars in the bulge of M31 compared to the disk of M31, it seems plausible that there may be differences in the characteristic decay curve of the magnitudes of individual novae. This project investigates whether or not the position of a nova within M31 is correlated to the rate of decay of the light curve.

Procedure

This study involved searching for novae in the Andromeda galaxy. Twenty-seven epochs of data of the central region of M31were looked at during this project (Table 1).

TABLE 1

EPOCH NUMBER AND DATES

Epoch Number	Date
E1	3 Sep 1995
E2	18 Jun 1997
E3	23 Jul 1997
E4	24 Jul 1997
E5	25 Jul 1997
E6	31 Jul 1997
E7	1 Aug 1997
E8	18 Nov 1997
E9	6 Jun 1998
E10	24 Jul 1998
E11	25 Jul 1998
E12	26 Aug 1998
E13	5 Sep 1998
E14	14 Oct 1998
E15	30 Oct 1998
E16	11 Nov 1998
E17	27 Jan 1999
E18	24 Jun 1999
E19	20 Jul 1999
E20	14 Jun 2000
E21	17 Jul 2000
E22	13 Sep 2000
E23	14 Sep 2000
E24	15 Oct 2000
E25	10 Nov 2000
E26	12 Jan 2001
E27	15 Jan 2001

Images from the .9 m, 1.3 m and 2.1 m telescopes on Kitt Peak were examined. The images were taken with a "Hydrogen Alpha" filter, which only transmits light of 656.3 nm wavelength. Since the original images were large- 2048 x 2048 pixels, each image was divided into 16 subraster images of 512 x 512 pixels. The 16 subraster images used were f01 through f16. The naming convention for the images is "m31eXXfYY", where "XX" is the epoch number and "YY" is the field number (Rector, 2001). The field number corresponds to one of the subrasters shown above; it is a number between 1 and 16. Table 2 shows the M31 fields. The epoch number indicates when the observation was completed. Currently there are 27 epochs of observations available for M31 on the RBSE CD ROM.

TABLE 2
ANDROMEDA FIELDS

1	**2**	**3**	**4**
5	**6**	**7**	**8**
9	**10**	**11**	**12**
13	**14**	**15**	**16**

The subraster images were divided among the members of the research group. Scion Image software was used to stack the images from a single field. The stacked images were then animated and examined for the occurrence of nova. If any novae were discovered coordinates were recorded. The magnitudes of known standard stars were input into the software program. From that information the magnitudes of the novae were determined. Magnitude decay curves for discovered novae were created using Vernier Graphical Analysis. The slopes of the decay portion of the light curves were then calculated using the auto curve fit function in Graphical Analysis. Brightness of the novae was plotted on the y-axis and dates of the novae were plotted on the x-axis. Epochs were translated into Julian dates. Light curve slopes were compiled for the inner area of M31 (subrasters 6, 7, 10, 11). A separate compilation of light curve slopes for the outer portion of Andromeda (the remaining subrasters) was made. This was done so that a comparison of light curve decay between the inner portion and the outer portion of the galaxy could be made.

Coordinate transformation of M31 images to determine radial nova distances

In order to determine the relationship between the distance of a nova to the center of M31 and the rate of its light curve decay, the distance of the nova from the center of the galaxy was computed.

The center of the galaxy was defined to be the center of the subraster grid, specifically the corner in common between subrasters 6, 7, 10 and 11. The subrasters are already rotated and aligned with the equatorial coordinate system (Right Ascension and Declination). Each subraster is 512 by 512 pixels and every pixel is given a coordinate using x and y coordinates starting in the upper left hand corner of each subraster, increasing to the right for positive x and down for positive y. X and Y coordinates were reset to (0,0) in the upper right corner for each subraster.

A series of transformations of these coordinates was performed to take each nova's x and y coordinates and convert it into a system, which allowed the calculation of the distance of the nova in the center of the galaxy. This involved basically four steps:

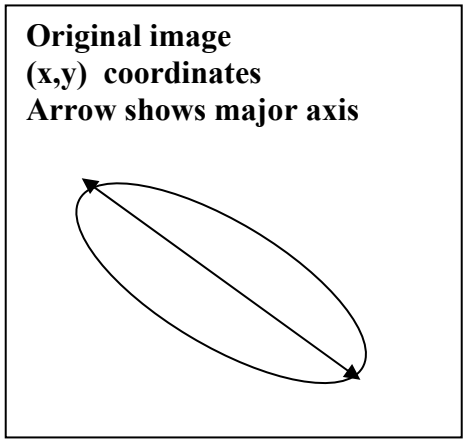

1) Conversion of the x,y pixel coordinates into standard Cartesian coordinates with 0,0 defined to be in the center of the subraster grid.
2) Rotation of the coordinate system to be aligned with the "major axis" of M31. The "major axis" is shown at left.
3) De-projecting the elliptical shape of the galaxy to make it circular.
4) Computation of the distance of the nova from the center of the de-projected, rotated coordinate system.

Figure 1 – Axes Of The Andromeda Galaxy

Step 1. Shifting the coordinate system is relatively trivial and involves combining the subraster coordinates and shifting the origin, plus reversing the direction of the y-axis by changing the sign of the y coordinates. For example, (0,0) in subraster 2 becomes the point (-512, 1024) in the new system because it is -512 pixels in the y direction from the x-axis and 1024 pixels from the y-axis.

Step 2. This involves determining the (r,θ) position vector of each nova with respect to the center of the coordinate system, then adding 37.7 degrees to account for the tilt of M31 with respect to the celestial equator (Simien, 1978).

Figure 2 – First Step In Rotation And Deprojection Of The Novae Locations

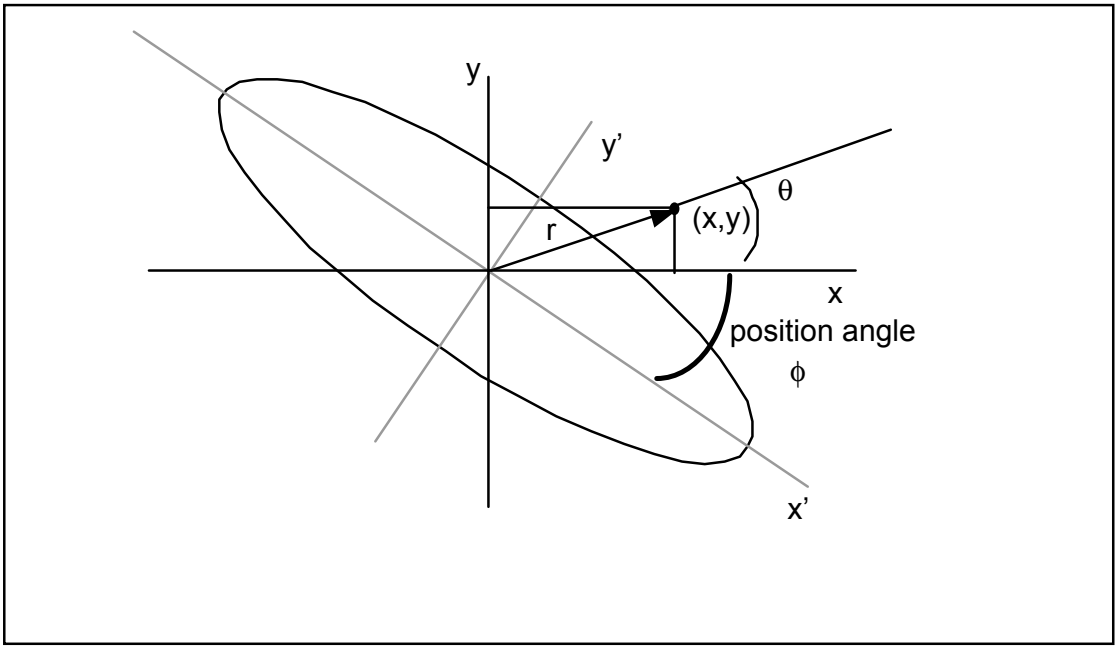

To do this, the x,y coordinates were found and the following formulas used.

$$r = \sqrt{x^2 + y^2}$$

$$\theta = \arccos\left(\frac{y}{r}\right)$$

In cases where y is negative, theta is greater than pi radians, so pi was added to theta.

Next, the position angle (ϕ) of the major axis of the galaxy was added to each theta. The position of each nova was computed in the rotated coordinate system using these formulas:

$x' = r \cos(\theta + \phi)$
$y' = r \sin(\theta + \phi)$

Figure 3 – Primed Coordinates In The Rotated Reference Frame

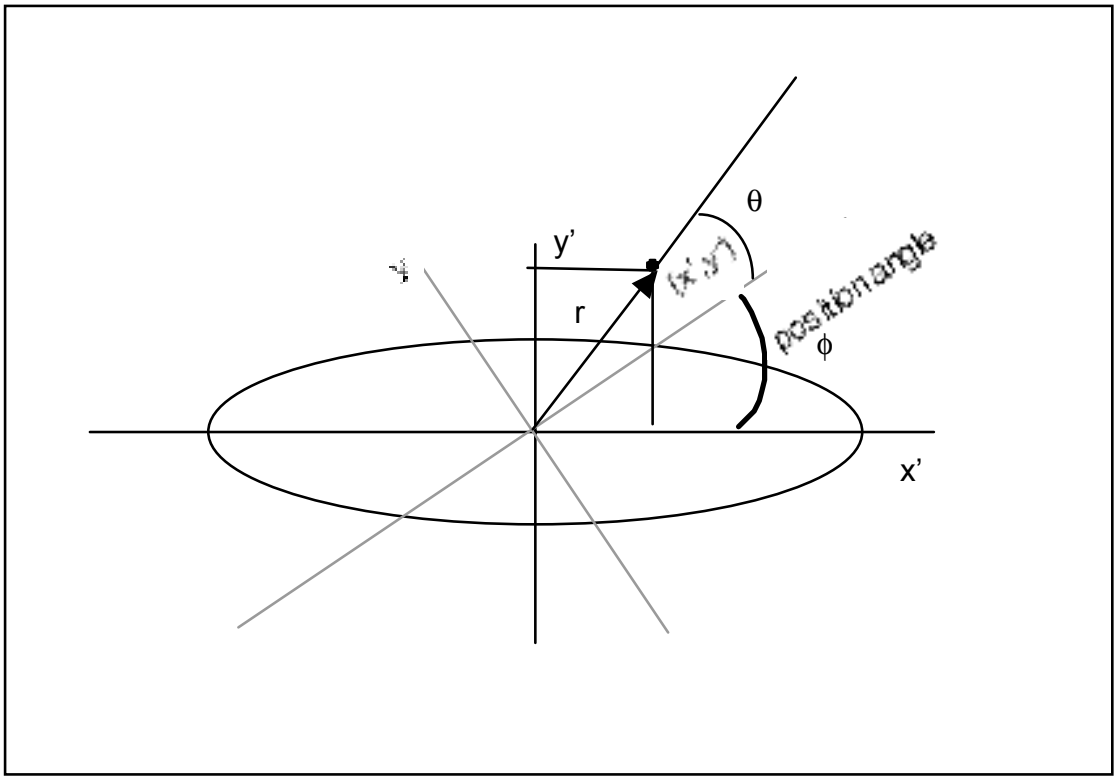

In effect, the image was rotated 37.7 degrees and the x, y coordinates were recalculated. The prime indicates the rotated coordinate system. The figure shows the approximate appearance of the galaxy after rotation.

Step Three. Next, the coordinates need to be de-projected. M31 is tilted 12.5 (de Vaucouleurs, 1958) degrees with respect to our line of sight. If it were not tilted with

respect to our line of sight, it would be an edge-on galaxy; if it were tilted 90 degrees, it would be a face-on spiral.

To de-project the coordinates, this formula was used:

y' /y" = sin δ,

Figure 4 – Geometry For Deprojecting Y-Coordinate

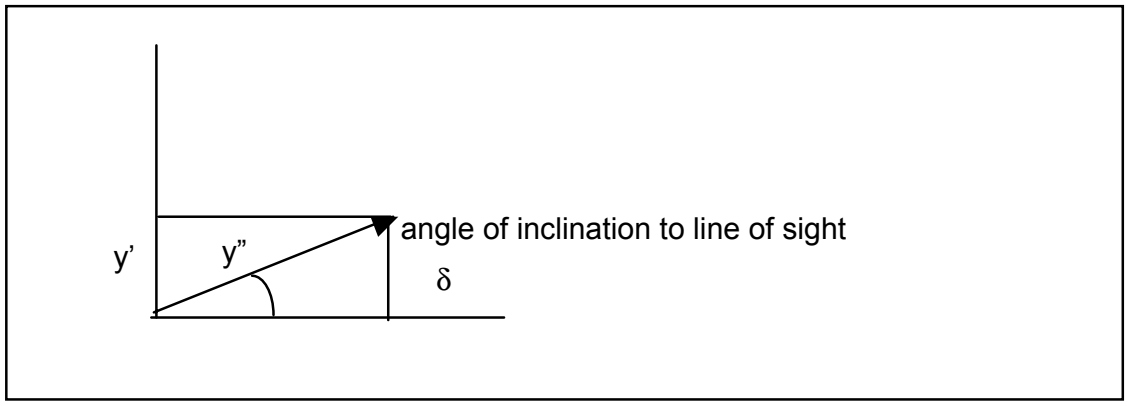

Where δ is the angle with respect to the line of sight, y ' is the rotated coordinate, and y" is the rotated and de-projected y- coordinate.

Since the galaxy is symmetrical along the x-axis (one side is not appreciably larger than the other as viewed from earth is) the x projection is unnecessary. In other words, x' = x" and does not require de-projecting.

This leaves the coordinate of each nova in the rotated, de-projected coordinate system as (x",y").

Step Four. The final step is to determine the distance of each nova from the center of the coordinate system by using the Pythagorean Theorem again on the new coordinates using this formula:

$$r'' = \sqrt{(x')^2 + (y')^2}$$

This is the value used to generate the distance vs. decay curve graphs.

RESULTS

Twelve novae for which light curves could be determined were studied. The locations of these novae were rotated and deprojected to determine their distances from the center of M31 as shown in Table 3 below.

TABLE 3

Coordinate Transformations to Rotate and Deproject Novae Positions

	IP Software coordinates		Rotated & Deprojected		distance of nova from center of M31	
nova	x	y	x"	y"	(pixels)	r"
f05n01	291	535	-879.00	-283.41	923.56	
f06n01	1012	623	-254.72	1432.00	1454.48	
f06n02	644	840	-413.19	-401.01	575.79	
f07n01	1143	952	50.13	599.43	601.52	
f07n02	1253	982	155.51	800.55	815.52	
f10n01	982	1313	209.96	-937.81	961.03	
f11n01	1388	1429	-40.34	-2508.97	2509.30	
f11n02	1224	1150	-81.19	-1025.69	1028.90	
f11n03	1091	1055	-34.05	-302.63	304.54	
f14n01	812	1806	645.95	-2259.72	2350.23	
f15n01	1199	2012	465.72	-4106.21	4132.53	

The locations of the twelve studied novae are plotted in Figure 5 and their derotated locations are shown in Figure 6.

Figure 5 – Location Of Twelve Studied Novae As Recorded In Original Image

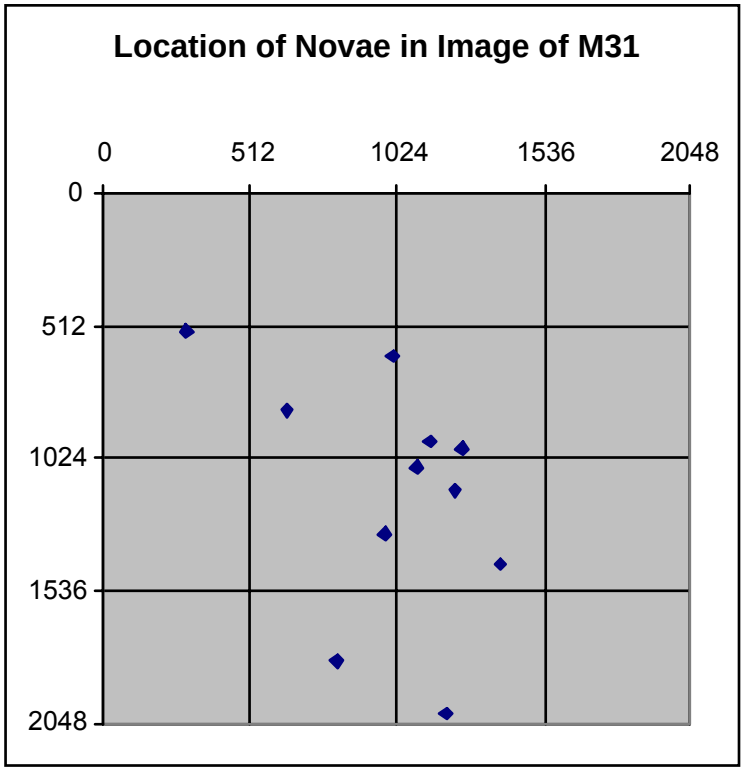

Figure 6 – Rotated And Deprojected Locations Of Studied Novae In M31

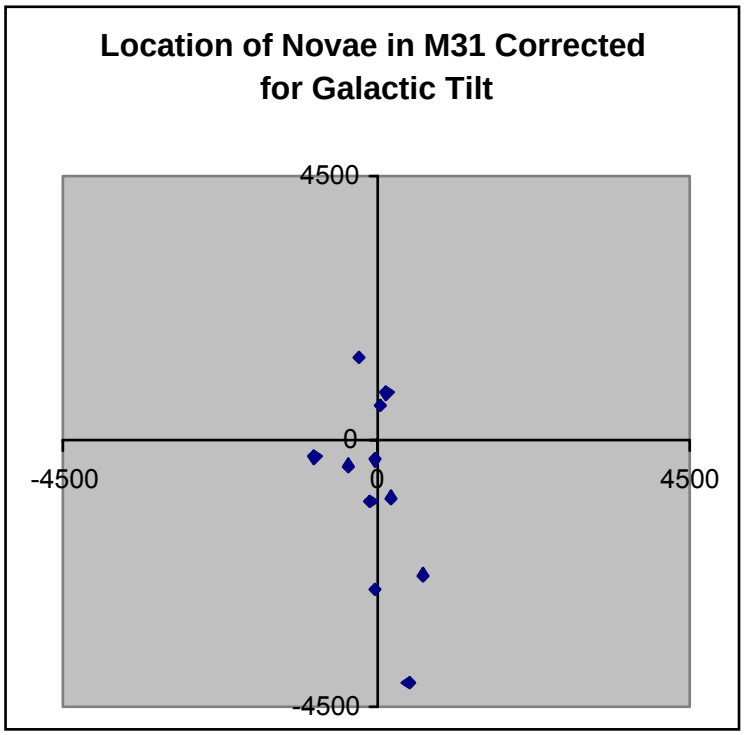

The light curves for the twelve studied novae are plotted in Figure 7 below. The slopes of these curves are listed in Table 4. The range of the novae decay rates was between 12 and 225 days/magnitude. By the previously quoted AAVSO definition of the division between fast and slow novae we detected four fast novae and eight slow novae. Figure 8 is a plot of the relationship between the decay of magnitude and distance from the center of M31.

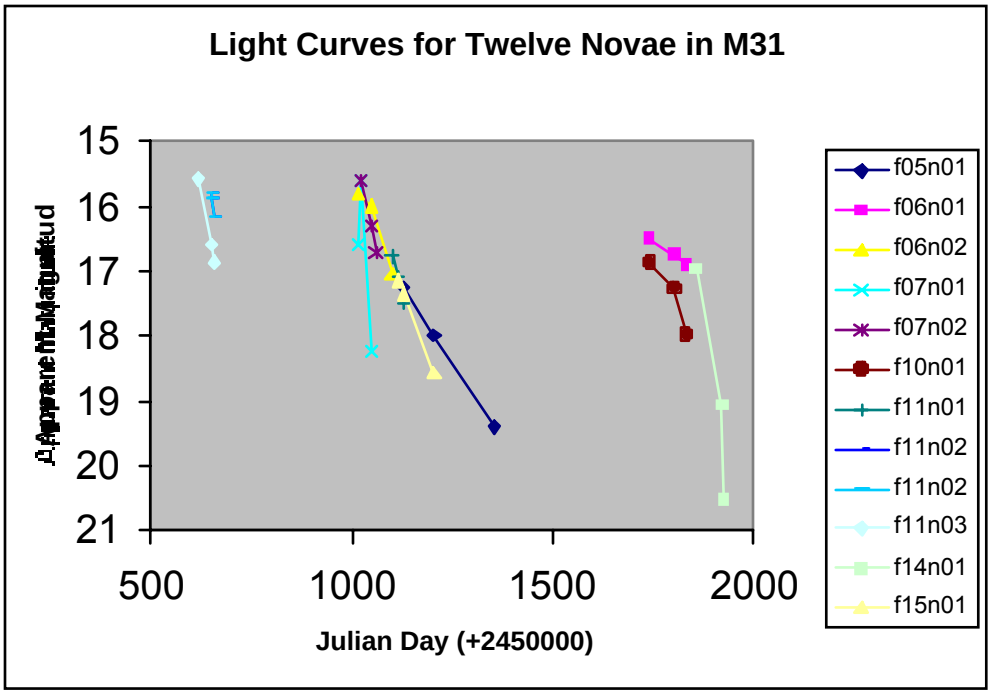

Figure 7 – Light Curves For Twelve Novae In M31

Table 4

Decay Rates for Studied Novae

Nova:	R.A.	Dec.	Decay Rate (Julian days/mv):	Mean Squared Error:
f05N01	00:43:28	+41:21:40	105.1	1.19e-6
f06N01	00:42:45	+41:20:41	225.8	9.86e-6
f06N02	00:43:07	+41:18:18	78.9	3.57e-2
f07N01	00:42:37	+41:16:56	12.2	7.10e-29
f07N02	00:42:30	+41:16:36	39.1	2.73e-3
f10N01	00:42:47	+41:12:51	138.3	4.54e-2
f11N01	00:42:22	+41:11:32	38.8	2.08-3
f11N02	00:42:32	+41:14:42	28.6	3.19e-3
f11N03	00:42:40	+41:15:47	34.5	1.40e-2
f14N01	00:42:56	+41:07:16	22.4	2.80e-1
f15N01	00:42:33	+41:04:55	63.2	154e-4

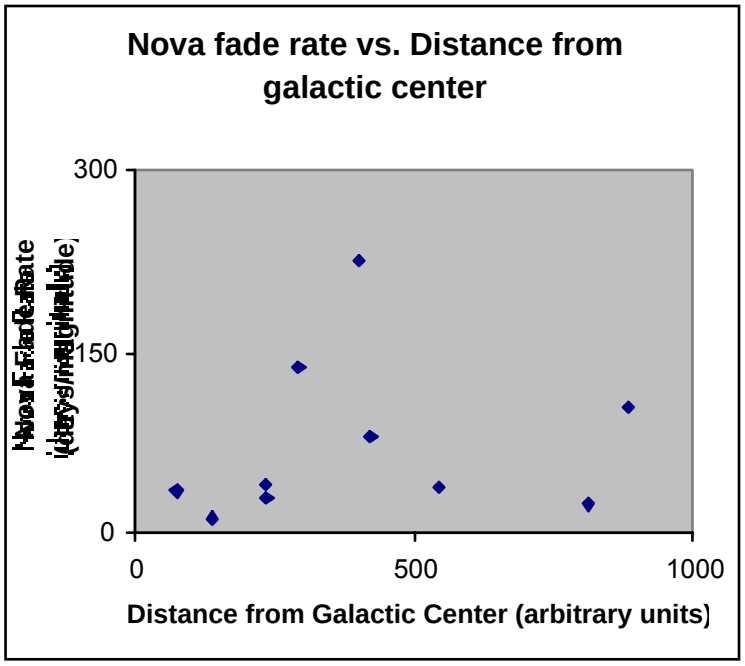

Figure 8 – Novae Fade Rate Vs. Distance From Galactic Center

CONCLUSION

Based on the final graph, no relationship was seen between the position of novae in M31 and the rate of decay of the light curves. There are several possibilities for why no relationship is seen. It is possible that there is no intrinsic difference between the novae, which implies that the hypothesis is not proven. The age and metallicity of the progenitor stars which produce novae, and hence their position in the galaxy, does not cause a change in the decay rates. Yet decay rates differ as shown by this data and background references. It could be that other variables, such as the spectral class of the star, are more important in determining decay rates.

There may be flaws in the methodology in selecting and measuring novae. The sample was limited by the procedure for selecting candidates in those extremely slow novae would not necessarily have been detected. Sequential epochs were used which were not necessarily separated by long periods of time. Also, there were extended gaps in the epochs by date that may have caused the overlook of extremely short novae. The measurements concentrated on later epochs and may have missed novae in earlier epochs.

NEXT STEPS

Our results suggest at least two different approaches that may result in more definitive results. The existing epochs, plus any later ones generated for the TLRBSE program, should be examined more carefully for both long and short term novae to get additional data.

Another possibility is that there are other variables besides metallicity, age, and location, which affect decay rate. If the nova remnant can be detected and spectra collected, then

other variables could be investigated. This will obviously take a larger telescope than those previously used for this work.

ACKNOWLEDGEMENTS

We would like to express our gratitude to the following organizations and people who have helped us in our endeavors with this project.

NSF (National Science Foundation)

NOAO/TLRSE (National Optical Astronomy Observatory/Teacher Leaders in Research Based Science Education)

U of A (University of Arizona)

KPNO (Kitt Peak National Observatory)

WIYN (Wisconsin Indiana Yale NOAO Consortium)

REFERENCES

Ciardullo, R., Shafter, A. W., Ford, H. C., Neill, J. D., Shara, M. M. and Tomaney, A. B. 1990, ApJ, 356, 472

De Vaucouleurs, G., 1958, AsJ, 128

Hatano, K., Branch, D. and Fisher, A., 1997, ApJ, 487, L45

"M31", search. Netscape.com/nscp_results.adp?source+NSCPTop&querry=M31, July 22, 2002

Rector, T. A. and Jacoby, G. H., "Nova Search: Cosmic Easter Eggs", TLRBSE, 2001

Shafter, A. W. and Irby, B. K., 2001, ApJ, 563, 749

Sharov, A. S., Alksnis, A., Zharova, A. V. and Shokin, Y. A., 2000, AsL, 26:7, 433

Simien, F., et.al. , 1978, Astronomy and Astrophysics, A&A, 67, 74

Spitzer, R., "Do Novae Repeat ? A Study of Novae Discovered in M31 Between the Years 1090-2000, 2000, The RBSE Journal, 26

"Variable Star of The Month, May 2001: Novae", www.aavso.org/vstar/vsotm/0501.stm, July 22, 2002

Novae Characteristics With Respect To Distance From The Center Of M31

Mary Margaret Callahan, Seattle Girl's School, Seattle, WA – TLRBSE 2004
Richard Smith, Buena High School, Ventura, CA -- TLRBSE 2004
Sharon Price, Kalaheo High School, Kailua, HI – TLRBSE 2004
Shayne Zurilgen, Brookside School, Stockton, CA – TLRBSE 2004

ABSTRACT

Prompted by the interest to understand more about planetary nebula and the possibility of using novae as distance indicators, research has been conducted to identify characteristics of novae and relationships of those characteristics. This study simplifies this research by investigating specific characteristics of novae identified in the Andromeda Galaxy (M31). The characteristics specifically measured were the decay rate of novae, the extinction time of novae and the maximum magnitude of novae as related to their distance from the center of M31. Images of M31 were produced using the NOAO .9m telescope at Kitt Peak. Data recorded from previous studies through the TLRBSE program was considered for this study. The hypothesis was that there would be a relationship between the distance of a nova from the center of the galaxy with other common characteristics such as magnitude, decay rate and extinction time.

The images were analyzed using ImageJ software to identify and then determine position of novae which could be confirmed for more than at least one epoch. Then magnitudes of these novae were measured using the MIRA software and the known magnitudes of standard stars. Using calculations to measure distance and the slope of the decay rate, a graph was created that suggested that there was a weak, but statistically insignificant, relationship between decay rate and position of a nova. There was also little to no relationship identified between extinction time or maximum magnitude and the position of a nova from the center of the galaxy. An interesting observation of the graphs led to the observation that there may be different populations of nova and the use of binning of this information suggests the possibility of such a relationship. The data available was limited, reducing the ability to confirm this relationship and it is suggested that further study be completed to come to a firm conclusion. Also, because the areas of study only included one field rather than the whole area of M31, the results may not be complete. Systematic errors included the inability to measure true distance using three dimensional positioning and the assumption of linearity of decay rates.

BACKGROUND KNOWLEDGE

White dwarfs are the most common stars in a galaxy. They are important because they are old stars that began their lives as medium mass stars similar to our sun. These stars fused hydrogen to helium but did not fuse carbon. They then drove away their outer layers into planetary nebula, leaving behind a carbon and oxygen core (Seeds, 2003). Novae occur in binary systems between a white dwarf and a red giant. They are identified by a sudden bright flare in a star field which then slowly dies out. These sudden flares occur as a result of hydrogen gas being pulled off of the neighboring red giant and accumulating on the surface of the white dwarf. Pressure from this gas raises

its temperature until fusion occurs, blowing away the layer of accumulated hydrogen gas. Because of their increase in brightness and their emission of x ray wavelengths, novae can be identified. They are found in areas that Cepheids are not, which make these objects possible tools of distance indicators (Ciardullo *et al*, 1990).

Novae vary in terms of how brightly they flare (maximum magnitude), how fast they die out (decay rate), and how long they last after reaching maximum brightness before disappearing completely (extinction time). The detection threshold for novae is roughly 19th magnitude in H-alpha (Rector, et al, 2000).

Livio (1997) reports that more massive white dwarfs result in more energetic and faster decaying nova and Camacho and Miller (2001) find that brighter novae have faster decay rates. In contrast Ciardullo (1990) found no correlation between magnitude and decay rate. According to Della Valle (1994), older star populations result in smaller white dwarfs. Older stars are characteristic of the centers of spiral galaxies. Green (2003) reports no difference in magnitude between novae in the galactic center and those from the outer edge. In addition, Clark (2003) states no relationship exists between nova lifespan and distance from center of the galaxy. Boley (2002) reports no relationship exists between magnitude and decay rates and distance from the galactic center. In contrast Swartz (2002) reports novae nearer galactic centers are brighter and have shorter life spans than outlying novae.

To help understand more about planetary nebulas and to use novae as distance indicators, more should be known about novae and predictable models of evolutionary steps should be created. The first step toward accomplishing this is by correctly identifying characteristics of novae as well as identifying relationships between those relationships.

RESEARCH QUESTIONS

What is the relationship between the characteristics of novae and their distance from the center of the Andromeda Galaxy? Namely, what relationship, if any, is there between the distance from the center and decay rate, extinction time and maximum magnitude of the nova?

HYPOTHESIS

Research by Livio (1997) and Della Valle (1994) suggests that novae in the center of a galaxy will have a slower decay rate and be less energetic (lower magnitude). It was therefore expected that a relationship between decay rate and distance from the center of the galaxy, as well as magnitude and distance from the center of the galaxy would be identified. Furthermore, it was expected that higher decay rates would occur with increasing distance, and it was expected that lower magnitudes (brighter) would occur with increasing distance. This was due to research that supported that the centers of galaxies are typically populated by older stars resulting in smaller white dwarfs. In a related issue, it was expected that shorter extinction times would occur with increasing distance from the center in accordance with their decay rates.

PROCEDURE

Images from the Andromeda galaxy were produced using the NOAO 0.9 m telescope at Kitt Peak. These images consisted of 3 fields covering Andromeda's central bulge (field 1) and its arms (fields 2 and 3). Field 1 was selected for study because the higher density of stars in the bulge increased the number of novae available. Field 1 was further divided into 16 subrasters as shown in Fig. 1.

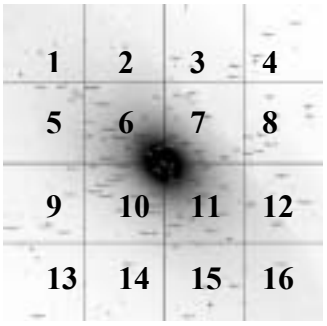

Fig. 1: Field One Subrasters

Each time the images were produced, they were labeled as epochs and numbered. Subrasters 1, 2, 5, 6, 7, 10, 11, 12, 15 and 16 were examined using ImageJ software. In each subraster, epochs 42 to 61, representing images from June 14 through September 21 2003, were compared or "blinked" to detect novae occurring in more than one epoch. Additional novae were selected by reviewing the RBSE Journal from 2001 through 2003. Novae identified in the RBSE Journal were reviewed to confirm their position and occurrence. Although many novae were identified, only twenty-two novae were considered for this study. The novae that were not visually identified in at least two consecutive epochs, or were measured at less than 19.5 magnitude, or did not have a change in magnitude that resulted in less energy were eliminated from the study. Dates of occurrence were recorded using the Julian calendar. The date and intensity of the maximum magnitude and the date and intensity of the last appearance were recorded for each nova. Each image containing a nova was calibrated using 3 standard stars and the magnitude of the nova determined using Mira software.

Magnitudes and dates were used to calculate two quantities: the decay rate in units of magnitudes per day and extinction times. Extinction time was determined as the difference between the first observed date and a calculated date (extinction date) at which the nova would reach a threshold value of magnitude 19.5. The threshold magnitude of 19.5 was established by determining the magnitude of the dimmest stars visible on a random image using ImageJ software. This value was consistent with that reported by Rector et al, (2000). The extinction date was calculated by applying the slope-intercept form of a linear equation to the decay rate and the initial date and magnitude data. The distance from the center of Andromeda was calculated by applying the Pythagorean Theorem to RA and Dec and the result given in degrees. These values were used to determine the relationships between decay rate and distance, extinction time and distance, and maximum magnitude and distance.

RESULTS

Novae locations, times of occurrence (first and last occurrence measured on the Julian Calendar), and magnitudes for the selected novae are shown in Table 1. Also included are the derived characteristics of decay rate, extinction time and distance from the center of M31.

Table 1: Novae Characteristics In M31

RA	Dec	Julian start	Julian end	Δ days	Maximum Mag	Minimum Mag	Δ mag	decay rate (mag/day)	Extinction time (days)	Distance (Degrees)
42 50 02	41 16 42 22	451101	451129	28	16.434	17.071	0.637	0.0228	135	0.01941
42 39 82	41 17 04 92	452477	452501	24	16.745	17.150	0.405	0.0169	163	0.02077
42 46 70	41 14 49 44	451101	451206	105	16.316	19.631	3.315	0.0316	101	0.02583
42 49 72	41 18 01 36	452883	452904	21	16.990	17.221	0.231	0.0110	228	0.03312
42 38 65	41 14 20.44	451354	451380	26	15.653	16.492	0.839	0.0323	119	0.03399
42 41 21	41 18 32 67	452825	452904	79	15.870	17.490	1.620	0.0205	177	0.04105
42 32 14	41 14 42.90	450653	450771	118	15.853	17.964	2.111	0.0179	204	0.04248
42 30 46	41 16 34 93	451019	451101	82	15.786	18.174	2.388	0.0291	128	0.04374
42 46 82	41 12 52 46	451711	451925	214	17.193	19.440	2.247	0.0105	220	0.05792
43 03 53	41 16 05 13	450653	450662	9	14.867	15.079	0.212	0.0236	197	0.06130
43 10 35	41 14 59 65	450771	451019	248	15.220	19.020	3.800	0.0153	279	0.07217
43 06 97	41 18 09 60	451019	451206	187	15.749	17.833	2.084	0.0111	337	0.07504
42 19 35	41 16 17 39	450653	450971	318	15.861	20.347	4.486	0.0141	258	0.07753
42 22 18	41 11 32.36	451101	451206	105	16.170	18.600	2.430	0.0231	144	0.09785
42 15 90	41 12 00 26	452854	452904	50	17.060	18.590	1.530	0.0306	80	0.10624
43 12 54	41 21 49 35	450618	450662	44	16.982	17.656	0.674	0.0153	164	0.12136
42 16 00	41 21 00 45	450771	451052	281	17.433	18.710	1.277	0.00454	455	0.12603
43 23 58	41 21 40 57	450618	450662	44	17.395	17.682	0.287	0.00652	323	0.14455
42 50 43	41 07 49 74	450653	450971	318	16.685	18.182	1.497	0.00471	598	0.14475
43 28 83	41 21 42 64	450971	451129	158	16.232	17.335	1.103	0.00698	468	0.15793
42 08 54	41 08 16.30	450618	450662	44	16.583	17.552	0.969	0.0220	132	0.16316
42 33 90	41 04 58 02	451062	451206	144	15.076	18.584	3.508	0.0244	182	0.18780

Increasing distance of novae from the galactic center was not significantly correlated with novae decay rates, as shown in Fig. 2.

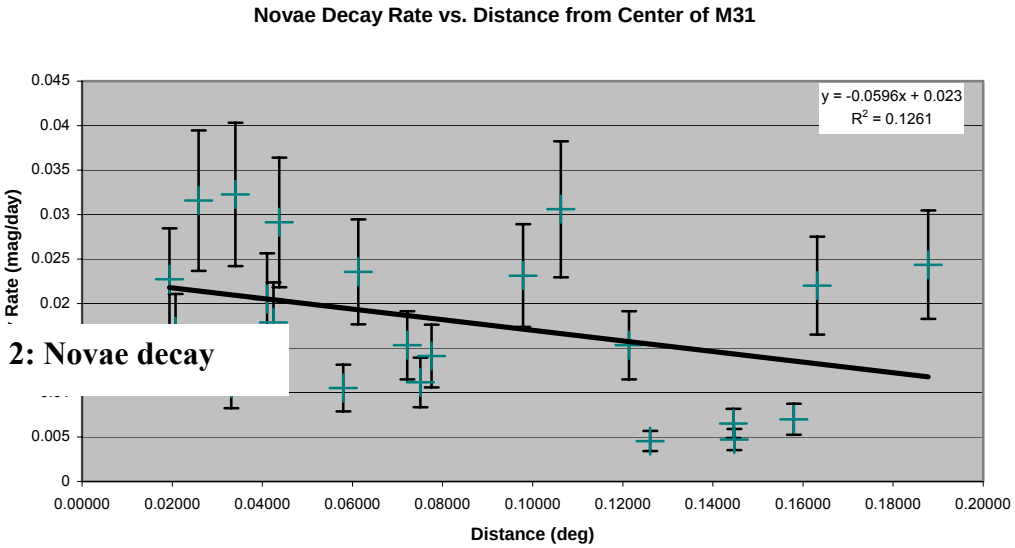

Fig. 2: Novae decay

Fig. 2: Decay Rate Vs. Distance

No correlation was observed between maximum magnitude and distance, as shown in Fig. 3.

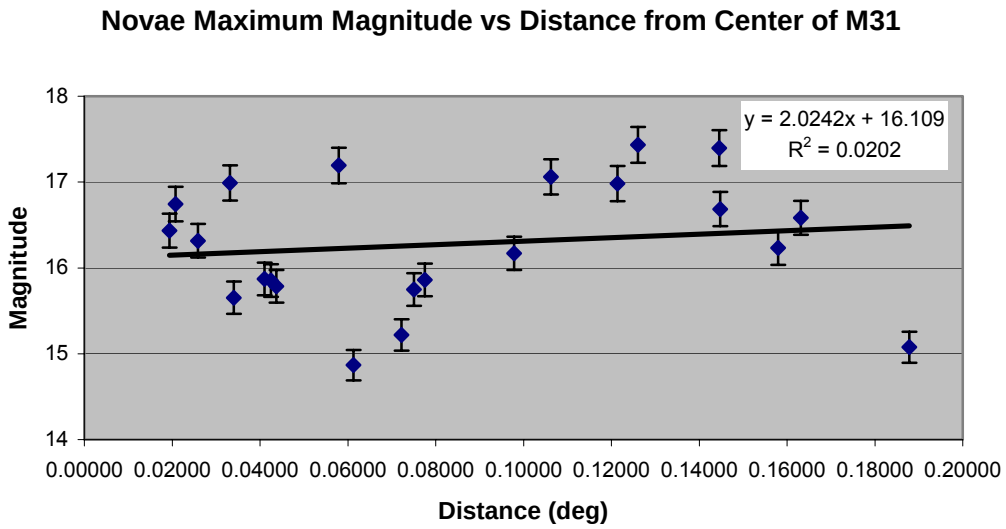

Fig. 3: Maximum Magnitude Vs Distance

Decay times were not correlated with distance as shown in Fig. 4. This data was treated as a frequency distribution of novae classified as having decay times either greater or less than 300 days and distances either greater or less than 0.125 degrees. The frequency

distribution was analyzed using a X^2 test and the apparent distribution was not statistically significant (See Table 2).

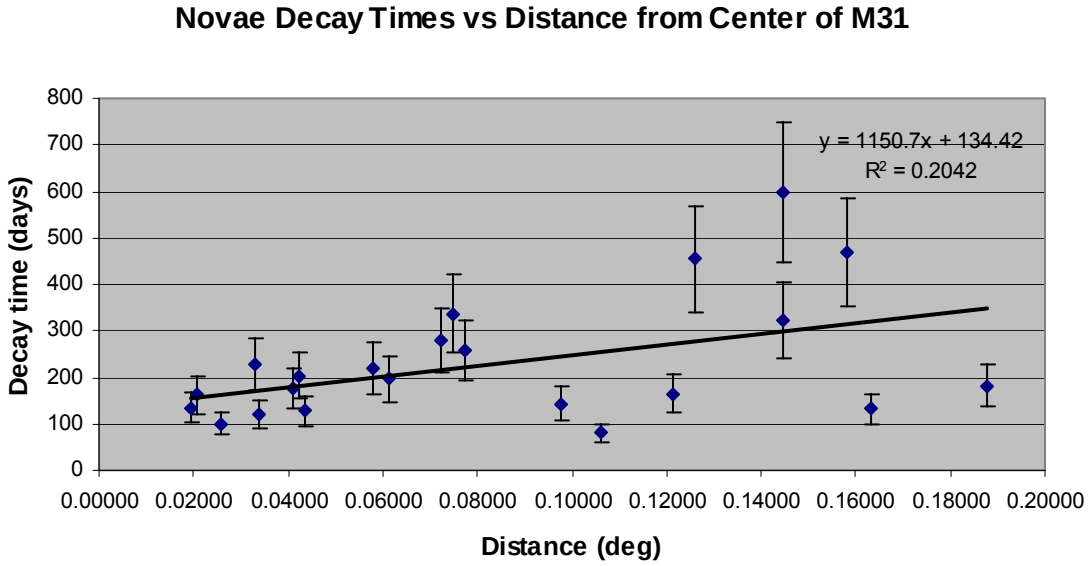

Fig. 4: Decay Times Vs Distance

Table 2: Frequency Distribution Of Novae By Distance And Decay Time

		Distance (deg)	
		< 0.125	> 0.125
Decay Time (days)	> 300	1	4
	< 300	15	2

(X^2 (1, N=22) = .00257 with critical value at p<.05 being 3.84).

Novae were separated into inner or outer classes based on their distance from the center of M31. A cutoff value of 0.125 degrees was used as it separated subrasters 1, 2, 5, 12, 15, and 16 (outer subrasters) from subrasters 6, 7, 10, and 11 (inner subrasters). Average values were determined for each of these classes and are recorded in Table 3.

Table 3: Characteristics Of Andromeda Novae

	Mag. max.	Decay Rate (mag/day)	Decay Time (days)
Inner (less than 0.125 degrees) N = 16	16.172 +/- 0.1	0.021 +/- 0.005	183
Outer (0.126 degrees or larger) N = 6	16.567 +/- 0.1	0.012 +/- 0.003	360

No difference was found between average magnitudes of either class as shown in Fig. 5.

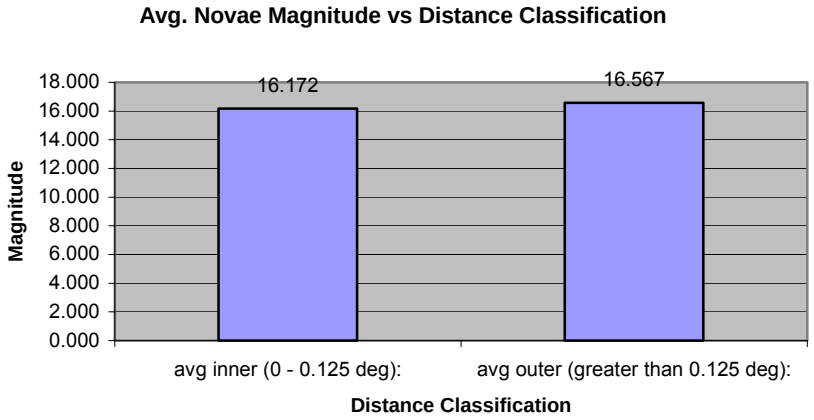

Fig. 5: Novae Average Magnitude Vs Distance Classes

A significant difference was found in the averages of decay rates between the two classes as shown in Fig. 6.

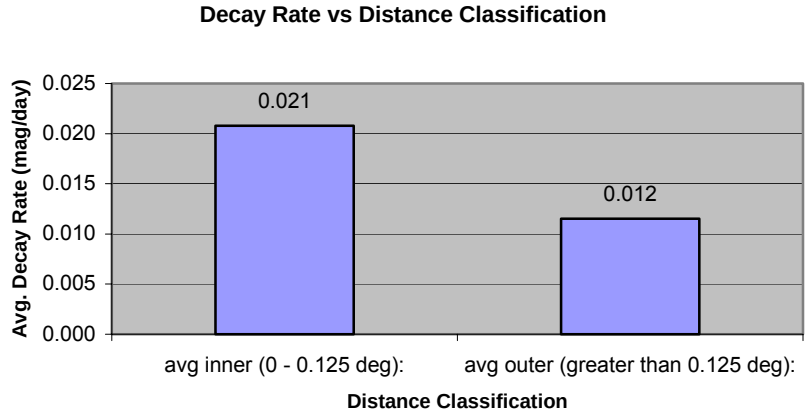

Fig. 6: Novae Average Decay Rate Vs. Distance Classes

A difference was found in the averages of decay times between the two classes as shown in Fig. 7.

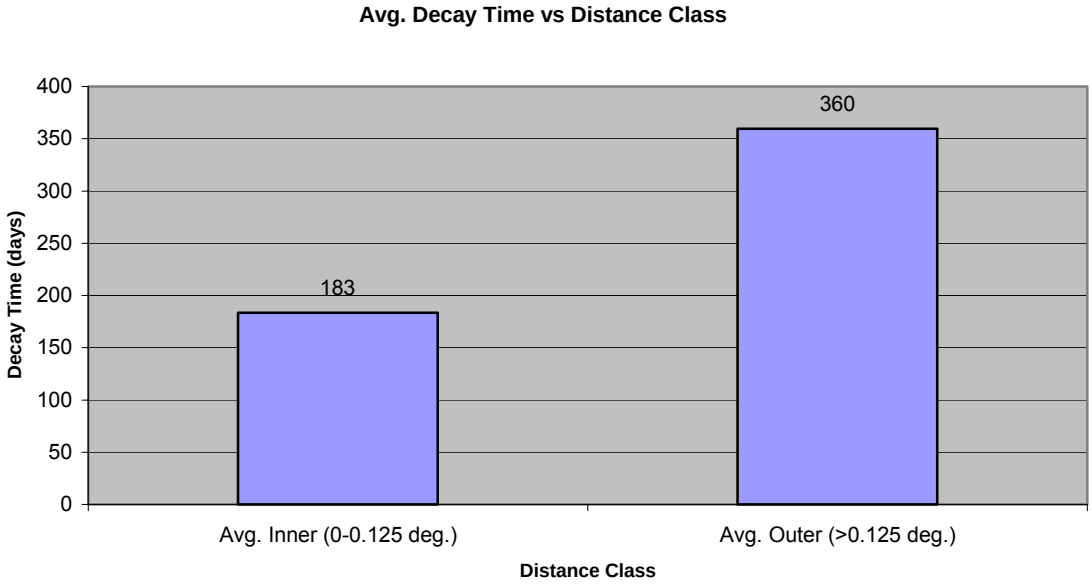

Fig. 7: Novae Average Decay Times Vs. Distance Classes

DISCUSSION

It was expected that novae further from the center of M31 would be brighter, have faster decay rates, and shorter decay times than novae closer to the center. In fact, no statistically significant correlations with any of these measures and distance from the center of M31 were confirmed. This is consistent with the reports of Green (2003), Boley (2002), and Clark (2003). It is possible that the obscuring effects of dust and gas closer to the center of M31 mask novae with greater magnitude than those further away (Croft, 2004). It is also possible that distances measured were not great enough to detect statistically significant different populations.

The relationship between novae magnitude and decay rates was also examined as shown in Fig. 8. This data was treated as a frequency distribution of novae classified as having decay rates either greater or less than .02 mag/day and magnitudes greater or less than 16. The frequency distribution was analyzed using a X^2 test and the apparent distribution was not statistically significant (see Table 4). This is in accordance with the findings of Ciardullo (1990).

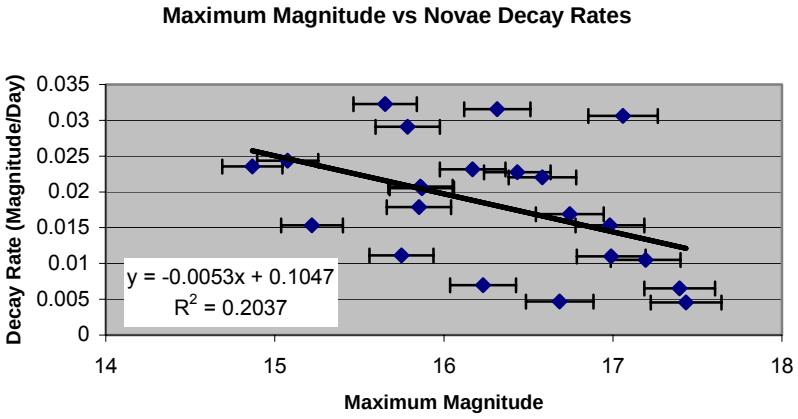

Fig. 8: Maximum Magnitude Vs. Decay Rates

Table 4: Frequency Distribution Of Novae By Decay Rate And Magnitude

		Magnitude	
		14 - 16	16 - 18
Decay Rate (mag/day)	0.02-0.035	5	5
	0 – 0.02	3	8

(X^2 (1, N=21) = .280 with critical value at p<.05 being 3.84).

Errors in this investigation included accuracy of magnitude and position determinations. Magnitude was measured with an error of up to +/- of 0.09 magnitudes, which resulted in average errors of 22% in measurements of magnitude changes. Most of this error was associated with two measurements of only 0.2 change in magnitude. By eliminating observations with magnitude changes resulting in more than 50% error, the average error dropped to 14% but did not change results significantly. The error limits of position values were not determined. Another source of error was the assumption of linearity in decay curves. In fact, the slope of these curves depends heavily on when, in the decay process, the measurements are obtained and the interval between measurements. This error can be reduced by ensuring that data points are taken relatively far apart. In this study only the first and last observations were considered. When data representing observations taken less than 1 month apart were omitted, the results did not change significantly. A smaller source of error is the possibility of underestimating novae distance. As distance is calculated in two dimensions, it is possible that novae at long distances may appear short if lying directly in line with the Earth.

In light of these results, further investigations of the potential extinction due to dust and gas near the galactic center should be conducted. One suggestion may be to compare the apparent magnitude of novae using both short and long wavelengths. Measuring the magnitude and decay rates of novae at greater distances from the galactic center should clarify the relationship between these novae characteristics and distance. Such measurements could establish the distribution of slow and fast novae populations. Analysis of novae data in fields 2 and 3 of the TLRBSE Nova Project may provide more information. Finally, analyzing spectra produced by newly discovered novae should

reveal information related to their composition. Detection of heavier elements thought to catalyze fusion reactions in larger novae found relatively far from the galactic center could lead to a greater understanding of novae dynamics (Howell, 2004)

REFERENCES

Boley, P. 2001, *A Search for Novae in the Andromeda Galaxy - Year Three,* The RBSE Journal, 2001, 35.

Boley, P. 2002, *A Search for Novae in the Andromeda Galaxy - Year Four,* The RBSE Journal, 2002, 11.

Calver T. et al. 2001, *Do Novae Repeat? A Study of Novae Discovered in M31 Between the Years 1980-2000*, The RBSE Journal, 2001, 26.

Camacho L., and Miller R. 2001, *Magnitudes of Novae in M31*, The RBSE Journal, 2001, 19.

Ciardullo, R. et al. 1990, *The Hα Light Curves of Novae in M31*, The Astrophysical Journal, 356, 472.

Clark, N. 2003, *The Lifespan of Novae in the Andromeda Galaxy*, The RBSE Journal, 2003, 23.

Croft, S., 2004. Personal conversation. Tucson, Arizona. TLRBSE Summer Program.Green, B. 2003, *Is the Magnitude of a Nova Greater Towards the Galactic Middle or the Outer Edge?*, The RBSE Journal, 2003, 21.

Howell, S., 2004. Personal conversation. Tucson, Arizona. TLRBSE Summer Program.

Kaufmann M., Merica D. 2001, *Novae in the Andromeda Galaxy*, The RBSE Journal, 2001, 23.

Livio, M. 1997, in *The Extragalactic Distance Scale*, STScI Symposium #10, 186.

Rector, T. et al. 2000, BAAS, 195, 36.08. (A Search for Novae in the Bulge of M31, Author List: Rector, T.A., Jacoby, G.H., Corbett, D.L., Denham, M., RBSE Nova Search Team National Optical Astronomy Observatories, 2000)

Seeds, Michael. 2003 *Foundations in Astronomy.* 7th ed. Thomson Learning Inc., Brooks/Cole. Ca. USA

Swartz, D. 2002, *The Brightness and Life of Novae Near the Galactic Center Compare the Outer Edge*, The RBSE Journal, 2002, 16.

ACKNOWLEDGEMENTS

We would like to thank all of the TLRBSE staff for providing us with the opportunity and experience to do real research at Kitt Peak which allowed us to conduct this study. A special thanks to our leader, Jeff Lockwood, to our mentors, Travis Rector and Steve Howell. Also important in our success was the support of Richard Cool and Katie Garmony who showed us how to produce images of M31.

Lyman Alpha Emission Lines In Quasars

Lisa Ly, Jia Leung, and Heather Johnson
Cranston High School East, Cranston, RI
Teacher: Howard Chun, RBSE 1999

ABSTRACT

The spectra of a number of quasars from the FIRST Survey were analyzed using Graphical Analysis to determine whether the appearance of Lyman alpha emission lines increase or decrease with higher redshifts. Researchers claim that due to the plethora of Lyman alpha forests in the earlier stages of the universe that there will be less Lyman alpha emission lines as a result of absorption by the forests. However, seeing that higher redshifts indicate earlier stages of the universe's evolution, quasars with higher redshifts are thought to have formed earlier in the universe's development. Because of their young age and higher energy, quasars that are farther away are thought to emit more Lyman alpha radiation. According to the data collected, quasars with higher redshifts actually do display a higher number of Lyman alpha emission lines.

BACKGROUND

A quasar is a celestial object that is about the size of the solar system, but emits as much energy as one or more galaxies. They are characterized by their great redshifts and their astonishing energy output. A quasar is an active galactic nucleus, or an AGN. Scientists believe that they are very distant, and in fact, they are probably the most distant of all celestial objects. Because they are so far away, it is probable that they occurred when the universe first began, and they are no longer in existence today. Several researchers claim that the farther the quasars, the more likely Lyman alpha absorption lines are detected. This is so because there appears to be a larger number of what scientists designate as "Lyman alpha forests" that intercept the Lyman alpha emission lines so that it appears as though the lines are being absorbed rather than emitted. Scientists attribute both the great redshifts of the quasars and the higher abundance of Lyman alpha forests to the theory that both quasars and Lyman alpha forests existed more frequent in the early evolution of the universe.

PROCEDURE

Quasars were analyzed using the Graphical Analysis program. The elements found were classified according to the redshifted emission lines found in the quasar continuum, and the redshifts were determined by comparing the theoretical wavelengths with those that were found for each element. The flux of the continuum at the wavelength in which Lyman alpha was found was obtained to determine the strength of the emission line.

DATA

The spectra of various quasars from the FIRST Survey were analyzed using Graphical Analysis. Refer to Table 1 for the elements present, redshift, and flux of each quasar, and see Example 1 for a model of the quasar continuums analyzed. Table 2 charts the frequency with which the major elements appear in quasars that have a redshift of below 1, between 1 and 2, and greater than 2.

Table 1

Name	Elements	Red Shift	Flux (A)
ffs0800	CIII, Lyα	1.62	2.35E-13
ffs1439	CIII, CIV	1.63	
ffs0816	OIII, MgII	1.65	
ffs0747a	CIII, CIV	1.71	
ffs1427	CIII, CIV	1.72	
ffs1424	OIII, Hβ	1.72	
ffs1335	CIII, CIV	1.73	
ffs1608	CIII, CIV	1.76	
ffs1606	MgII, OIII	1.78	
ffs1545	MgII, CIII	1.79	
ffs1359	CIII, CIV	1.83	
ffs1639	MgII, CIII	1.88	
ffs0811a	CIV, Lyα	1.89	7.23E-14
ffs0957	MgII, CIV	2.00	
ffs1036b	CIII, CIV, Lyα	2.00	7.31E-14
ffs1658	CIII, CIV	2.11	
ffs1351	CIV, Lyα	2.16	6.15E-14
ffs1620	MgII, CIII	2.16	
ffs0738a	CIII, CIV	2.19	
ffs0018	MgII, Lya	2.21	
ffs1616	Lyα, CIV	2.26	1.18E-13
ffs1619	Lya, CIV	2.35	3.89E-13
ffs1011	MgII, Lyα	2.38	4.90E-14
ffs1238	OIII, Hβ	2.42	
ffs1030	CIV, Lya	2.43	6.54E-14
ffs1723	Lyα, CIV	2.53	3.58E-14
ffs1406	CIV, Lyα	2.56	5.14E-14
ffs1535	Lyα, CIV	2.57	1.44E-13
ffs1641	Lyα, CIV	2.75	5.51E-14
ffs0813	CIII, Lyα	2.80	8.39E-15
ffs1724	Lyα, CIV	3.56	1.19E-13
ffs1006	CIII, Lyα	3.60	1.94E-14
ffs1001	CIII, Lyα	3.73	2.22E-14

Table 2

Redshift < 1

Element	Percentage*
OIII	76%
Hβ	57%
MgII	38%
CIII	19%
CIV	10%
Lyα	0%

1< Redshift < 2

Element	Percentage*
OIII	21%
Hβ	15%
MgII	53%
CIII	74%
CIV	35%
Lyα	6%

Redshift > 2

Element	Percentage*
OIII	5%
Hβ	20%
MgII	35%
CIII	35%
CIV	65%
Lyα	75%

* Percentage of quasars in which element is present

Row Num	Data Set 1: Data X	Y
1868	7425.5	3.42E-16
1869	7427.9	3.41E-16
1870	7430.2	3.43E-16
1871	7432.6	3.46E-16
1872	7434.9	3.51E-16
1873	7437.3	3.50E-16
1874	7439.6	3.49E-16
1875	7442.0	3.49E-16
1876	7444.3	3.45E-16
1877	7446.7	3.38E-16
1878	7449.0	3.34E-16
1879	7451.3	3.31E-16
1880	7453.7	3.28E-16
1881	7456.0	3.28E-16
1882	7458.4	3.28E-16
1883	7460.7	3.27E-16
1884	7463.1	3.28E-16
1885	7465.4	3.31E-16
1886	7467.8	3.28E-16
1887	7470.1	3.29E-16

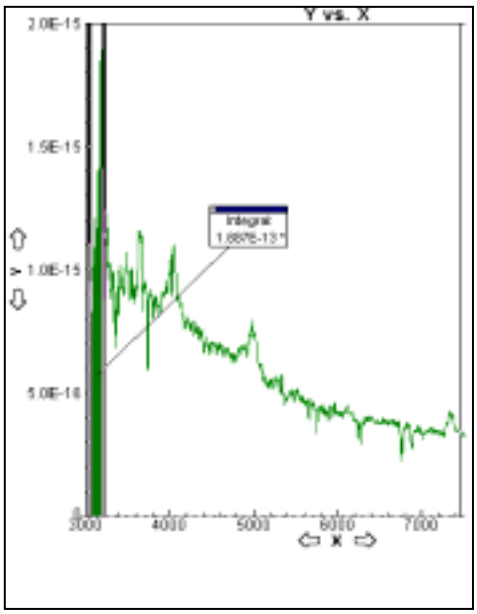

DISCUSSION OF RESULTS

Results from the analysis show that Lyman alpha emission lines appear more often in quasars with high redshifts rather than those with lower redshifts. The quasars observed were divided into three groups: those with redshifts less than 1, between 1 and 2, and greater than 2. The percentages of quasars of each group that emitted Lyman alpha lines show a steady increase as follows: 0 % in quasars with a redshift less than 1; 6% in quasars with a redshift between 1 and 2; and 75% in quasars with a redshift greater than 2. The Lyman alpha emission lines were also analyzed to determine whether they appear more often because they are present more often or because the emission lines were becoming progressively stronger with distance. However, after analyzing the flux of each quasar's spectrum, the data show that there is no pattern and no correlation between the strength of the emission line and distance. On the contrary, research shows that the Lyman alpha lines should be absorbed by the Lyman alpha forests and the appearance of Lyman alpha emission lines should not increase with distance. However, because only the quasars from the FIRST survey were analyzed, it is possible that there are little or few Lyman forests in this region and that they did not interfere with the collection of data.

REFERENCES

Quasar spectra files, FIRST survey, supplied by NOAO, RBSE Program

Astronomy Picture of the Day. <http://antwrp.gsfc.nasa.gov/apod/ap980224.html>

Quasars as lighthouses: the Lyman-alpha forest at low and high redshift.

<http://www.astr.ua.edu/keel/agn/forest.html>

Surveys for High Redshift Quasars. http://www.astro.psu.edu/users/dps/surveys.html

Quasars As Evidence Of Universal Acceleration

Chris Bertschinger
Wauwatosa East High School, Wauwatosa, WI
Teacher: Gary Sampson, TLRBSE 2003

ABSTRACT

The term "Active Galactic Nuclei" (AGN) is actually an umbrella term used to describe a number of astronomical objects, usually galaxies, which appear to contain a nucleus that completely outshines the rest of its surrounding galactic disk. There are five sub-categories of AGN: BL Lacs, Quasars, Radio Galaxies, Starbursts, and Ellipticals. Starbursts, Radio Galaxies, and Ellipticals are generally galaxies that are near to our own Milky Way Galaxy. The next most distant AGN are the BL Lacs followed by quasars.

In this study, quasars from the FIRST data set were analyzed for redshift and used as distance markers to ascertain whether or not there was any evidence to support the idea that the universe has changed its rate of expansion since the Big Bang and to determine what effect, if any, this may have had on early galaxies. Preliminary data did show a distinct accumulation of matter at a distance of seven billion light years.

BACKGROUND

Since their discovery by Maartin Schmidt in 1963, quasars (an acronym for quasi-stellar radio source) have proven to be among the most intriguing astronomical objects in the observable universe. Although they were at first thought to be radio signals from extraterrestrials, modern theory predicts that quasars are actually super-massive black holes located in the nuclei of distant galaxies. Quasars were also discovered to be moving at velocities of almost half that of the speed of light making them also the most distant observable objects in the sky ranging from a "close" two billion light years to a staggering thirteen billion light years away. Due to a quasar's enormous distance from the Earth, it takes light billions of years to reach telescopes on Earth; meaning that when observing quasars, the observer is seeing the universe as it existed billions of years in the past.

HYPOTHESIS

The aim of this research study is to determine the different red shifts of the samples in the FIRST data and determine which of them are quasars. Any quasars found are then to be used to search for definitive areas of higher, or lower, mass density at varying distances that would indicate the acceleration of the expansion of the universe.

PROCEDURE

The first step of this study was to examine each of the one hundred and fifty one objects in the FIRST data folder on the RBSE disk. Each file was examined using Graphical Analysis. On every graph, the two highest peaks were measured and entered into the Microsoft Excel Macro (also provided by RBSE). Excel then determined the red shift, distance, and velocity of each object. After determining each of the aforementioned criteria, the objects were then classified into each of the five sub-categories of AGN with

quasars composing just over half of all objects. The quasars distances were then graphed on Excel.

RESULTS

File (ffs)	Red shift	Velocity (km/s)	Distance (ly)
301	2.48	1.74 x 10^5	6.97 x 10^9
722	1.624	1.62 x 10^5	6.5 x 10^9
732	1.438	1.58 x 10^5	6.32 x 10^9
733	1.441	1.58 x 10^5	6.32 x 10^9
737	0.097	3.22 x 10^4	1.29 x 10^9
738b	3.06	1.78 x 10^5	7.14 x 10^9
740	0.712	1.25 x 10^5	5.01 x 10^9
800	1.613	1.62 x 10^5	6.49 x 10^9
811	2.695	1.76 x 10^5	7.04 x 10^9
816	1.393	1.57 x 10^5	6.27 x 10^9
847	0.061	2.12 x 10^4	8.49 x 10^8
859	0.302	7.79 x 10^4	3.12 x 10^9
905	1.293	1.52 x 10^5	6.08 x 10^9
928	1.902	1.67 x 10^5	6.7 x 10^9
955	2.111	1.7 x 10^5	6.81 x 10^9
957	2.975	1.78 x 10^5	7.12 x 10^9
1001	3.7	1.81 x 10^5	7.26 x 10^9
1005	2	1.61 x 10^5	6.76 x 10^9
1006	3.67	1.81 x 10^5	7.25 x 10^9
1011	2.42	1.74 x 10^5	6.95 x 10^9
1019	1.75	1.65 x 10^5	6.6 x 10^9
1030	1.75	1.65 x 10^5	6.6 x 10^9
1036a	3.64	1.81 x 10^5	7.25 x 10^9
1036b	2.01	1.69 x 10^5	6.76 x 10^9
1039	0.79	1.31 x 10^5	5.23 x 10^9
1047	0.03	1.09 x 10^4	4.36 x 10^8
1054	0.99	1.42 x 10^5	5.68 x 10^9
1106	0.15	4.63 x 10^4	1.85 x 10^9
1112	1.5	1.6 x 10^5	6.38 x 10^9
1119	1.53	1.6 x 10^5	6.41 x 10^9
1131	1.855	1.67 x 10^5	6.67 x 10^9
1143	2.6	1.75 x 10^5	7.01 x 10^9
1144	2.6	1.75 x 10^5	7.01 x 10^9
1152	0.48	1.03 x 10^5	4.13 x 10^9
1157	1.8	1.66 x 10^5	6.63 x 10^9
1210	1.95	1.68 x 10^5	6.73 x 10^9
1223	2.4	1.74 x 10^5	6.94 x 10^9
1238	2.4	1.74 x 10^5	6.94 x 10^9
1254	1.65	1.63 x 10^5	6.52 x 10^9
1257	1.5	1.6 x 10^5	6.38 x 10^9
1306	1.6	1.62 x 10^5	6.48 x 10^9
1318	0.05	1.77 x 10^4	7.07 x 10^8
1334a	1.35	1.56 x 10^5	6.22 x 10^9

1334b	0.18	5.35 x 10^4	2.14 x 10^9
1335	1.7	1.64 x 10^5	6.56 x 10^9
1349	1.2	1.51 x 10^5	6.03 x 10^9
1351	2.15	1.71 x 10^5	6.83 x 10^9
1359	1.83	1.66 x 10^5	6.65 x 10^9
1406	2.56	1.75 x 10^5	7.00 x 10^9
1408	0.846	1.34 x 10^5	5.37 x 10^9
1410	0.14	4.38 x 10^4	1.75 x 10^9
1430	0.22	6.23 x 10^4	2.49 x 10^9
1448	2.5	1.74 x 10^5	6.98 x 10^9
1450	0.71	1.25 x 10^5	5.00 x 10^9
1501	2.3	1.73 x 10^5	6.90 x 10^9
1517	0.137	4.3 x 10^4	1.72 x 10^9
1533	0.76	1.29 x 10^5	5.15 x 10^9
1534b	3.1	1.79 x 10^5	7.15 x 10^9
1534c	1.29	1.54 x 10^5	6.15 x 10^9
1535	2.14	1.71 x 10^5	6.83 x 10^9
1537	0.46	1.01 x 10^5	4.03 x 10^9
1545	1.77	1.65 x 10^5	6.61 x 10^9
1546	1.25	1.52 x 10^5	6.10 x 10^9
1557	3.7	1.81 x 10^5	7.26 x 10^9
1602	1.78	1.65 x 10^5	6.62 x 10^9
1606	1.76	1.65 x 10^5	6.60 x 10^9
1608	3.97	1.82 x 10^5	7.29 x 10^9
1614b	1.55	1.61 x 10^5	6.43 x 10^9
1616	2.26	1.72 x 10^5	6.88 x 10^9
1619	2.35	1.73 x 10^5	6.92 x 10^9
1620	2.1	1.7 x 10^5	6.81 x 10^9
1627	2.54	1.75 x 10^5	6.99 x 10^9
1628	2.25	1.72 x 10^5	6.88 x 10^9
1630	0.18	5.35 x 10^4	2.14 x 10^9
1639	0.87	1.36 x 10^5	5.43 x 10^9
1641	2.75	1.76 x 10^5	7.06 x 10^9
1656	0.65	1.2 x 10^5	4.81 x 10^9
1658	2.11	1.7 x 10^5	6.81 x 10^9
1706	3.38	1.8 x 10^5	7.2 x 10^9
1708	1.34	1.55 x 10^5	6.21 x 10^9
1723	2.52	1.75 x 10^5	6.99 x 10^9
1724	0.6	1.16 x 10^5	4.63 x 10^9
2341	0.7	1.24 x 10^5	4.97 x 10^9

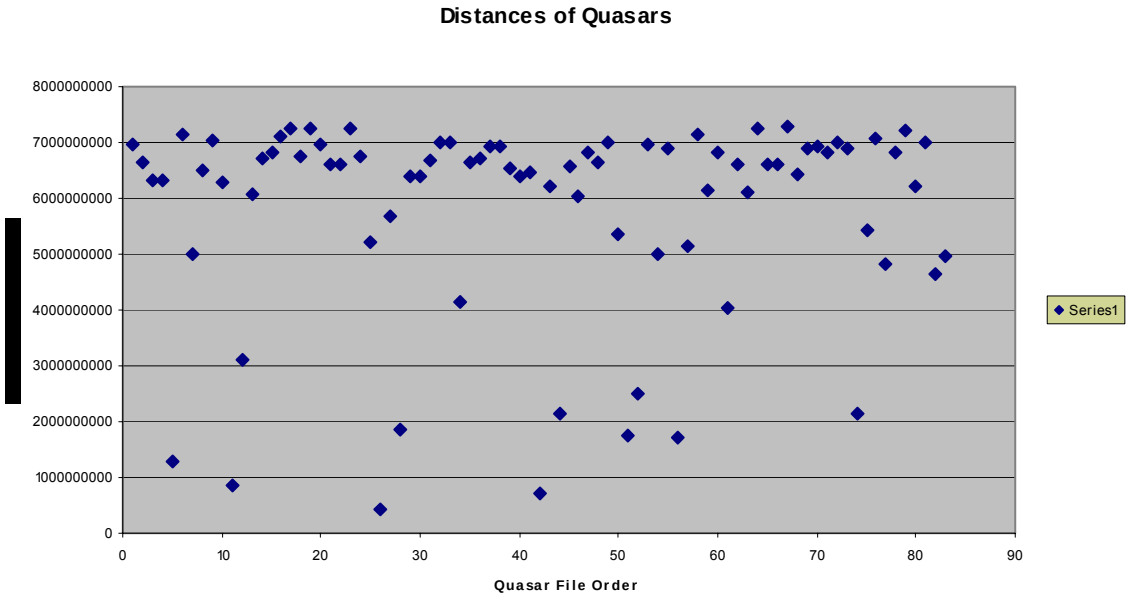

CONCLUSION

Based on the graph shown, there is an apparent mass accumulation around the seven billion light year mark. This result could be the beginning boundary of "quasar space", the area of the universe where quasars are common and more numerous, or it could be the first of many more accumulations of quasars. However, this is not an accurate answer due to the small number of quasar numbers and limitations of the telescopes to only see quasars up to a distance of eight billion light years. This study will have to be put on hold until more quasars are made available through RBSE and the observational equipment is upgraded.

REFERENCES

Beaudry, Karyn *et al*. Investigating and Categorizing AGN Objects. TLRBSE Journal 2000.

Michelle Miller and Randy Buhrman. Does Distance Affect Types of AGN. TLRBSE Journal 2003

Keel, Bill. Quasars Explained. Astronomy Magazine Feb 2003: 34 – 41.

Anderson, Scott F. et al. High Redshift Quasars Found In Sloan Digital Sky Survey. The Astronomical Journal, Aug 2001. p. 503 – 517.

Greene, Brian. The Fabric Of The Cosmos. New York: Alfred A. Knopf Publishing, 2004.

Rector, Travis. AGN Spectroscopy: Studying Nature's most Powerful "Monsters". TLRBSE Journal: Tucson Arizona 1999.

The Correlation Of Distance With Luminosity In Quasars

Richie Foy, Erin Sisson, Jessica Smith
Graves County High School, Mayfield, KY
Teacher: Velvet Dowdy, TLRBSE 2003

ABSTRACT

The spectra of Active Galactic Nuclei can reveal many extremely important characteristic of the object. These characteristics include distance, velocity, red shift, luminosity, flux, etc. By using the knowledge attained from these sources, one can see relationships unrevealed that would otherwise be impossible to attain.(Arp, Halton; Russell, David) This project focused on the relationship between the AGN (quasars) to find a correlation between the distance of an object and its luminosity.

INTRODUCTION

Quasar are an extremely luminous object at the center of some distant galaxies. The word quasar is a shortened form of the term quasi-stellar (starlike) radio source, which was applied to the first type of quasar identified. Because quasars look much like stars in photographs, they are sometimes called quasi-stellar objects. Most quasars are about the size of the solar system. But they can be a trillion times brighter than the sun. Many astronomers believe quasars are the most distant objects yet detected in the universe. Some are estimated to be as far as 12 billion to 16 billion light-years from the earth.(Bremer, M.N.; Baker, Joanne C.; Lehnery, Matthew D)

Astronomers determine how distant a quasar is by measuring its red shift. Red shift is a shift in the wavelength of light given off by an astronomical object toward the longer, or red, wavelengths of the object's spectrum. It indicates an object is moving away from the earth. The more distant the object is, the larger is its red shift.(Chang, John; O'Brien, Mark) All quasars have large red shifts.

Quasars give off enormous amounts of energy in the form of visible light, ultraviolet light, infrared rays, X rays, gamma rays, and in some cases, radio waves.(Gareth, James) Energy from quasars takes billions of years to reach the earth. For this reason, the study of quasars can provide information about early stages of the universe.

RESEARCH QUESTION

What is the correlation between the luminosity and distance in quasars?

The emission lines of different quasars were measured in order to calculate the red shift, flux, distance, and luminosity of each of the quasars

METHODS

To complete this task we Graphical Analysis 3.1.1 Demo was used to calculate the emission lines of quasars. The calculator TI-83 was used to calculate the red shifts, flux, and distance of each of the quasars. Finally PowerPoint was used to graph the date we collected and calculated.

The data was collected by the 2m telescope on Ktt Peak in Arizona. It was donated for student's use by the NOAO.

To complete this research project we determined which spectra were quasars in Graphical Analysis. After this was completed we had to compare the ratios and found the red shift by using the formula

$$Z = (lobs) / (lrest) - 1$$

After the redshift was determined, the distance of the object from earth was found bye using the equation:

$$d=cZ/H0(1+.5Z)/(1+Z)$$

The variables of the equation stand for the following things: c=speed of light, z=redshift, H0 is Hubble's constant of 75 km s-1Mpc-1

Next Graphical Analysis was used to determine the flux. Once the flux was found, the luminosity was found by using the formula:

$$L=4pfd2(1+Z)2$$

After this was accomplished, the figures were converted into centimeters, and then Mpc.

Additional research included information about quasars, red shift, and other similar experiments. This research helps us to better understand the galaxy and universe in which we live.

RESULTS

The Graphs are attached. Two different sets of data were used, one of which (Graph 1) was the data that was researched. The other set (Graph 2) was conducted by another group with a similar research project. The data from a similar project was used because it was necessary to compare the correlation being that there was so few data collected most recently. It can be assumed that the data that was collected most recently was extremely selective to make sure it was truly a quasar. It can also be assumed that the other project was not as selective as the more recent one. (Keel, Bill)

DATA RECENTLY RESEARCHED

Quasar	1st &2nd Line	Flux	Distance	Lunimosity
Gb171937	3976.5852	1.2284*10^25	8.41	1.0846*00^28
Ffs1619	4074.5949	5184.9535	.02	79.22
Ffs620	3734.7869	1.1575	110.32	1.6754*10^30
Gb234734	4602.1809	1.4197*10^25	302.94	1.9048*10^33

Data Collected by Previous Research Project

No data except, for the graph, was attainable from the project which had previously been conducted. However, it was possible to compare the graphs of the two data sets.

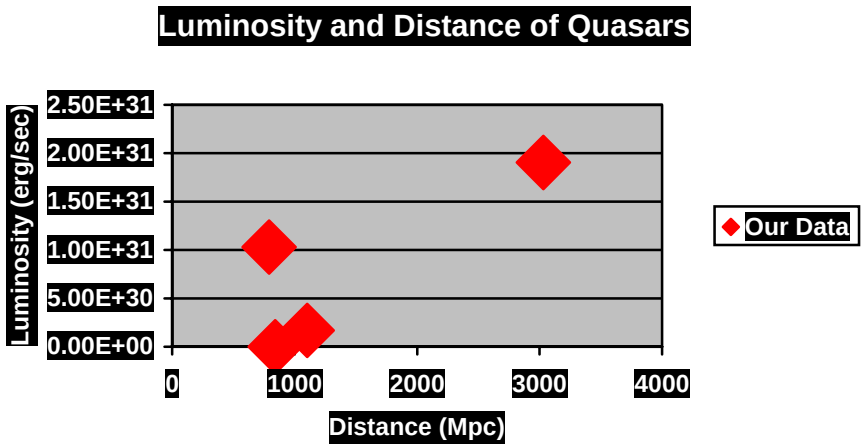

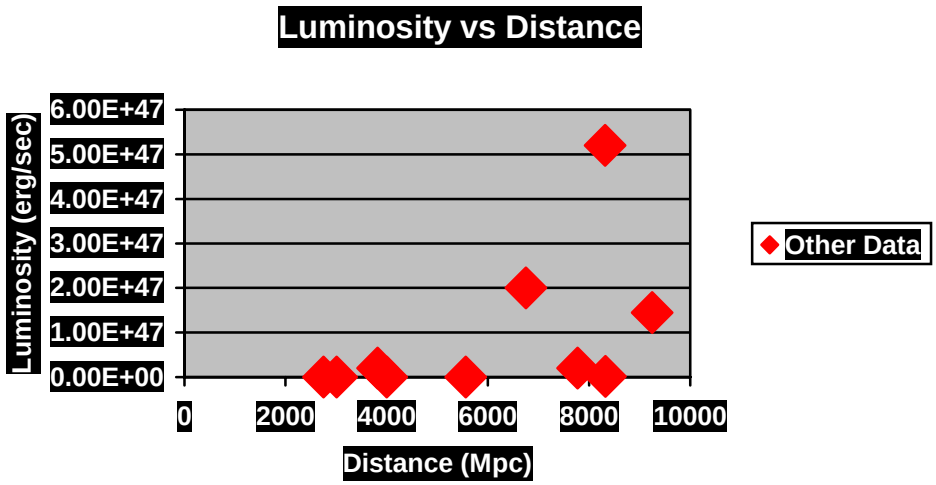

CONCLUSION

The conclusion is that there is a direct positive correlation between distance and luminosity of quasars, through graphing and analyzing the more recent data compared to that of others. It is apparent that there is a positive correlation because, for the most part, when the distance increases so does the luminosity.(Schmidt, Maartin; Gunn) When comparing the recent data to the previous data, it can be concluded that the data is very similar because they both have positive correlations. The results of the two sets of data differ because in the previous data, there is an extremely clear correlation. However, in the more recent data, the correlation is not as clear. In order for it to be more clear a larger number of data sample would need to be collected. Being that in the previous data there was a positive correlation, it was assumed that if more data had been collected for the recent data that there would have been a positive correlation as well. It was also noticed that there was one piece of data on each graph that strayed away from the mainstream data. This revealed that it is a possibility that there are many different AGN in space that the scientific community is not aware of.

Error in Analysis: The graphs were difficult to make due to scale difficulties. It was also difficult to locate a large number of quasars. Also, clouds of gas between the object and Earth may be moving at different velocities and directions, causing a lower red shift in the absorption lines. (Simoneeti, John) There was no discernable bias. However, the number used for Hubble's constant is being disputed in the scientific community.(Waddington)

SUGGESTED FURTHER STUDY

There should be a study of a larger sample of data to contribute to the accuracy of the study.

REFERENCES

Arp, Halton; Russell, David. *A Possible Relationship between Quasars and Clusters of Galaxies*; The Astrophysical Journal, Volume 549, Issue 2, pp. 802-819. March 2001.

Bremer, M.N.; Baker, Joanne C.; Lehnery, Matthew D. *A quasar in a compact group of galaxies at z=0.7*; Monthly Notice of the Royal Astronomical Society, Volume 337, Issue 2, pp. 470-476. December 2002.

Chang, John; O'Brien, Mark. *Quasars*. http://www.rdrop.com/users/green/school/quasars.htm. March 2004.

Department of Physics & Astronomy. *Quasars*. University of Tennessee. http://csep10.phys.utk.edu/astr162/lect/active/quasars.html. March 2004.

Gareth, James. *Quasars.* http://freespace.virgin.net/gareth.james/astro/alevel/quasars.html. March 2004.

Keel, Bill. *The Einstein Cross Gravitational Lens 2237+030*. http://www.astr.ua.edu/keel/agn/qso2237.html. March 2004.

Lochner, Jim. *Active Galaxies and Quasars*. Imagine the Universe. http://imagine.gsfc.nasa.gov/docs/science/know_l1/active_galaxies.html. March 2004.

Schmidt, Maartin; Gunn, James. *Surveys for High Redshift Quasars*. http://www.astro.psu.edu/users/dps/surveys.html. March 2004

Schmidt,M. *Modern Cosmology in Retrospect*. Cambridge Univ. Press. p.349. 1990.

Simoneeti, John. Frequently Asked Questions About Quasars. Department of Physics at Virginia Tech. http://www.phys.vt.edu/~jhs/faq/quasars.html#q7. March 2004.

Sipior, M.S.; Feigelson, E.D. *Luminous X-Ray Sources in a Volume Limited Sample of Low-Luminosity AGN*; Two Years of Science with Chandra, Abstracts from the Symposium held in Washington, DC, September 5-7, 2001.

Trentham, Neil; Blain, A.W. *The temperatures of dust-enshrouded active galactic nuclei*; Monthly Notices of the Royal Astronomical Society, Volume 323, Issue 3, pp. 547-554. May 2001.

Waddington, I; Dunlop, J.S.; Peacock, J.A.; Windhorst, R.A. *The LBDS Hercules sample of mJy radio sources at 1.4 GHz – II. Redshift distribution, radio luminosity function, and the high-redshift cut-off*; Monthly Notices of the Royal Astronomical Society, Volume 328, Issue 3, pp. 882-896. December 2001.

Elements Found In The Spectral Lines Of Quasars

Erin Perry
Fairfield High School, Fairfield, PA
Teacher: Mr. C. Katsu, RBSE 2001

PROBLEM

Over the vast expanses of time we as Homo sapiens have become a species dedicated to attempting to solve the mysteries of this universe, from Galileo and Kelper's astronomical laws, to Einstein's Byzantine theory of relativity. In this astronomy project, I located the different elements found in Quasar absorption and emission lines. Once this was completed, I then found the red shift of each of the Quasars I observed, and then could find their relative distance to Earth by using the Doppler Formula. From this information, I tried to find relationships between the elements found in the Quasars, and their distance to Earth.

BACKGROUND

Quasars are small, powerful sources of energy believed to be the active cores of very distant galaxies. These cores in mention were first detected as sources of radio energy, and so researchers could find no evidence of visible optical wavelengths. The first to be studied once found on a telescope was 3c273, which proved at best to only look like a small pinpoint of light. After 3c48, only the second quasar ever to be found was discovered, scientists learned that the spectra of quasars was equivalent to the combination of continuous spectra and a few un-definable emission lines.

There are a few individual elements related directly to quasars that make them specifically unique. One such item is their unmistakable red shift pattern. All quasars seem to be accompanied by a clearly identifiable extraordinary red shift pattern, meaning in part that the red shifts can be interpreted to mean exceptionally large distances. For

instance, normal galaxies at the distances specified by the red shift patterns of quasars would be invisible, and yet quasars are evident on photographs. Another extreme quality of quasars is their ultra luminosity, characterized by their ability to be ten to hone hundred times more luminescent than that of a regular galaxy. The brightest quasar ever to be studied was quasar 3c273, which also happened to be one of the very first studied. What it is that makes this quasar so bright, is that it contains three H Balmer lines red shifted by 15.8%. One of the last unmistakable qualities of the specified quasars is their tendency for their light to fluctuate rapidly, and erratically. These particular wonders of the night sky can also change brightness in a month, or week, or even a single day. If this already isn't enough information to compute, not that the size of quasars are extremely small compared to their luminosity of distance. Quasars are only one light week, to one light day in diameter.

PROCEDURE

After accessing my G file I open up numerous folders before locating the AGN file under data analysis. This program allows me to access numerous different AGN and it will then be my task to choose which are Quasars, and which of the AGN I should ignore. Once I find a Quasar, I will then carefully observe the peaks and dips in the graph representing the Quasars emission and absorption lines. Beside this graph is a data table showing every line that makes up the graph. Once I click on a certain peak, whatever line happens to be on will be highlighted on my left, and it will then by my responsibility to record all information. After I have sufficient numbers from the graph, I will then match the correct numbers to their corresponding elements as found in an accurate list of weak emission telluric absorption bands, and strong emission lines commonly seen in AGN. Then I again matched the numbers that had identical elements and found the quotient of each. From this information I could then find the ratio of that particular element in an emission line ratio table to correctly locate the accurate element from that Quasar. After finding the red shift of each of the Quasars, I then placed the numbers derived into the Relativistic Doppler Formula, which relates the radial velocity to the speed of light and the red shift of the Quasar in mention. Thus I found each of their relative distances to Earth.

CONCLUSION

Unfortunately my conclusions are incomplete because I feel like I still have not looked at enough data to adequately compose a correct conclusion paper. I do believe I have found a pattern among the nine different Quasars I spent many weeks going over and over again. The pattern I have observed is that among the Quasars that are the closest to Earth, out of the nine I have observed, the last numbers of the element are smaller, than the ones that go with the Quasars that are far away. An O3 did not appear in any of the quasars close to Earth, only showing up in those that were very distant, another example is that of Ne5, which only could be viewed in the furthest Quasars from Earth. Due to inadequate research, I can only assume that this pattern will be repeated in other Quasars that have not been observed yet.

DISCUSSION

In the five different examples of quasars that I looked at, there appeared a number of different elements. There of course were some elements that were the same, but many of

them varied, between one, and all of the different examples. The reason for this is that even though quasars are similar, they can't all be exactly the same. One of the main factors in their unique differences is their fundamental makeup, or the way in which their particular atoms interact with each other to form the different elements, that eventually make up the quasars themselves.

There were not any factors that I did not have under my control at any time, because I was not actually conducting experiments. I have been merely recording and observing. I could have made errors in the process of coping down the correct numbers, but I've gone through my work, and the numbers that I've entered in my data, are correct.

The only way to say for certain that the same elements will continue to repeat themselves in each quasar is to continue to observe and record them. Unfortunately, I had run short on time as far as getting adequate research done, so I did not observe enough quasars to get a detailed or accurate account of exactly which elements are recurrent, or are not recurrent, or if a pattern even exists at all.

The data that I've been studding, recording, and observing is specific to quasars. The spreadsheets that I've used, the data tables I've developed will only work for this particular type of AGN. This is because there are so many different kinds, that if my research were to include even one more type of galaxy, then the whole process would be thrown off, and the data would cease to be accurate.

If someone had wanted to improve upon my project, I would recommend beginning where I had left off. To save time, they would not have to repeat going over the same data that I already have, they can simply build on it. If someone really had wanted to go in depth, they could also expand on my project, while doing the same with other kinds of AGN. With a wide variety of galaxies to research, the possibilities are endless. There are so many things that any number of different galaxies could have in common, not including elements.

Elements Found In Quasars

Quasar 1210	**Hy, Ne3**
Quasar 1119	**Ne3, H**
Quasar 1359	**O2, Ne3**
Quasar 0800	**O3, Ne5**
Quasar 1257	**O2, Ne3**
Quasar 1318	**Hd, O2**
Quasar 1501	**Ne3, H**
Quasar 1005	**Ne5, O3**
Quasar 1349	**Ne3, H**

A Study Of The Flux/Luminosity Ratios Of Mg II And Radio Emissions In AGN's

Sherry Brown, Edmonds Woodway High School, Edmonds, WA – TLRBSE 2003
Tim Lundt, Burchell High School, Wasilla, AK – TLRBSE 2003
Brian Rogan, Gann Academy, Waltham, MA – TLRBSE 2003
Tom Vining, Desert Mountain High School, Scottsdale, AZ – TLRBSE 2003

ABSTRACT
Spectra of galaxies show that each type of galaxy has a distinct suite of spectral emissions both in the visible and radio wavelength. For several types of galaxies, these were examined to try and determine a correlation between Mg II and radio emissions in an attempt to validate the current model of AGN structure.

BACKGROUND
Galaxies come in many different types and can be both "quiet" and active. This project undertook the study of active galaxies in an attempt to determine if the pattern of emission can be correlated with the current model for nuclei of active galaxies.

AGN's

AGN's (Active Galactic Nuclei) are galaxies with strong emission spectra indicative of a strong source of energy in the core of the galaxy. It is postulated that AGN's contain a blackhole of enormous size that powers the galaxy.

NORMAL GALAXIES
Most galaxies can be considered "normal". Their spectra mirror their composition, primarily dust, gas and stars. Their spectra should have lots of absorption lines and few if any emission lines.

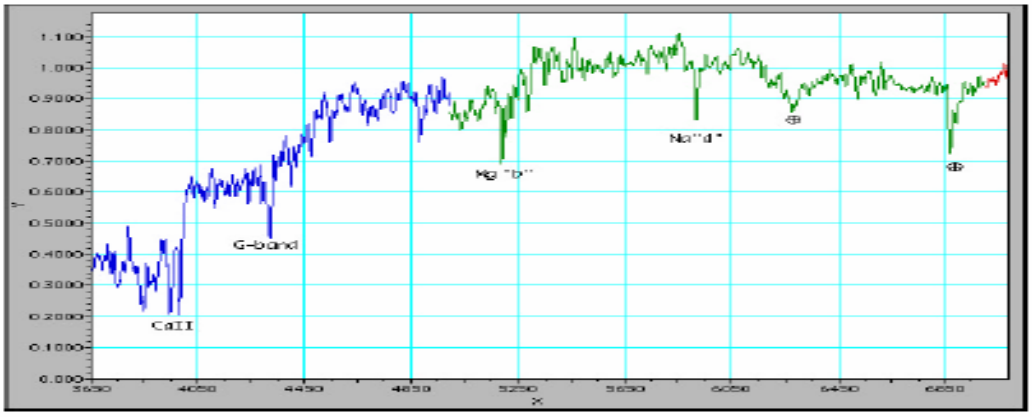

STARBURST GALAXIES

All galaxies go through a cycle of star formation and death. Some galaxies, however, can form stars more rapidly, producing stars at a rate far exceeding a normal galaxy. These are known as starburst galaxies. Their spectra consist of narrow emission lines in addition to the galactic spectrum.

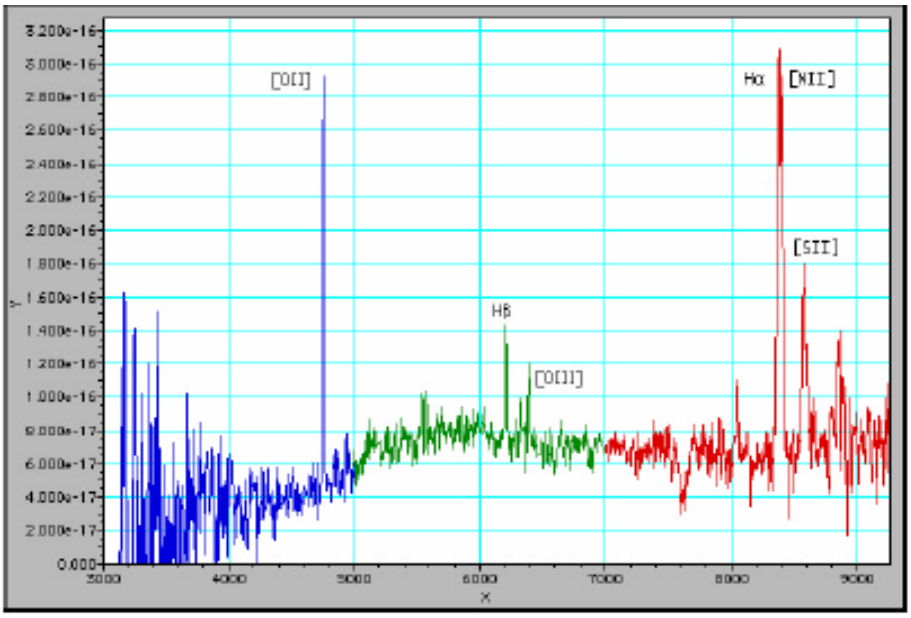

Fig 2. Spectra Of A Starburst Galaxy

RADIO GALAXIES

Radio galaxies look like normal galaxies but they produce enormous amounts of radio energy. Optically, their spectra consist also of narrow emission lines and they can be easily confused with starburst galaxies. The primary difference is that the OII, OIII and NII lines are much stronger than the Hα and Hβ.

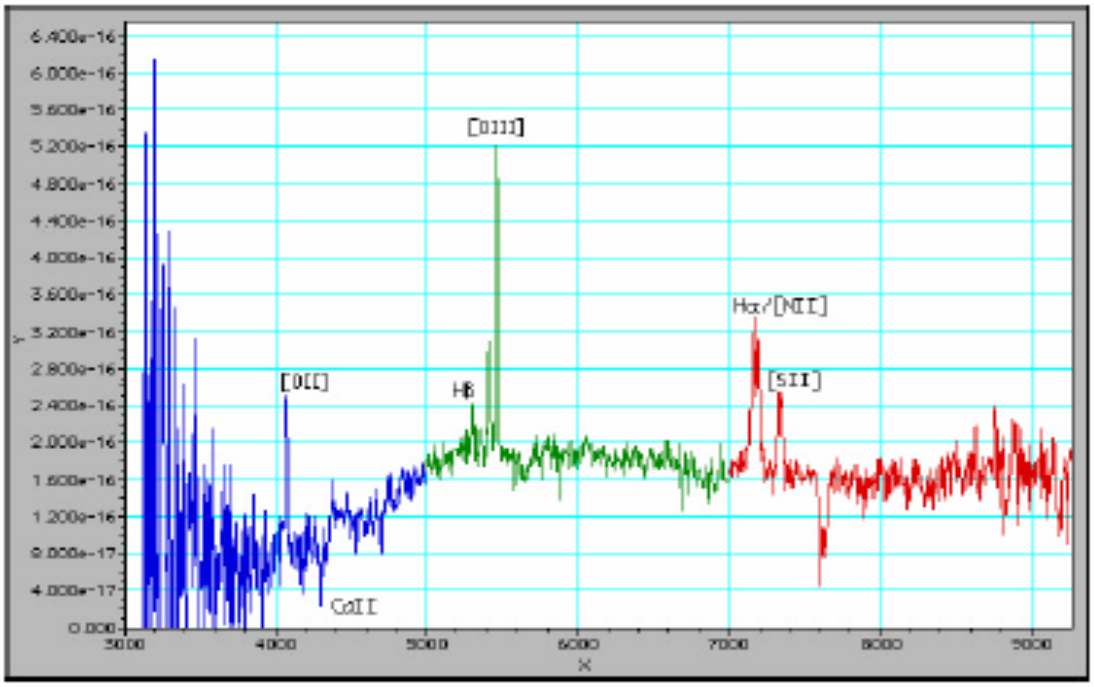

Fig 3. Spectra Of A Radio Galaxy

QUASARS

Quasars are the most distant of all AGN's. Their spectra don't resemble normal galaxies. They have a smooth continuum with strong emission lines. Unlike a galaxy, synchotronic radiation rather than stars produces their continuum.

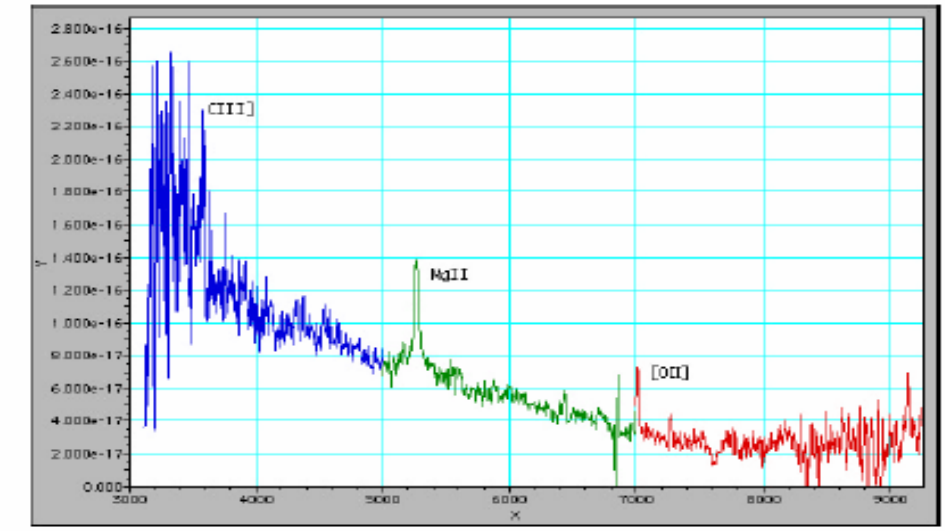

Fig 4. Spectra Of A Quasar

BL LAC OBJECTS

These objects have no strong emission lines. However, they do have a CaII break in their spectra unlike quasars, which rarely have that characteristic in their spectrum.

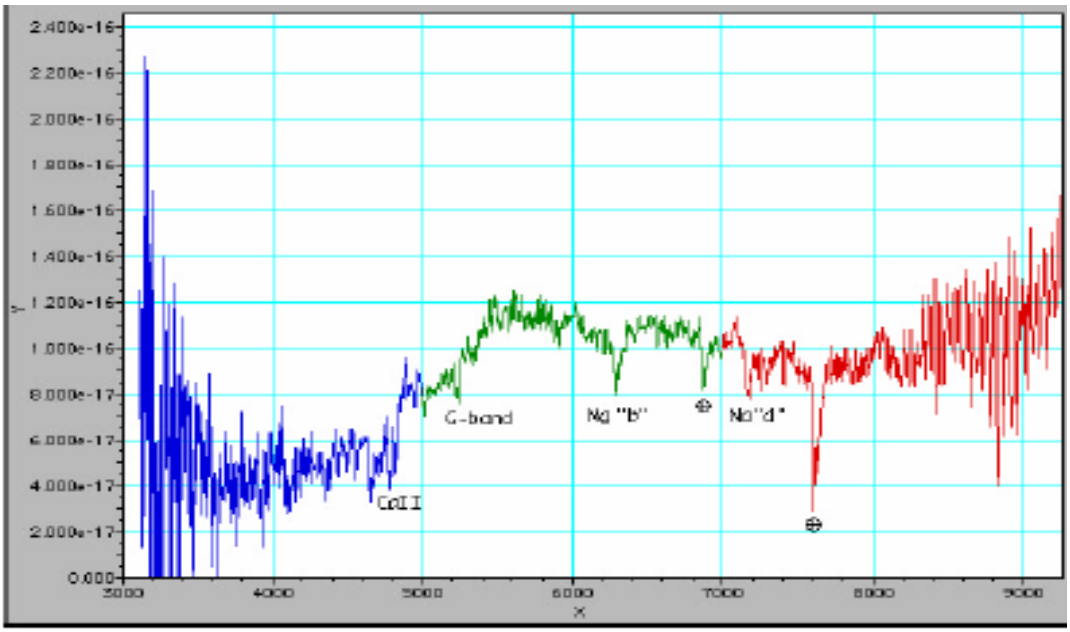

Fig. 5. Spectra Of A BL Lac Object

RESEARCH PROBLEMS

The research problem being investigated had three essential questions that were trying to be answered:

- **-How can we differentiate between different AGN's?**
- **-What is the current model that would explain our data?**
- **-Is there a correlation between Mg II emission in the surrounding clouds and the radio emission jets generated by the AGN?**

PROCEDURE

Each type of galaxy, both normal and active emits a characteristic spectrum. By looking closely at the emission pattern for each object, its identity can be determined from the characteristic lines.

For this study, a database of several hundred AGN spectra were surveyed and separated based on the criteria discussed in the background section. A flowchart was devised to help differentiate each of the objects.

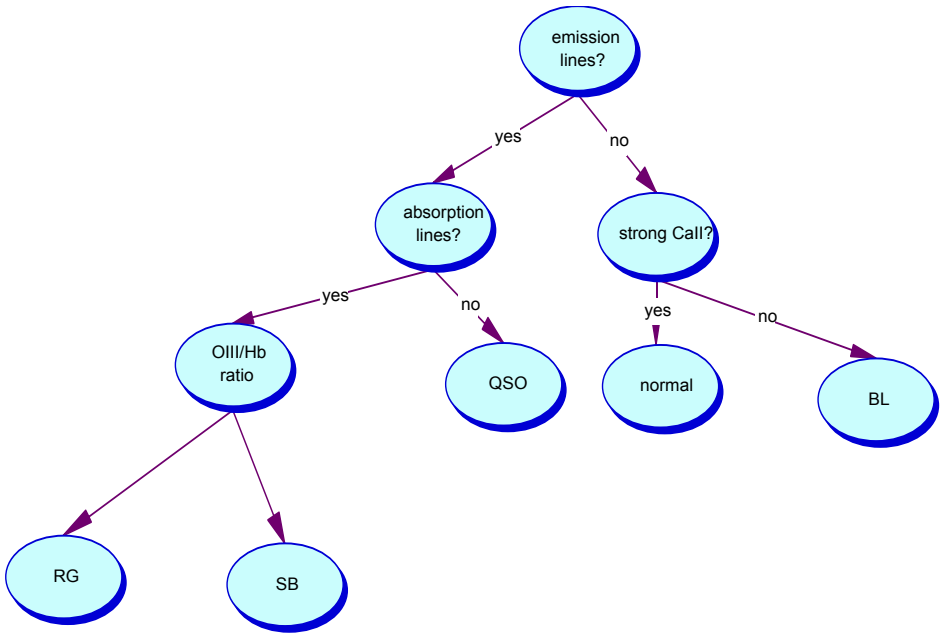

Fig 6. Flowchart Of Spectral Characteristics
(Rg=Radio Galaxy Sb=Starburst Galaxy Qso=Quasi Stellar Object Bl=Blac Object)

The radio wavelength flux and its luminosity were each plotted vs. the Mg II wavelength flux and luminosity to see if there was a correlation between them.

The results were determined in the following manner:

Table 1 – Calculating Flux

MgII rest wavelengths (λ_{rest}) = 2796, 2803
MgII redshift wavelength (λ_z) = (1+z) λ_{rest}

MgII emission flux = total flux – background flux
Total flux = area under curve
Background flux = (λ_z^{MgIIa} - λ_z^{MgIIb})(average continuum flux)

$$\text{MgII emission flux} = \text{Total flux} - (\lambda_z^{MgIIa} - \lambda_z^{MgIIb})(\text{average continuum flux})$$

Where λ_z^{MgIIa} = the MgII wavelength at the beginning of the broadening
Where λ_z^{MgIIb} = the MgII wavelength at the end of the broadening
λ_z^{MgIIa} ,λ_z^{MgIIb} and average continuum flux are all measured visually using Graphical Analysis

The results were then plotted for Flux and Luminosity for Radio vs. Mg II in both cases.

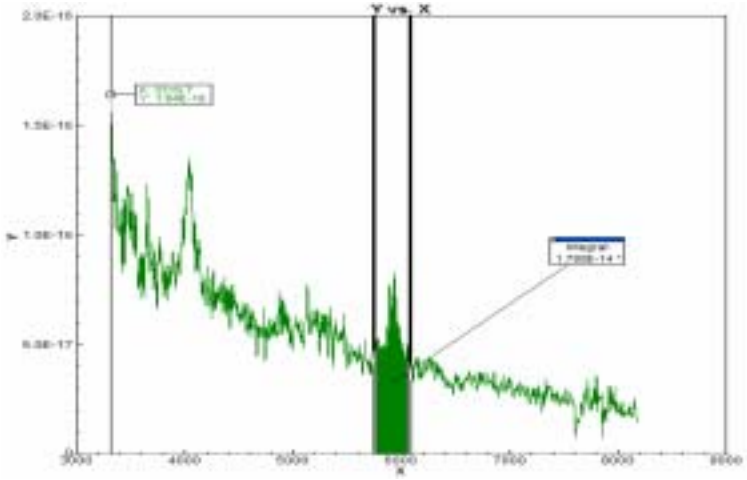

Luminosity
Radio vs Mg II

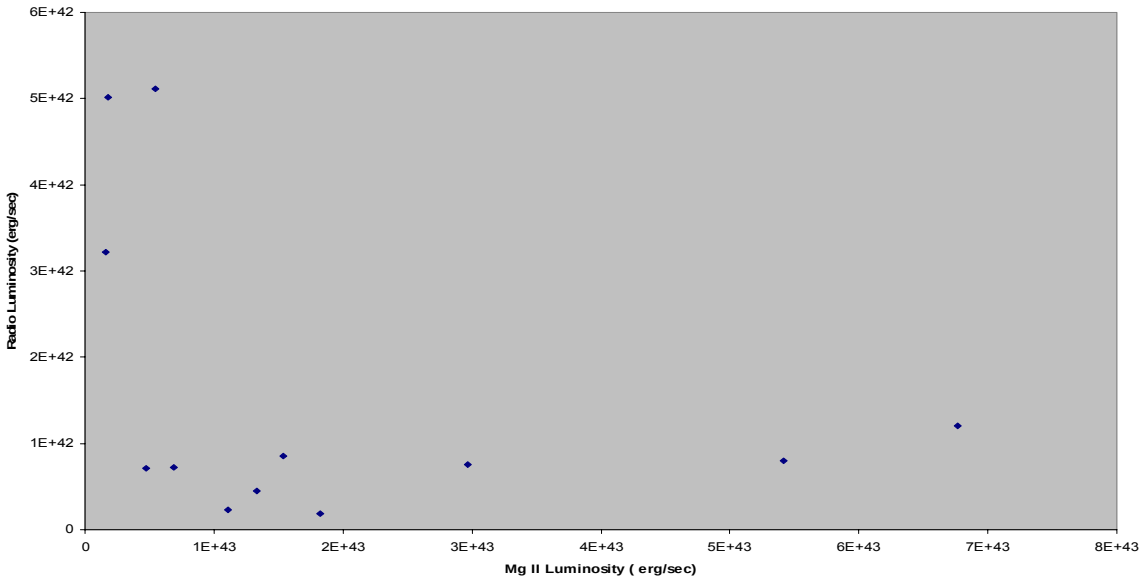

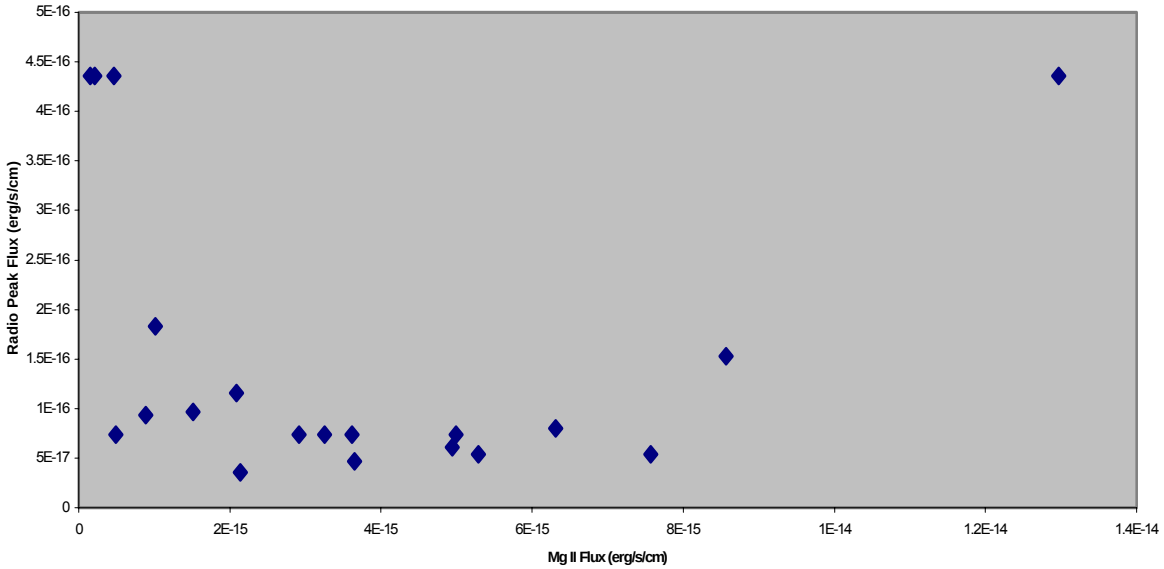

CURRENT MODEL

The current model of AGN's is illustrated in figure 7. A compact object such as a black hole is postulated to be in the center of a galaxy with clouds of gas surrounding the source. Mg II lines should be produced from heating and in some AGN's, jets should be produced that eject material at high velocity.

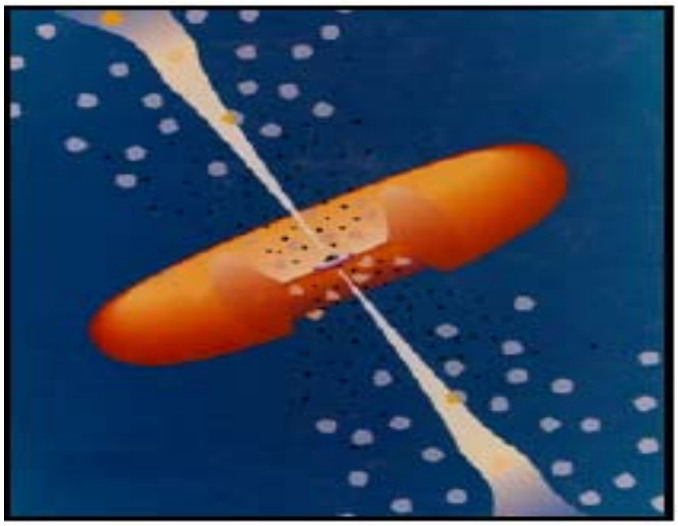

Fig 7. Current Model Of Agn Structure

CONCLUSION

Unfortunately, there was no correlation that could lead to the conclusion that the Mg II emission lines were produced by any material being ejected from the AGN or in any way could be related to the structure of the object.

There are several possibilities as to why no correlation was seen. There may not have been enough objects with strong emission lines. Of the total number of objects selected, some did not have as clear-cut a set of lines as others and the selection criteria were not always met.

NEXT STEPS

The next steps in this project would be to increase the database of objects being investigated, analyze other frequencies besides Mg II and to look at spectra in other wavelengths where a correlation might be clearer.

ACKNOWLEDGEMENTS

We would like to acknowledge the help of Dr. Travis Rector whose guidance on this project enabled the investigators to develop the project and carry out the analysis. We also wish to acknowledge the help of all of the staff of TLRBSE who provided us with the data and the opportunity to use the .9 meter telescope at Kitt Peak. In addition, the following organizations helped in making this project possible.

NSF (National Science Foundation)\
NOAO/TLRBSE
University of Arizona
KPNO (Kitt Peak National Observatory)

References

An Analysis Of Mkn 501 A Blazar

Makayla O'Neill, Ashley Armstrong, Mallory Perkins, Charlene Siza
Graves County High School, Mayfield, KY
Teacher: Velvet Dowdy, TLRBSE 2003

ABSTRACT

The purpose of this project was to analyze the properties of the blazar Mkn 501. The focus was to see if the spectrum of the blazar changed at different time periods. The blazar's light curves were notably different during various times. The curves of the spectra rose to different levels. The light curves did not have dramatic emission or absorption lines so the composition could not be determined with the resources available. The spectra analyzed showed that the spectrum of the blazar did change over time.

INTRODUCTION

For this research project the star MKN 501 was chosen and as research began it was discovered that MKN 501 was a Blazar. A Blazar is an irregular variable star that is very bright and can vary rapidly in luminosity. Blazars appear as point-like objects in the sky and are classified as active galactic nuclei and aren't very different from quasars, with jets directly pointing to the observer. The jet orientation of Blazars explains most of their peculiar characteristics which includes high luminosity, the very rapid variation, and the sometimes superluminal motions found in high-resolution images which are the very faint lines found in the spectrum. Rapid fluctuations of blazar brightness indicate that the energy producing region is small. Blazars emit polarized light with a featureless and nonthermal spectrum. Blazars can be found in the center of a galaxy and are thought to be powered by a supermassive black hole. (Wikipedia)

Blazars are also known as BL Lac Objects or BL Lacertaes. BL is a progressive ID a lot like license plates and Lacerta is the constellation where it resides. The real nature of BL Lac objects remains unknown. It's found that when near us, they are totally enigmatic and featureless. If they were extra-galactic, given their relatively high apparent magnitude, they would have been among the most luminous objects in the Universe. (Wikipedia)

Not much information has been found on Bazars because the quest to find them is difficlut because thavior has yet to be fully understood. Research is continued in attempts to someday fully understand what and how they work.

RESEARCH QUESTION

Does the fluctuating brightness of a blazar affect the patterns of the spectra of a Blazar? It was hoped to find that the spectrum does vary with changes of patterns in the spectra.

METHODS

Mkn 501 was chosen for this research project. However, as further research was obtained it was discovered that Mkn 501 was actually a blazar, not a star as was originally thought. In order to obtain research many resources and other materials were used. The spectra of Mkn 501 were used to determine the emission and absorption lines. Since Mkn 501 is a blazar, it only contains emission lines. The spectra taken on different days and times

were analyzed. The dates include: November 14,1979; September 29, 1987; May 7, 1987. A curved line was used to find the highest point. Star Classify, written and donated by Harlan DeVore, was used to obtain the different elements that Mkn 501 contains. Emission lines from each spectrum were analyzed and the wavelength was typed in Star Classify to determine the elements that Mkn 501 contains. This reveled that each emission line contained different elements from the ones previously analyzed. The red shift of the blazar was determined to find the correct peak number. The red shift of the blazar was found on Simbad. Most of the information was found using Simbad Astronomical Database. Data collected by the 2 meter telescopes on Kitt Peak in Arizona was also used. The data and software donated by NOAO was used as well. The properties of a blazar confirmed that Mkn 501 was indeed a blazar.

RESULTS

The results of the investigation were that the spectrum does vary with the varying brightness of a blazar. After looking at the spectra and wavelength it was apparent that each emission line contained different elements. However, Mkn 501 contains high amounts of hydrogen. According to Simbad it was a Spectral Type B. This type contains neutral helium, but strong hydrogen. The table of elements shows that Mkn 501 does contain more hydrogen than the other elements found. It proves that Simbad was correct in saying that Mkn 501 was a Spectral Type B.

Elements of Mkn 501

Wavelength	Elements
3681.7	H infinity
3706.072	H infinity
3730.444	O II
3786.5	H 11
3901.049	He I
4464.047	He I
4588.345	TiO

14/11/79

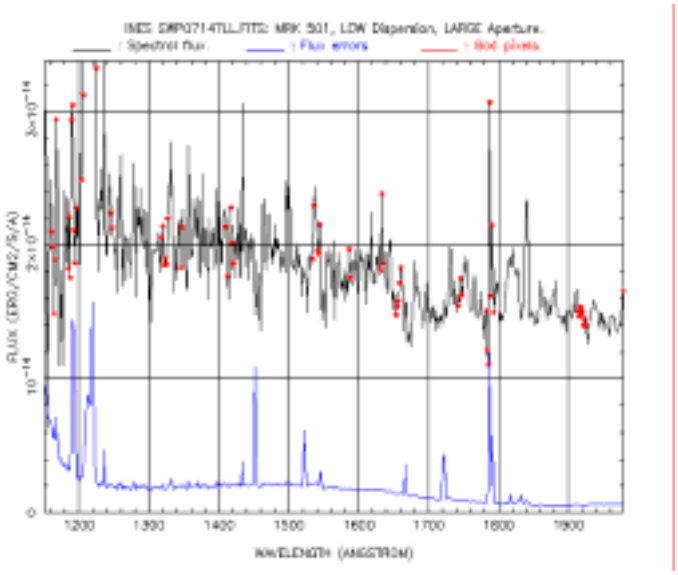

SPECTRA 1

The first spectrum was taken on November 14, 1979. Compared to the other spectra, it has more bad pixels. The emission lines in this spectrum were profound and noticeable. The emission lines were stronger than in the other spectra graphs. Large amounts of hydrogen were found in the emission lines. Blazars do not have absorption lines so they were not analyzed. As time passed the emission lines appeared smaller. However, there was one point when the emission line just shot up. It was a bad pixel, however. The very

faint lines in the spectra were caused by the jets. The jets also account for the high luminosity and rapid variation.

29/09/86

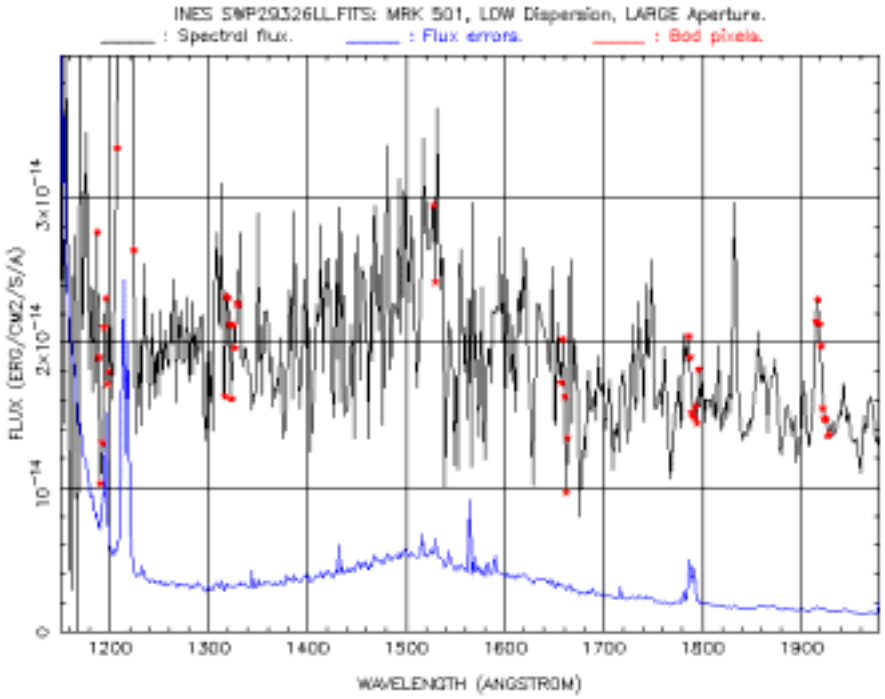

SPECTRA 2

The second spectrum was taken in 1986. The emission lines were more profound than in 1979. There were still bad pixels but not as many as in '79. The variation in the luminosity can be seen in this spectrum. Many of the emission lines shot up and just as dramatically dropped down again. The faint lines caused by the jets had fewer emission lines that those shown in '79. The emission lines were higher in this spectrum than in the previous. By the spectra it can be seen that throughout the day the spectrum of the blazar fluctuated due to the rapid variation in luminosity.

07/05/87

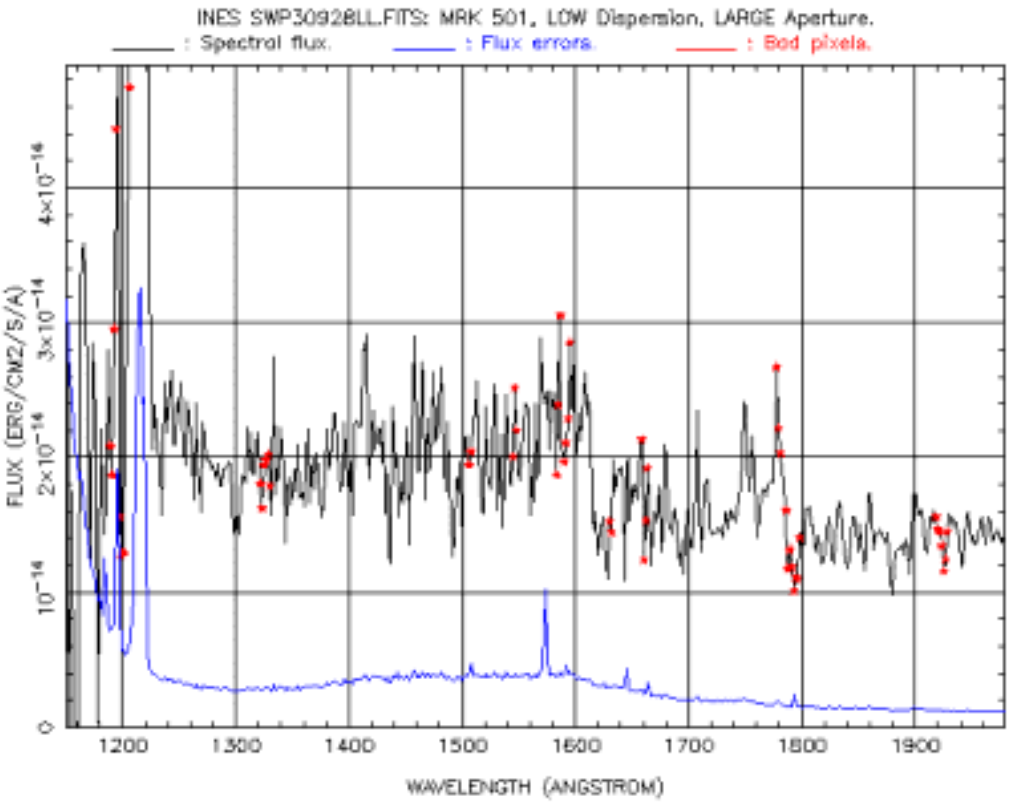

SPECTRA 3

The third spectrum was taken in 1987. It varies dramatically with the one taken almost a year earlier. The emission lines aren't as profound and intense as previous ones. The faint lines have very few emission lines and the ones that are present aren't as profound. In fact, they are really small compared to previous ones. From '79-'87 there was a drastic change in the emission lines found in the faint lines. There was also a drastic downward slope in '87.

All three spectra show that the spectrum of the blazar, Mkn 501, fluctuated due to the rapid variation in luminosity. This change was apparent not only in the spectra but also in the faint lines. The red shift of the blazer, Mkn 501, was found on Simbad. The red shift of Mkn 501 was .033640. The spectra of Mkn 501 proved that the spectrum fluctuated due to the varying luminosity.

CONCLUSION

There is a variation in the spectrum of a blazar. This is apparent because at different times the luminosity of the blazar fluctuated and the spectra was vastly different. The elements in the emission lines were different at times, but strong amounts of hydrogen were present in each spectrum. In the first spectra, taken in 1979 there were many emission lines. There were also several bad pixels. The emission lines started out strong but decreased as the day went on. There was one emission line that just shot up, but it was a bad pixel. In the next spectra, taken in 1986 there were strong but few emission lines. Almost a year later in 1987 the spectrum was vastly different. Emission lines still existed, but there were so many bad pixels that it was difficult to determine if the elements contained would be accurate. The blazar seemed to start off with high wavelengths but decreased in the last spectra. The luminosity of the blazar continually fluctuated as time went by, and still fluctuates today. If the spectrum was analyzed today there would probably be a tremendous difference in the wavelengths and luminosity, as was seen in the spectra of Mkn 501 in 1979, 1986, and 1987.

The jets of the blazar account for the high luminosity and the fluctuating brightness of the blazar. The special jet orientation explains most of a blazar's peculiar characteristics: the high luminosity, the very rapid variation, the sometimes superluminal motion found in high-resolution images, and the very faint lines found in the spectrum (Wikipeda). These lines are found at the bottom of the spectra graphs in each spectra. Some show strong emission lines, others don't.

Although, a variation in the spectrum of Mkn 501 was found, there may have been problems that were encoutered throughout the investigation. One of the main problems that was continually run into and could have affected the results was the bad pixels found in each spectra. The bad pixels could have affected the elements that were found in each emission line and possibly the curved line. The bad pixels may have also affected the outcome of the element in 1979, where the emission line just shot up. The bad pixels could have affected the wavelength that was found using Star Classify. Other factors affecting the blazars spectroscopy may have been the black hole in the middle and other outside forces. These forces may have played a role in the luminosity that was read. Their may also have been objects between Earth and the blazar that could have affected the luminosity that was seen. For example, it may have appeared bright but with the object in the way it could have been brighter than was imagined.

Even with the bad pixels and other factors that could have affected the outcome of the results, it was found that the spectrum of a blazar varies depending on the brightness of the blazar.

FURTHER RESEARCH

For additional research other factors affecting the spectrum would be a related topic. With the current question only one factor was chosen. Also for further study the composition and distance of a blazar could be an interesting subject. While researching the blazar, a black hole was discovered in the center. With this finding, the black hole involvement in the blazar would provide further research.

REFERENCES

www.astro.soton.ac.uk/~crk/PH227/ node50.html

http://astro.fisica.unipg.it/blazarsintheweb.htm

http://www.chara.gsu.edu/PEGA/find_ redshift.shtml

www.simbad.com

http://en.wikipedia.org/wiki/Blazar

Barth A.J., Ho L.C., Sargent W.L.W. Journal from February (II) 2002

De Paolis F., Ingrosso G., Nucita A.A., Zakharov A.F. Journal from November (I) 2003

Edwards P.G., Piner B.G. Journal from November 2002

Howard E.S., Webb J.R., Pollock J.T., Stencel R.E. Journal from January 2004

Ghisellini G. Journal from 2003

Mastachiadis A., Kirk J.G. Journal from 2002

Spectroscopy Of Gamma Draco Compared To A Standard K Class Star

Jared Fulcher, Jodie Beadles, Kelli Gough, Andrew Perkins
Graves County High School, Mayfield, KY
Teacher: Velvet Dowdy, TLRBSE 2003

ABSTRACT

The research question explored in this project was, "How does the spectroscopy of Gamma Draco compare to the spectroscopy of a standard K class star?" The results indicate that Gamma Draco does not emit the same elements as a standard K class star and thus proves its semi-variable nature. Then a comparison will be made upon the spectral class of Gamma Draco in 1980. It can therefore be concluded that Gamma Draco is a semi-variable star because it does not have the same emissions as a regular star in its same class and also Gamma Draco changes spectral classes in 1980.

INTRODUCTION

This project is a study of the semi-variable star Gamma Draco, located at +51.29° Declination and 17h 56m Right Ascension (Kidger, 2003)Semi-variable stars are stars that vary in their light output. There are several reasons a star's brightness might change. There are over 30,000 known semi-variable stars, and thousands more are suspected of being semi-variable (Variable Stars, 2004). Gamma Draco is actually a binary system of stars. Since Gamma Draco is an eclipsing binary, one of its stars dims when the other star passes in front of it, and it brightens again when the star moves out of the way (Compton's, 1998). Semi-variable stars are observed by the scientific community to determine the long-time behavior of a star, provide professional astronomers with data needed to analyze variable star behavior, to schedule observations of certain stars, to correlate data from satellite and ground-based observations, and to make computerized theoretical models of variable stars (Variable Stars, 2004). Research on semi-variable stars is important because it provides information about properties such as mass, radius, luminosity, temperature, internal and external structure, composition, and evolution. This information can then be used to understand other stars (Decin, 2004).

Gamma Draco is in the spectral class K5III (Simbad, 2004). This project is intended to expand on the current understanding of the nature of semi-variable stars as compared to the nature of standard stars. To do this, the emissions of Gamma Draco will be compared to the emissions of a standard K5 star. The emissions of a standard K5 star are strong unionized metals and weak hydrogen (The Classification of Stellar Spectra, 2004). A standard K star also has temperature of 3900K-5200K (DeVore, 2004).

RESEARCH QUESTION

"How does the spectroscopy of Gamma Draco compare to the spectroscopy of a standard K class star and how does the spectral class of Gamma Draco change?"

This study is expected to reveal a pattern of emissions and of spectral class changes that can conclude the semi-variable nature of Gamma Draco.

METHODS

Graphical Analysis 3.1 Demo- data on CD donated by the National Optical Astronomy Observatory

Spectra data obtained by the Coude Feed on Kitt Peak in Arizona

Simbad Astronomical Database-data; spectra

Star Classify- an Excel program created and donated by Harlan DeVore, TLRBSE participant, 2003

Compton's Interactive Encyclopedia- data

AAVSO- data

Gamma Draco was chosen from a list of stars that were provided by the head of the study (Coude Feed on Kitt Peak, 2004). Spectra were obtained from an Internet database (Simbad Astronomical Database, 2004). Once the emission lines of the spectra were identified the lines were then computed using Star Classify, an Excel program (DeVore, 2004). With the Star Classify program the emitted elements of Gamma Draco were then recorded. After processing three spectra of a reasonable time period the elements were compared to the elements emitted by a standard K5 star. A table was then formulated to present the results of the comparisons.

After finding the results of the emission comparisons a conclusion could be reached of the pattern of Gamma Draco's emissions. Then studying three spectra obtained in 1980, the peak of the light curve was found (Simbad Astronomical Database, 2004), which is used to find spectral class (Howell, 2003). On finding these peaks, Star Classify was then used to determine the spectral class of Gamma Draco during 1980 (DeVore, 2004). Finding the spectral class for the three spectra, a discovery was made of Gamma Draco's evolution from a B-class star to an A-class star (Aspin, 2003).

RESULTS

Date	Element	Ionization
12-26-80	**Al II**	**Single ionized**
06-09-80	**Al II, Si IV, O IV**	**Single ionized, Triple ionized**
04-20-80	**C III, C II**	**Double ionized, Single ionized**
Standard K5 Star emissions: unionized metals and the weakest hydrogen (DeVore, 2004)		

This table represents the elements emitted by Gamma Draco. The emissions of a standard K5 star are presented at the bottom and in comparison Gamma Draco does not emit the elements of a standard K5 star.

Date	Peak (in Angstroms)	Temperature	Spectral Class
12-26-80	1250	23176K	B-class
06-09-80	1250	23176K	B-class
04-20-80	3250	8914K	A-class
A standard K star has temperature between 3900K-5200K			

This table represents the findings of comparing the spectral class of Gamma Draco in 1980.

CONCLUSION

The study of Gamma Draco revealed that Gamma Draco does not emit the elements of a standard K5 star. Thus the semi-variable nature of Gamma Draco is proven. Then with the study of the spectral classes of Gamma Draco on each date another conclusion was reached. During the year of 1980 Gamma Draco appeared to be a B-class star. Thus Gamma Draco was a hotter star in 1980. This conclusion could help identify a pattern in the semi-variable nature of Gamma Draco. Gamma Draco can be found to be hotter and brighter in the latter part of the twentieth century.

The study could have been falsified by the spectra obtained on the Simbad Astronomical Database. Each of the spectra had bad pixels and each emission line was only an estimation as to its size. The light curves also found on the spectra were estimates and may have been inaccurate.

FURTHER STUDY

A future study of Gamma Draco could include research of Gamma Draco's absorption lines and compare them to its change in spectral classes. Also a comparison could be made of Gamma Draco emissions or absorptions to its magnitude.

REFERENCES

Aspin; The evolutionary state of stars in the NG 13335 star formation region; March 2003Compton's Encyclopedia; Binary Star Systems; March 2004

Coude Feed, Kitt Peak, Arizona; Spectral Data; 2004

Decin; ISO-SWS calibration and the accurate modeling of cool star atmospheres. II General Results; March 2003

DeVore, Harlan; Star Classify Excel program; 2004

Howell, Steve; Spectroscopy of semi-variable stars Draft; October 2003

Kidger; High precision near infrared photometry of a large sample of bright stars visible from the northern hemisphere; June 2003

Simbad Astronomical Database; 2004 -- simbad.u-strasbg.fr/Simbad

The Classification of Stellar Spectra; 2004
lheawww.gsfe.nasa.gov/users/allen/spectral_classification.html

Variable Stars; 2004 – www.aavso.org/vstar

Analysis Of The Spectrum Of Gamma Herculis

Tiffany Dowdy, Janie Bowlin, Jon Ladd, Brandon Speed
Graves County High School, Mayfield, KY
Teacher: Velvet Dowdy, TLRBSE 2003

ABSTRACT

Several different groups of scientist have done tons of research on the subject of "stars". Our group took the star Gamma Herculis (gamma her) and investigated an analyzed the spectrum of the star. We discovered several interesting facts about gamma her and its spectrum. Unfortunately we were unable to come to a solid conclusion about the entire spectrum of Gamma Herculis, and what it all means.

INTRODUCTION:

Stars are very interesting subjects. Several different scientists have studied these amazing objects. This particular star, gamma herculis, is a semi variable star. A semi variable star is a star that changes the apparent brightness over a period of time. This change in brightness may be very diminutive or may be a great deal of change in the spectrum. The time in may take a star to "change" its brightness may also vary from time to time. For a given star it may only take a second or two, while for another star it may take years between each "change". This expansion of time, in which it takes the star to change, helps scientist to classify the star into different types of variable stars.

Gamma Her is a very special type of variable star. It is known as an eclipsing binary star. An eclipsing binary star is not just one star. The word "binary" hints at the fact that in reality it contains two stars. An eclipsing binary star is a pair of stars that rotate around each other and occasionally eclipsing one another to the viewer. The period of rotation for an eclipsing binary star may appear rather fast being that it ranges from one day at a time.

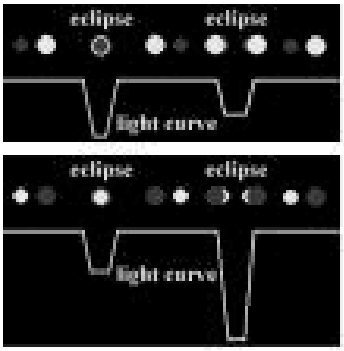

Fig. 1

Fig. 1 is a chart that shows the relationship between the eclipsing stars and the spectrum that it gives off. As the stars move in front of one another the spectrum does not show that as much light is being given off. This can account for some of the spectrum being that it is so different at times in gamma herculis.

Gamma Herculis has also been used as a standard star for the MK spectral and luminosity classification. The star has been observed sporadically usually for the purpose of including the necessary values into charts, we used emission lines and absorption line to chart this data.

RESEARCH

Our group searched for several different facts about the star gamma her. We were able to use the Internet as a semi reliable source. We searched for previous research questions that involved gamma her. The spectrum, it's self, of gamma her was very difficult to obtain. We wanted to analyze the spectrum of gamma her and discover the differences between time periods. We hope to find that gamma herculis is in fact a semi variable star, and that the charts that have been recorded about this star will help to prove this point.

METHODS

Our group was given information about the entire project. Most of this information was obtained at Kitt Peak. WE were able to obtain different charts on the semi variable star and eclipsing binary stars throughout difference search engines over the Internet. Graphical analysis and star classify helped us to analysis the data that we found on the star through the charts.

RESULTS

Research on the star gamma her was very limited due to the simple fact that semi variable stars have just not been researched as much as some other stars. WE discovered that gamma her is an eclipsing binary star. There are some speculation to the actual spectrum of gamma her. Gamma her is for certain a semi variable star. Little is known about the partner star of gamma her. Since little is know about this star it is difficult to come to the conclusion that gamma her is the only semi variable star of the two. In fact it might even be that the partner star is also a semi variable star. If it is discovered that the partner star is also a semi variable star, then this may cause misconceptions in the reading of the charts that have be compiled about gamma her. Some of the mishaps of the partner star may cause things to show up on ht gamma her's spectrum that are not truly there.

Starting off we looked at the different charts that have been compiled over gamma her.

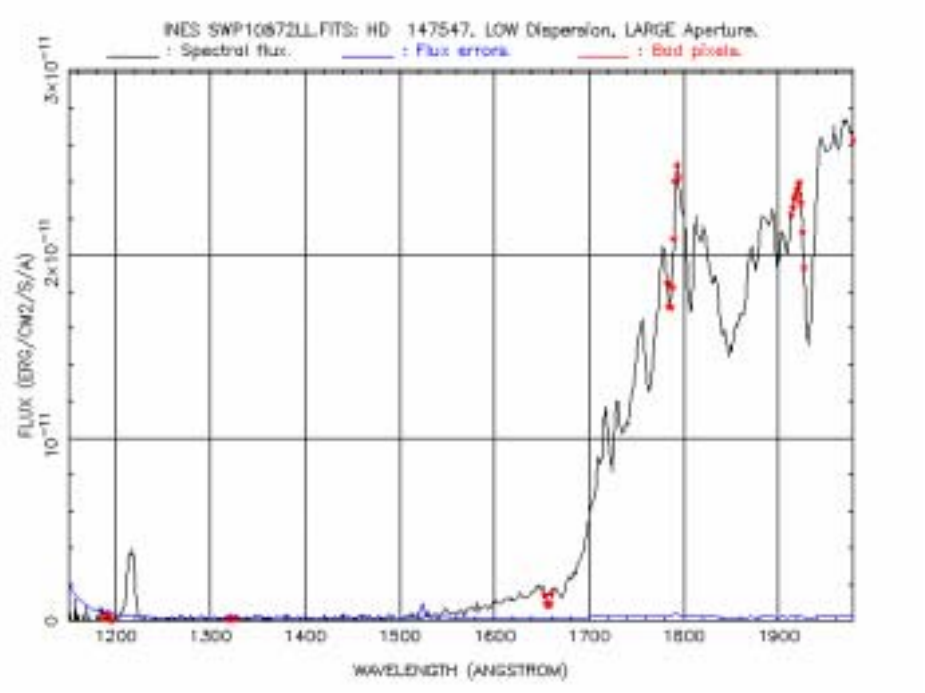

When analyzing this chart we used star classify to help us find out what element was being given off by each line.

Lines	element	actual #
-1220	Lya	1215.2
-1550	CIV	1545.9
-1720	CIVII	1665.9
-1880	ALII	1857.4
-1970	CIII	1908.3

Absorption lines	elements	actual #
-1725	OIII	1665.9
-1850	ALII	1857.4
-1929	CIII	1908.3

Star classify gave us the element that showed up as being closes to what we, the views, were seeing on the chart. Emission lines are the lines that spike up. The line # is the number that was seen on the chart. THE element is the element that this particular line gave off. The actual # is the # that the element really shows up as. Absorption lines are the ones that appear to come down. All points on the charts are not valid some of the points were bad pixels. These pixels were labeled by the dot that appears on the chart.

Within one given time period a semi variable star's, such as gamma her, emission and absorption lines are given off may vary greatly. The above chart ranges form 1200- just over 1900. As one follows the chart form 1200 the lines start to bottom out. At around 1500 the lines gradually increase. From 1650-1800 there is a huge incline in the lines themselves.

This increase shows the intensity of the variable star gamma her. Semi variable stars are very random when one looks at their charts.

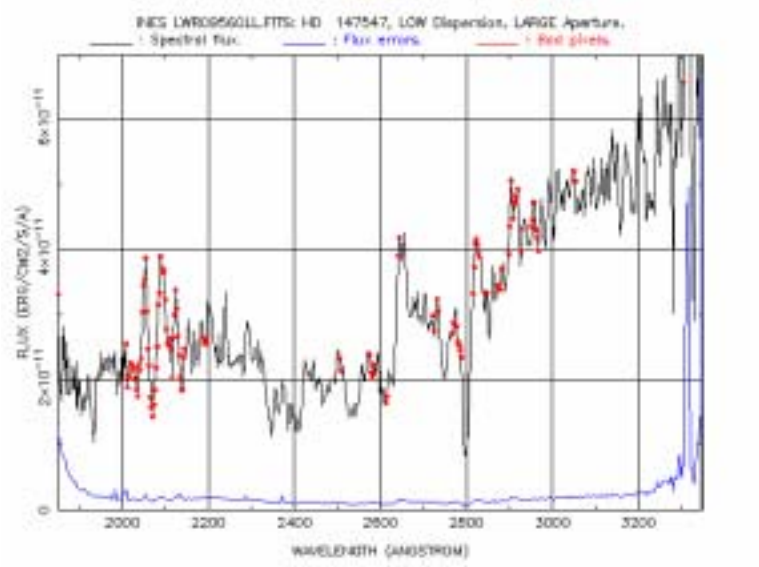

Chart 2:

Lines	elements	actual #
-1040	OVI	1033.3
-2450	NE IV	2439.2
-3010	FE	2994.4
-3300	NE V	3346.8

ab lines

Lines	elements	actual #
-2350	CII	2326.0
-2750	MgII	2800.3
-3160	He I	3188.0
-3280	Ne V	3346.8

This chart is of the same star, but only eight minutes later. As one can see this chart is very different form this other spectrum chart. This chart, like the other spectrum chart, helps to prove the fact that these perceptual types of stars are very random. Even with the short period of time between the two there is a great deal of difference between the line and the elements that they give off. The spectrum of gamma her changes without any pattern of time or element. This star is very random in its pattern and there for is properly classified as a semi variable star.

CONCLUSION

When looking and analyzing the lines that were given off by gamma her, one must be careful to take into account the fact that its an eclipsing binary star. Since there is very little research on gamma her's partner star we are unable to know if the partner star is

also semi variable. IT is semi variable then we are not positive that it is not giving off emission lines that would show up when we look at gamma her's spectrum. It is very possible that lines were transferred form one star to another due to the solitary fact that the stars are in close contact and appear to move in front of one another. This would cause all of the data that has even collected to be misleading and unable to be used. There for we are unable to come to a concrete decision on the analysis of the spectrum of gamma herculis.

FUTHER STUDY

More research is truly need to completely understand the spectrum of gamma her. There needs to be more available spectral charts. A wide range of data is needed that shows the long periods of times the changes may occur and the results of those changes.

One may also want to research other eclipsing stars. The Do-Si-Do method is a method used to analyze eclipsing binary stars. When researching variable stars it might be interesting to study variable stars in globular clusters.

Overall it makes an interesting project to research stars that have never really been researched before.

RESOURCES

http://web.byu.edu

www.sai.msu.su/groups/cluster/gcvs/gcus

www.aas.org/publications

www.space.com/

http://godot.u-strasbg.fr/cgi-ines/plotspectra?mainserver=ines.laeff.esa.es&filename=LWR09560LL.FITS

http://seds.lpl.arizona.edu/~spider/spider/ScholarX/variables.html

http://adc.gsfc.nasa.gov/adc/quick_ref/ref_varstar.html

http://wwwmacho.mcmaster.ca/DLW/Variable.html

http://members.aol.com/astroalcove/variables.html

http://www.ebicom.net/~rsf1/binaries.htm

http://zebu.uoregon.edu/~soper/MilkyWay/cepheid.html

http://www.pd.astro.it/hosted/PlanetV/planetarium/models/L23_06S.html

http://www.stormpages.com/swadhwa/stellarevolution/lecture17.htm

http://www.astro.lsa.umich.edu/users/jpinkney/AST125/variables.html

http://csep10.phys.utk.edu/astr162/lect/variables/variables.html

http://www.sai.msu.su/groups/cluster/gcvs/gcvs/intro.htm

http://seds.lpl.arizona.edu/~spider/spider/Vars/vars.html

http://hoa.aavso.org/variablestars.htm

In Pursuit Of Population III

Julie Krugler
Grosse Pointe North High School, Grosse Point, MI
Teacher: Ardis Maciolek, RBSE 1998, TLRBSE 2001

ABSTRACT

Population III stars are the first, metal-poor stars which formed after the Big Bang. This study aimed to find a low mass Population III star in the as well as to better define their characteristics and the parameters of the search for them. Spectra of 20 stars and the sun were taken at Kitt Peak National Observatory using the Coude Feed Spectrograph. The data were reduced by removing the effects of stellar radial velocity, atmospheric extinction and earth motions. The spectra were then analyzed by comparing them with standard stars and model stars constructed using the Vienna Atomic Line Database. Their chemistry, abundances and metallicities were determined. Stars with low metallicities and spectral oddities were found and compared with well-known low metal stars to determine how their characteristics are different than the standard model. In conclusion, this study suggests that G and K dwarfs may be legitimate candidates for Population III stars or at least early Population II stars which may be used to reveal the chemistry of the first stars.

INTRODUCTION

The first stars formed shortly after the creation of the universe. These stars theoretically had very low metal abundances due to the initial elements present during the Big Bang. Up until recently, scientists believed that all the first stars were too big and too hot to have survived until today. This theoretical group of stars has never been detected, but is known collectively as Population III.

The idea of seeking a Population III star stemmed from an article in Nature magazine. HE 0107-5240 was found to be the most metal deficient star known to date. Unlike what was predicted by previous models, it was a low mass star. The theoretical model of a Population III star includes the criteria of having very low metal abundances in its spectra. HE 0107-5240 was a part of the Metal-Poor Halo Stars project of the Hamburg/ESO Survey.

The discovery of HE 0107-5240 has offered new hope in the quest for Population III stars. It introduces the concept that a low mass Population III star could exist, which changes the parameters of the search.

PURPOSE

The intent of this project was to search for low mass Population III candidates, and to help further clarify the characteristics of a potential Population III star.

MATERIALS AND PROCEDURES

DESIGNING THE STUDY

The first task in establishing the list of candidate stars was to define a set of parameters. These parameters included location in the galaxy, radial velocity, and metallicity. The stars included in this study were from a region in the galaxy called the halo. These stars typically are old, have highly negative radial velocities, and very weak metal lines. The halo is an ideal place to look for possible Population III stars because there is less interstellar extinction which would interfere with the spectra.

In "Population III by Popular Demand"[1] a Population III star is described as a star with an iron to hydrogen ([Fe/H]) ratio of -6 or below. However, for the purposes of this study, the [Fe/H] ratio was given a limit of -1 and below because published [Fe/H] ratios of known stars do not extend to -6. Most stars do not have a published [Fe/H] ratio and were therefore included only on the basis of its radial velocity and spectral classification.

Solar-type stars live about 10 billion years, with the age of universe is theorized at around 13.7 billion years[2]. Stars with slightly lower masses such as spectral types G5 and later could potentially have been created around the time of the Big Bang. The scope of this study was to look at stars with spectral classes of G5-K5. It was a fresh approach, since previously only high mass stars had been studied as possible candidates.

Once the parameters were defined, I searched through catalogues using VizieR to find stars which were spectral types G5-K5 within the RA and declination range, and with a magnitude of 9.5 or lower. I also used the Starry Night software program to figure out the RA and Dec. ranges for Kitt Peak on the observing nights and to calculate the position of the moon to ensure each target star was visible. A few stars with normal metal contents were included in the group as comparison stars.

INSTRUMENTATION AND SET-UP

I, along with another student and my teacher, observed at Kitt Peak National Observatory on the Coude Feed Spectrograph. Over two nights we observed for approximately 25 hours.

Due to limitations in the set-up of the spectroscope, a range of only 1300 Angstroms could be studied. The range of 3700 – 5000 Å was chosen because the lines which are critical to the determination of metallicity are located at that area of the spectrum. The resolution limit of the spectroscope was 1 Angstrom and the blue filter was used.

CALIBRATION TECHNIQUES

Certain measures are taken to assess the capability of the instrument and to standardize it. In order to do this, a series of calibrations were completed, including zero bias frames, flat fields, and Fe-Ar lamps. The spectrum of the sun was also collected during the same time of the calibrations. Also providing an important aspect to data reduction and controls was the use of a standard star, HD17520.

---

[1] Beers, T.C. (1999)

[2] http://www.space.com/scienceastronomy/map_discovery_030211.html

DATA COLLECTION

In order to acquire data that was accurate, a photon count of around 10,000 was ideal to ensure a solid signal-to-noise ratio. The observed stars had fairly bright magnitudes, but it was better to take a series of exposures and stack them rather than to take a single exposure. However, not all stars had the same visual magnitude. Thus, the integration times varied from 300-1800 seconds and one to five exposures were taken of each star to try to come as close to the photon count as possible.

DATA

Below is an explanation of the columns of the STAR DATA table:

RA – Right Ascension
Dec – Declination
Name – Star Name
Spectra – Spectral Type
VMag – Visual Magnitude
RV – Heliocentric Radial Velocity
Cat – Catalogue
FeH – Iron to Hydrogen Ratio
Teff – Effective Temperature
Mic – Microturbulence
(v-i) – V-I Index
# of Exp – Number of Integrations
int time/exp – Time per exposure (s)

STAR DATA TABLE

NAME	SPECTRA	VMAG	RV km/s	Cat	FeH	logg	Teff K	mic	(v-i)	# of Int	int time/exp s
BD +06 0648	K0	9.1	-141	KMPS	-1.95	0.8	4500			2	1500
HD 6734	K0IV	6.44	-95	R	-0.36	3.4	5000	0.75	1.24	1	1200
HD 8724	G5III	8.3	-110	FEH2	-1.6	1.5	4624	2	1.01	2	1500
HD 15596	G5III-IV	6.23	-118	FK		2.5	4755		0.97	1	1200
HD 17520	O9V	8.29	-46				35,000		0.29	2	1500
HD 28663	F2	9.6		BEERS					0.74	4	1500
HD 37634	G5	8.89			-0.63				0.71	1	1500
HD 48236	A5	8.9		KMPS					0.3	2	1500
HD 74462	G5IV	8.74	-168.1	FEH2	-1.37	1.7	4710	1.8	1.01	2	1500
HD 191570	F5IV	6.495	-40.2		0.04	4.44	6752		0.46	2	1200
HD 191615	G8IV	7.8	-94	R					0.97	2	450
HD 196658	K0	8.7	-104.8	GEN					1.15	2	900
HD 204587	K5	9.1	-86.7			4.67	4034		1.5	2	1200
HD 204894	K2	9.1	-126.8	GEN					0.93	2	1500
HD 216143	G5	7.82	-116	KGO	-2.11	1	4500	2.2	0.94	2	1200
HD 218857	G6w	8.95	-172	KGO	-2.17	2.41	5082	2.7	0.77	2	1500
HD 219953	K1V	8.87	-51		-0.43		5010		0.84	3	1600
HD 235397	G5	9.5	-94	GEN					0.83	2	1500
HD 251383	K2V	9.42	-92	R	0.33		4780		0.93	3	1500
HD 285246	A5	9.6		BEERS					0.22	5	1500

ANALYSIS

DATA REDUCTION

Many stars had highly negative radial velocities, and this altered the position of the spectral lines. First, the shift caused by them must be accounted for by using the non-relativistic Doppler formula. Secondly, the heliocentric radial velocities given in each of the catalogs made two corrections: a) for the Earth's orbit around the Sun and b) for Earth's rotation. One spectrum was corrected for their shift by comparing the observed wavelengths of certain spectral lines to their known values.

In order to portray the entirety of the photon counts, each of the text files were put into Excel and files for the same star were compared to each other for cosmic rays. Cosmic rays are light that saturates the pixel when it enters the spectroscope. These are not a part of the star's spectra and must be taken out. In order to do so, the cosmic ray is subtracted. After the subtraction, the spectra can then be stacked (added together) and then graphed using PSI Plot. These higher photon counts then increased the signal to noise ratio which more accurately portrayed the spectra of the star. The following plots demonstrate stacking.

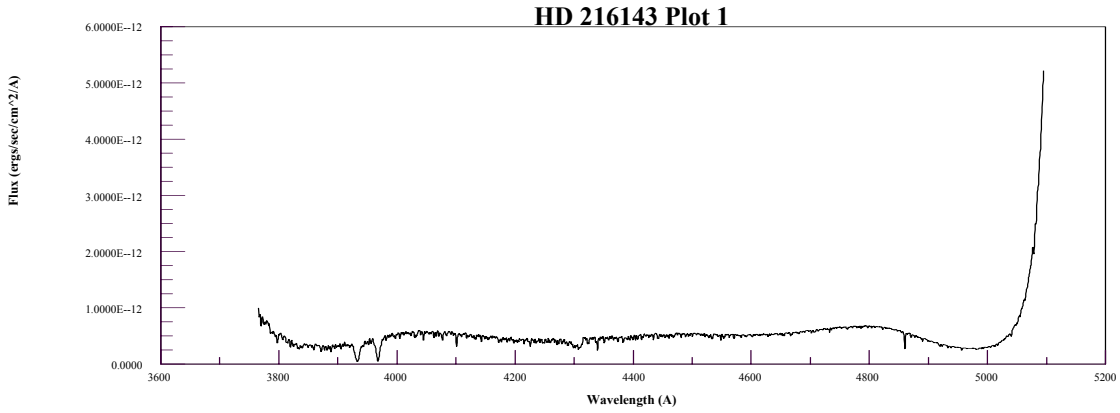

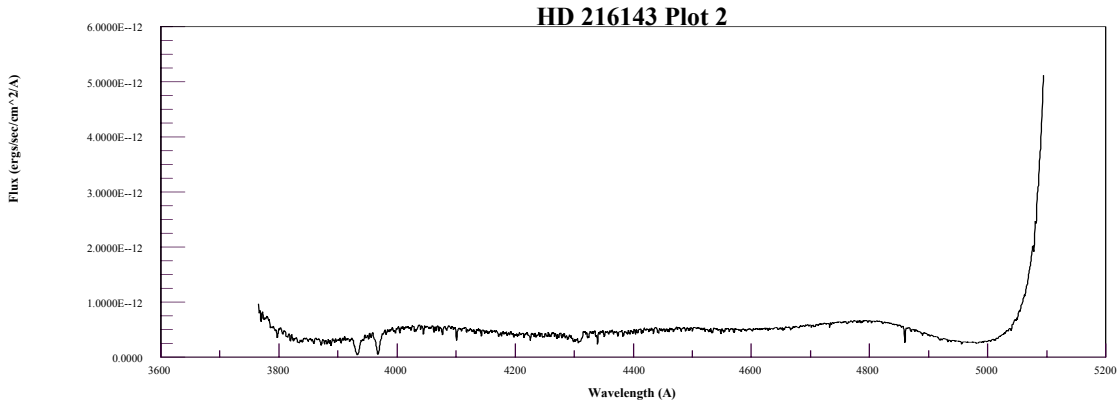

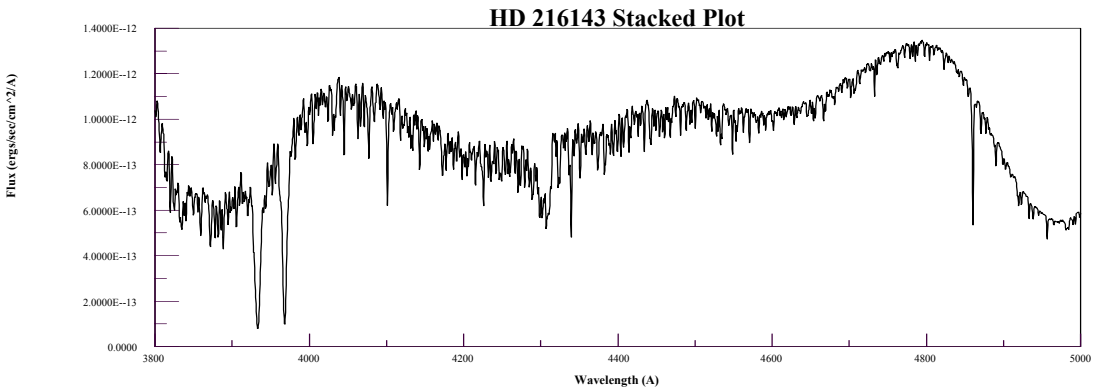

These Plots Show The Process Of Stacking.

Graphs one and two are examples of single integrations. The third graph is a 'stacked' plot where the flux values of the two integrations are combined and then terminated where the data becomes unusable.

DEVELOPING CHARACTERISTICS FOR LOW METAL VS. NORMAL STARS

In order to properly analyze the spectra of the observed stars, I first needed a model to which I could compare them. In order to create these, I registered with the Vienna Atomic Line Database (VALD). For each stellar spectral and luminosity class, a model star was created with VALD in order to compare any peculiarities in its spectra. In order to create such models, values for the abundances were either gathered from online sources when available or determined by analysis of the spectrum. If this was not possible, a query was sent that was based off the solar model and modified by an iterative method, which included changing the star parameters or its abundances. VALD serves its greatest and quickest purpose as a reference for the theoretical central depth of the spectral lines. This allows for a ratio between the data and the theoretical models to be created and that ratio is utilized in calculating abundances.

IDENTIFICATION OF LINES

In order to properly identify the lines of the spectra, both standard stars and the VALD were utilized. Some standard lines include the Ca II H and K which are two prominent features in each spectrum.

CHEMISTRY, SHAPES, BLENDS, SPLITS AND BINARIES

In order to determine the true chemistry of the star, certain spectral features must be weeded out as unusable data. When lines are too deep, they can become saturated. Saturation means that they have absorbed the maximum amount of light in their certain wavelengths. This means that any additional amount of the element present after the line is saturated cannot be estimated. Therefore saturated lines do not give a true representation of the elemental abundance. The lines which are the greatest use to this study are those which are smaller, clean symmetrical lines because they represent more closely a 1:1 proportion of area to elemental abundance.

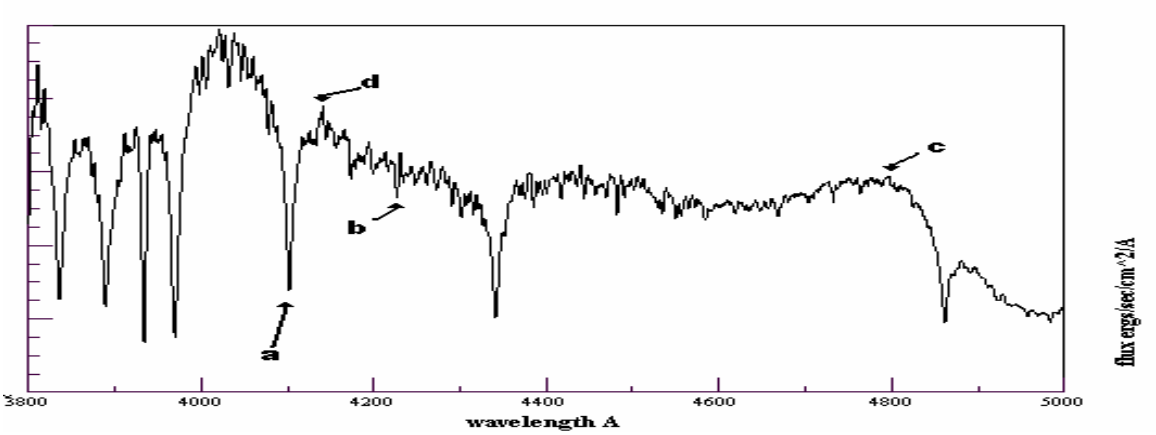

Plot 5. See Below Text For Explanation.

Point A depicts a Ca II line. Point A is not a useful line to calculate the abundances because it is much too deep (strong). Point B is a much better line because it is sharp and narrow. The line is not "saturated" and therefore changes in a 1:1 ratio as the amount of light at that wavelength is received. The best lines are no more than 20% deep from the normalized curve.

Points C and D show the highest points on the spectrum in the local area. Normalization takes these points and fits them as close to 1 as possible and changing the depths accordingly. Ideally the normalized curve can now be analyzed easily for the equivalent width, or area of the different spectral lines.

CALCULATION OF ABUNDANCES

In order to calculate the abundances of an element in a spectrum, the area of its absorption lines must be determined. This area is also known as the equivalent width. To do this, a curve must be fit to the spectrum to represent the continuum. The spectrum must also be rectified, or altered in such a way that its continuum is equal to a line depth value of 1. The central depth of the absorption lines is proportional to its equivalent width. In weak lines, the equivalent width tends to be proportional to the abundances.

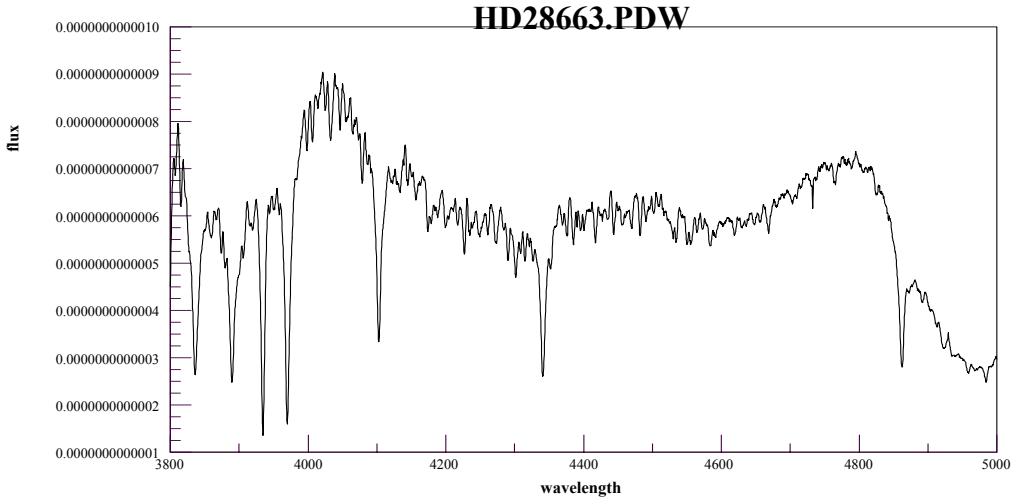

Plot 6. A Raw Data Plot Before Normalization.

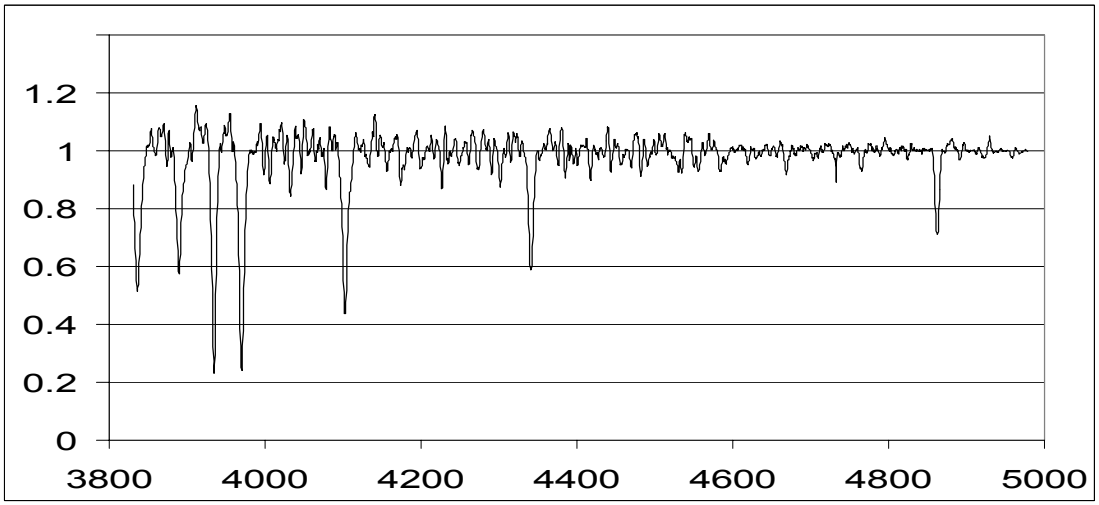

Plot 7. A Plot After Normalization.

Weak lines are best for calculating abundances because the equivalent width is basically equal to the abundance. However, there is another way to calculate the abundances using VALD. Matching the lines of the VALD query to the lines of the data, the line depths of the stars can be given a percentage depth. This percentage is then used in a logarithmic ratio of the abundance of an element to hydrogen.

VALD requires that the temperature, microturbulence, and the log of the surface gravity be given to construct the model star. It allows it to create the correct line depths for the spectral lines. When no elements are entered into VALD it defaults to the solar abundances. Central depth is the most important piece of information given by the query.
Ratios and standard abundances

One of the best indicators of metallicity is the iron to hydrogen ratio. A theoretical Population III star would have a [Fe/H] ratio of -6 and below. The lowest ratio of this survey was -.931. While this star is metal-poor, it is not of the extremely metal poor classes. This can be attributed to many factors. The resolution used was medium at 1 Å.

Higher resolution studies have been conducting indicating that these stars are more metal rich than this study indicates. The normalization of the spectra was performed in Microsoft Excel. Programs specifically used to handle spectra such as IRAF and Visual Specs did not work with the types of files in which the stars were recorded. However, these programs offer better normalization which gives a much better indication of the central depths.

CLASSIFICATION

Nine stars were reclassified. This is probably due to the change in the resolution of the survey. All of the stars of this study (with the exception of BD +06 0648) were taken from the Henry Draper Catalogue. The HD survey used a 2 Å resolution, whilst the Coude Feed has a resolution of 1 Å. The higher resolution allows for a more specific and detailed look as to the spectral and luminosity classification of the stars.

STATISTICS

In order to calculate the validity of the lines, the weakest line from each star was taken and evaluated. Using the Z test, it was determined that for 95% of the stars, the spectral lines had over a 90% chance of being valid (not noise). 80% of the stars had spectral lines that had over a 96% chance of being valid.

CONCLUSIONS

No Population III stars were found. The lowest metallicity gathered was -.931. However, the successful part of this project was the reclassification of several stars. For instance, star BD +06 0648 was initially classified as a K0 star. Upon further investigation this star was reclassified as a G0III. The prevalence of the Balmer series and the lack of metal lines between the Ca K and the CH band indicate its spectral and luminosity classes.

The reclassification of these stars and the metallicities taken from the stars revealed that none were Population III stars, however many were metal poor. Many of these stars were G and K dwarfs. This leads to the conclusion that type G and K stars are suitable candidates for the first stars. It tends that the late G and early K dwarves seem to be the most metal-poor.

EXTENSIONS

Supernova outbursts have often been blamed for ‘polluting’ other stars in their wake. Supernovae have produced the majority of the iron in the universe. They also produce large amounts of the alpha elements. Could there be a population III star that has been masked by a supernova outburst? I plan to take the abundances of carbon and nitrogen to see if these stars indicate that they could be r-process enhanced stars.

BIBLIOGRAPHY

Jaschek, Carlos, and Mercedes Jaschek. The Classification of Stars. Great Britain: University Press, Cambridge, 1990.

Tonkin, S.F. Practical Amateur Spectroscapy. Singapore: Springer-Verlag London Limited, 2002.

Zombeck, M. V. Handbook of Space Astronomy and Astrophysics. New York: Cambridge University Press, 1990.

WEBSITES USED

http://www.noao.edu/kpno/manuals/coude/node1.html#toc

http://www.go.ednet.ns.ca/~larry/astro/HR_diag.html

http://arxiv.org/PS_cache/astro-ph/pdf/0201/0201472.pdf

http://arxiv.org/PS_cache/astro-ph/pdf/0305/0305567.pdf

http://www.physics.sfsu.edu/~dnidever/nidever.pdf

http://www.eso.org/observing/dfo/quality/UVES/img/sol/sol_spec_4000.gif

http://www.eso.org/observing/dfo/quality/UVES/img/sol/sol_spec_3000.gif

http://www.astrogeo.va.it/astronom/spettri/stelle-Gen.htm

http://www.harmsy.freeuk.com/fraunhofer.html

http://vizier.u-strasbg.fr/viz-bin/VizieR

http://simbad.u-strasbg.fr/Simbad

http://aladin.u-strasbg.fr/java/nph-aladin.pl?-rm=14.1&-server=Aladin

http://www.shef.ac.uk/physics/teaching/phy103/solspec.html

http://www.shef.ac.uk/physics/teaching/phy103/gcluster.html

http://www.angelfire.com/on2/daviddarling/PopII.htm

The Message of Starlight: Stellar Spectroscopy

Emma Hookway and Elizabeth Hookway
Cranston High School East, Cranston RI
Teacher: Mr. Howard Chun, RBSE 1999

ABSTRACT

This survey studied the spectra of nearby stars found within the Milky Way galaxy. The spectral information was obtained from National Optical Astronomical Observatories. Stars within our galaxy were used so that, because they are moving relatively slowly, there will be no noticeable red or blue Doppler shift, therefore, the spectral lines observed are found where they normally would be along the spectra, and therefore easily identifiable. Once emission and absorption lines were observed, their spectral lines, were recorded in angstroms (A°), and compared to the list given of known absorption and emission wavelengths to determine the chemical composition of the star. It was predicted that, because our sun is an average G class star, most of the stars observed would resemble our sun. It was determined that hypothesis was correct. G class stars were the most common followed by A, F and K class stars. It was also predicted that in the most common class of average stars, hydrogen and helium would be the most common elements, because that is the case in our own sun. Hydrogen and helium are the fuel source in these common classed stars because of the P-P cycle. This prediction was also correct for F and K class stars, but incorrect for A class stars.

BACKGROUND

To better understand this lab, one may need general knowledge of spectroscopy. Spectroscopy is an analysis of the light energy we see as it is emitted from an object. In this experiment, spectroscopy is used to analyze visual light. This procedure is a common tool for astronomers, because spectroscopy can be used to measure a star's temperature, velocity, composition, mass, and distance, to name a few. Three types of spectra may be used for analysis, the continuous spectra, the absorption spectra and the emission spectra. To understand the absorption and emission spectra the Bohr model of the atom can be used. Absorption lines occur when an election becomes excited and moves to a higher energy state, and emission lines occur when an electron moves from an excited state back to the ground levels. Each element leaves its own specific "fingerprint" in the form of spectral lines. The study of spectroscopy revolutionized the study of astronomy in the 19th century. For the first time, astronomers could study the composition of stars, and they could also classify the stars. By studying the elements' "fingerprints" (absorption and emission lines) this lab will classify stars, while determining their composition.

HYPOTHESIS

Most of the stars observed will be "average stars," meaning that most of the stars observed will be F, G or K class stars. In these stars, hydrogen and helium will be the most common elements found because these are the elements the Sun uses for fuel and are therefore the most abundant in our Sun.

PROCEDURE

Using Wien's law and the peak wavelength of a stars spectroscopy graph, the temperature of each star was determined, and from this information a preliminary star class was concluded. To confirm that this classification was correct, the wavelengths of any emission or absorption lines on the graph were recorded; then, using a list of elements and their corresponding wavelengths, the elemental composition of the star was discovered. Then, a survey was taken of the stars' classes. Finally, another survey was taken of the elemental composition of the four most common star classes determined.

CONCLUSION

This demonstration classified over 50 different stars into their respective stellar classes: O, B, A, F, G, K, M, L, using stellar spectroscopy. It was predicted that most of these stars would be average, F, G, or K class stars that would resemble our sun (our sun is a G class star). This prediction proved to be correct. It was also predicted that within these stars, Hydrogen and Helium would be the most abundant elements because they are what provides the fuel for our sun and are therefore most abundant. This prediction proved to be correct for Hydrogen, but not Helium.

In this experiment, the class of the star was first predicted using the temperature of the star, which was determined using Wein's Law. The prediction was then verified using the knowledge of what elements were present in the star. In some cases, though, the prediction made using temperature, and the elemental findings in the spectra, did not correspond, and adjustments were made taking both into consideration. A possible explanation for this is a misjudgment of the peak wavelength, or a small redshift that was not accounted for. (A redshift is a shift in the spectra caused by the Doppler effect of a star's movements away from the earth.)

It was determined that, out of 61 stellar spectrums observed, 16 of those were G class stars, like our Sun. There were also 13 A class stars, 11 F class stars, and 10 K class stars. From this small survey it can be determined that most of the stars in our galaxy are average stars. Within these stars, 21 different elements were observed; the most abundant of these being some form of hydrogen. Helium, though, was less abundant than expected. It was only observed 7 times in all of the A, F,G, and K class stars for which the survey was taken. Such elements as Calcium, Sodium and Titanium were far more abundant, occurring more than 20 times in some cases.

In general, metallic elements were more abundant than helium. For example, Calcium II, was observed 30 different times in the 50 A, F, G, and K class stars observed. Titanium was also very abundant, being observed 20 times in the stars observed. Metals were more abundant in these stars because at the temperature at which the stars were observed, metals were more easily ionized when compared to helium.

(*These results were based on the student's observations; however, some elements that were not seen could have been present. The temperature might not have been correct, which explains why some elements were not seen, but they were still part of the composition of the star observed*.)

REFERENCES

An Amateur Spectroscopy Site. December 3 2003
http://www.geocities.com/tlaude2000

Bishop C. Stellar Spectroscopy.
htttp://www.ph.surrey.ac.uk/astrophysics/files/spectroscopy.html

Franknoi, Andrew, David Morrison and Sidney Wolff eds. Voyages Through the Universe. New York: Harcourt Inc., 2000

Stella Spectra. NOAO: RBSE Program

Wikipedia. Astronomical Spectroscopy. December 5, 2003
http://en.wikipedia.org/wiki/Stellar_spectroscopy

DATA

TOTAL NUMBER OF EACH SPECTRAL CLASS

O	B	A	F	G	K	M	L
0	1	13	11	16	10	6	1

TOTAL NUMBERS OF EACH ELEMENTS IN F, G, AND K CLASS STARS

Elements Present in:	F class stars	G class stars	K class stars	A Class Stars
Hα	7	10	5	10
Hβ	9	7	6	12
Hγ	8	2	2	12
Hδ	8	2	3	10
Hε	9	11	4	11
He I	0	1	1	0
He II	5	0	0	0
Ca I	0	5	4	0
Ca II	8	16	3	3
Na I	5	13	9	1
Ti II	5	11	4	0
Fe I	1	4	7	0
Fe II	1	0	0	0
N IV	1	0	0	0
N V	1	0	0	0
Mn I	0	4	3	1
Si IV	0	1	0	0
C II	0	1	0	0
C III	0	1	0	0
C IV	0	0	0	1
Sr II	0	1	0	0

SPECTRAL DATA

Name	Estimated Peak Wavelength (A°)	Calculated Temperature (K)	Predicted Color and Class	Elements Found	Line Wavelengths (A°)	Spectral Classification
41 Cygnus	4200	6900	Yellow – White K	Ca II, Hε, Hδ, Hγ, Hβ, Hα , Na I	3935, 3970, 4103, 4340, 4861, 6563, 5895	F
52 Cygnus	5841	4960	Orange K	Hε, Na I, Ca I, Mn I, Hα	3971, 5890, 4035, 4035, 6563	G
69 Cygnus	3900	7436	Blue – White B	Hε, Hδ, Hγ, C IV, Hβ	3970, 4861, 4340, 4658, 4861	A
Bd 392411	3800	7860.5	White A	Hε, Hδ, Hγ, Hβ, Fe II, He II(2)	2971, 4100, 4342, 4861, 4232, 4339, 4688	F
Eq peg-dat	7522	3851	Orange K	Na I, CN, Hε, Hδ, He II, Fe I, CH "G Band"	5895, 4225, 3971, 4103, 4339, 4337, 4340	M
Ev Lac	7600	3816	Orange K	Ca I, Hγ, Mg H, Hβ, Na I, Hα	4230, 4340, 4780, 4863, 5894, 6563	M
Hd 187282	4800	6035.4	Yellow – White F	Hε, Hα, Hβ, N IV, N V, He II, Na I	4342, 6565, 6861, 4058, 4603, 4688, 5890	F
Hd 313643	6706	4320	Orange K	Na I, CIII, C IV, Hα, HeI	5887, 5699, 5816, 6581, 7066	M
Hd 313846	7600	3816	Red M	C III, He II, Hβ, Hα	4649, 4686, 4863, 6565	L
Hd 331054	5600	5173.2	Orange K	Hε, Hα, Ca II, Ti II, He I, Na I	3971, 5651, 3934, 4302, 4387, 5891	G
Hd 331055	4600	6298	Yellow-White F	Ca II, Ti II, Hε, Hδ, Hγ	3934, 4302, 3971, 4103, 4341	F
Hd 331057	3909	7597	White A	Hε, Hδ, Hγ, Hβ, Hα	3977, 4101, 4340, 4863, 6565	A
Hd 331059	6395	4530.1	Orange	Hα, Hβ, Ca II, Fe	4862, 6563,	K

			K	I(2), Ca I, T II, He I, Na I	3968, 4041, 4326, 4226, 4304, 4388, 5891	
Hd 331061	4060	7135	White A	Hε, Hδ, Hγ, Hβ, Hα	3970, 4102, 4340, 4862, 6563	A
Hd 331063	4038	7355	White A	Ca 11, Hε, Hδ, Hγ, Hβ, Hα	393, 3970, 4101, 4341, 4861, 6563	A
Hd 331066	4080	7100.5	White A	Hε, Hδ, Hγ, Hβ, Hα, Mn I	3970, 4102, 4341, 4862, 5653, 4032	A
Hd 331072	7600	3812	Orange K	Ca I, TiO (2), He, Ca 11, Ca 1	4226, 4585, 4750, 4542, 3934, 4229	M
Hd 321078	4032	7355	White A	Ca II, Hδ, Hγ, Hβ, Hα	3933, 4101, 4341, 4861, 6563	A
Hd 331080	4200	6897.6	Yellow-White F	Hδ, Hγ, Hβ, Hα Ca II, He II (2), Na I	4101, 4342, 4829, 6563, 3935, 3970, 4339, 5890	F
Hd 331081	7521	3821	Red M	TiO, Ca II (2)	4585, 3939, 3973	M
Hd 331083	4673	6356	Yellow-White F	Ca II, Hε, Hδ, Ti II, Hγ, Hβ, Na I, Hα	3933, 3970, 4101, 4300, 4340, 4860, 5890, 6561	F
Hd 331085	4207	6886	Orange K	Hε, Hγ, Hβ, Ca II (2), Mn I, Fe I, Ca I, Na I	3971, 4340, 4861, 3934, 4046, 4325, 4226, 5891	G
Hd 331086	4207	6886	Yellow-White F	Hε, Hγ, Hβ, Hα, Hδ	3966, 4641, 4863, 6564, 4105	A
Hd 331090	4916	6041	Yellow-White F	Ca II, Hε, Ti II, Hβ, Na I, Hα	3930, 3970, 4300, 4860, 5890, 6560	G
Hd 331341	4625	6263.8	Yellow-White F	Hε, Hδ, Hγ, Hβ, Hα, Ca II, He II	3970, 4102, 4341, 4860, 6563, 3968, 4339	F
Hd 331086	3941	7351	White A	Hδ, Hβ, Hα, Ca II	4341, 4863, 6564, 3971	A
Hd 331087	4006	7414	White A	Ca II, Hε, Hδ, Hγ, Hβ, Na I, Hα	3933, 3970, 4101, 4340, 4861, 5895, 6563	A
Hd 332091	6546	5131.1	Orange K	Ca II (2), Mn I, Si IV, Ca I, Fe I, Na I	3933, 3968, 4035, 4089, 4225, 4325, 5890	G
Hd 332110	4055	7144	White A	Hε, Hδ, Hγ, Hβ, Hα	3972, 4103, 4342, 4861, 6562	A
Hd 355045	8000	3712	Red M	Ti II, Ti O, Mg H, Na I, Hα	4300, 4670, 4780, 5890, 6563	M
Hd 355094	6670	4343.0	Orange K	Hδ, Hγ, Hβ, Hα, Mn I, Ca I, Fe I, Na I	4101, 4340, 4861, 4563, 4035, 4226, 4325, 5890	K
Hd 356459	4006	7232	White A	Hε, Hδ, Hγ, Hβ, Hα	3969, 520 4342, 4859, 6565	A
Lam cyg	3937	7543	White A	Hε, Hδ, Hγ, HCI, Hβ	3970, 4101, 4349, 4471, 4861	B
Mkn 501	5223	5632	Yellow G	Hε, Fe I, Hδ, C II, Ti II, Na I, Hα	3970, 4045, 4101, 4267, 4300, 5890, 6563	G
Star O1	5470	5296	Yellow G	Hε, Ti II, Na I, Ca I	3972, 4306, 4893, 4226	G
Star 02	7191	4139	Orange K	Ca II, Hε, Ti II, Na I	3930, 3970, 4300, 5891	K
Star 03	3986	7267.4	White A	Hε, Hδ, Hγ, Hβ	3969, 4101, 4340, 4859	A

Star 04	**4637**	**6248**	**Yellow – White F**	**Hε, Hβ, Hγ, Hα, Ca II, Ti II**	**3972, 4861, 4341, 4862, 3933, 4300**	**F**
Star 05	**7012**	**4236**	**Orange K**	**Na I**	**5890**	**K**
Star 06	**5300**	**5466.0**	**Yellow G**	**Hε, Hβ, Hα, Ca II, Ti II, Na I**	**3971, 4861, 6563, 3932, 4304, 5895**	**G**
Star 07	**4793**	**6044**	**Yellow – White F**	**Hε, Hδ, Hβ, Ca II, Ti II, He II**	**3972, 4101, 4862, 3933, 4302, 4340**	**F**
Star 08	**6607**	**4495**	**Orange K**	**Hε, Hδ, Ti II, Hβ, Na I, Hα**	**3970, 4101, 4300, 4861, 5890, 6563**	**K**
Star 09	**6000**	**4828.3**	**Orange K**	**Mn I, Na I**	**4032, 5895**	**K**
Star 10	**5932**	**4883**	**Orange K**	**Ca II, Ti II, Na I**	**3932, 4306, 5893**	**G**
Star 11	**4543**	**6537**	**Yellow – White F**	**Ca II, Hγ, Hβ, Na I, Hα**	**3933, 4340, 4860, 5890, 6563**	**G**
Star 12	**5000**	**5794.0**	**Yellow G**	**Hβ, Hα, Ca II (2), Ti II, Na I**	**4861, 6565, 3937, 3968, 4301, 5895**	**G**
Star 13	**6086**	**4760**	**Orange K**	**Hε, Fe I, Ca I**	**3971, 4045, 4228**	**K**
Star 14	**5352**	**5549**	**Yellow K**	**Ca II, Hε, Ti II, Hβ, Na I, Hα**	**3930, 3970, 4300, 4860, 5890, 6563**	**G**
Star 15	**6000**	**4828.3**	**Orange K**	**Hβ, Ca I, Ti II, Fe I, Na I**	**3970, 42265, 4300, 4325, 5891**	**K**
Star 16	**5605**	**5169**	**Orange K**	**Ca II (2), Ti II, Hε, Hβ, Hα**	**3935, 3969, 4306, 3971, 4861, 6563**	**G**
Star 17	**4504**	**6594**	**Yellow – White F**	**Hε, Fe I, Hδ, Hγ, Hβ, Na I, Hα**	**3970, 4045, 4101, 4340, 4860, 5890, 6563**	**K**
Star 18	**6010**	**4820.3**	**Orange K**	**Hβ, Hα, Mn I, Ca I, Fe I, Na I**	**5861, 6563, 4033, 4226, 4323, 5891**	**K**
Star 19	**5759**	**5030**	**Orange K**	**Ca II, Sr II, Ca I, Ti II, C III, Fe I**	**3935, 4074, 4226, 4444, 4641, 4326**	**G**
Star 20	**4756**	**6244**	**Yellow –White F**	**Ca II, Hε, Fe I, Hδ, Ti II, Hγ, Hβ, Na I, Hα**	**3933, 3970, 4045, 4101, 4300, 4340, 4861, 5890, 6563**	**F**
Star 21	**5800**	**4994.8**	**Orange K**	**Hε, Ca II, Mn I**	**3971, 3933, 4030**	**G**
Wolf 1364	**4032**	**7185**	**White A**	**Hε, Hδ, Hγ, Hβ, Hα**	**3971, 4101, 4341, 4861, 6564**	**A**
Xi cyg	**8000**	**3816**	**Red M**	**Na I**	**5895**	**M**